Hypochlorous acid stress responses in bacteria

By

Wei-Yun C. Wholey

A dissertation submitted in partial fulfillment
of the requirements for the degree of
Doctor of Philosophy
(Cellular and Molecular Biology)
in The University of Michigan
2012

Doctoral Committee:

Professor Ursula H. Jakob, Chair
Professor James Bardwell
Professor Victor DiRita
Professor Emeritus Robert A. Bender
Associate Professor Matthew R. Chapman

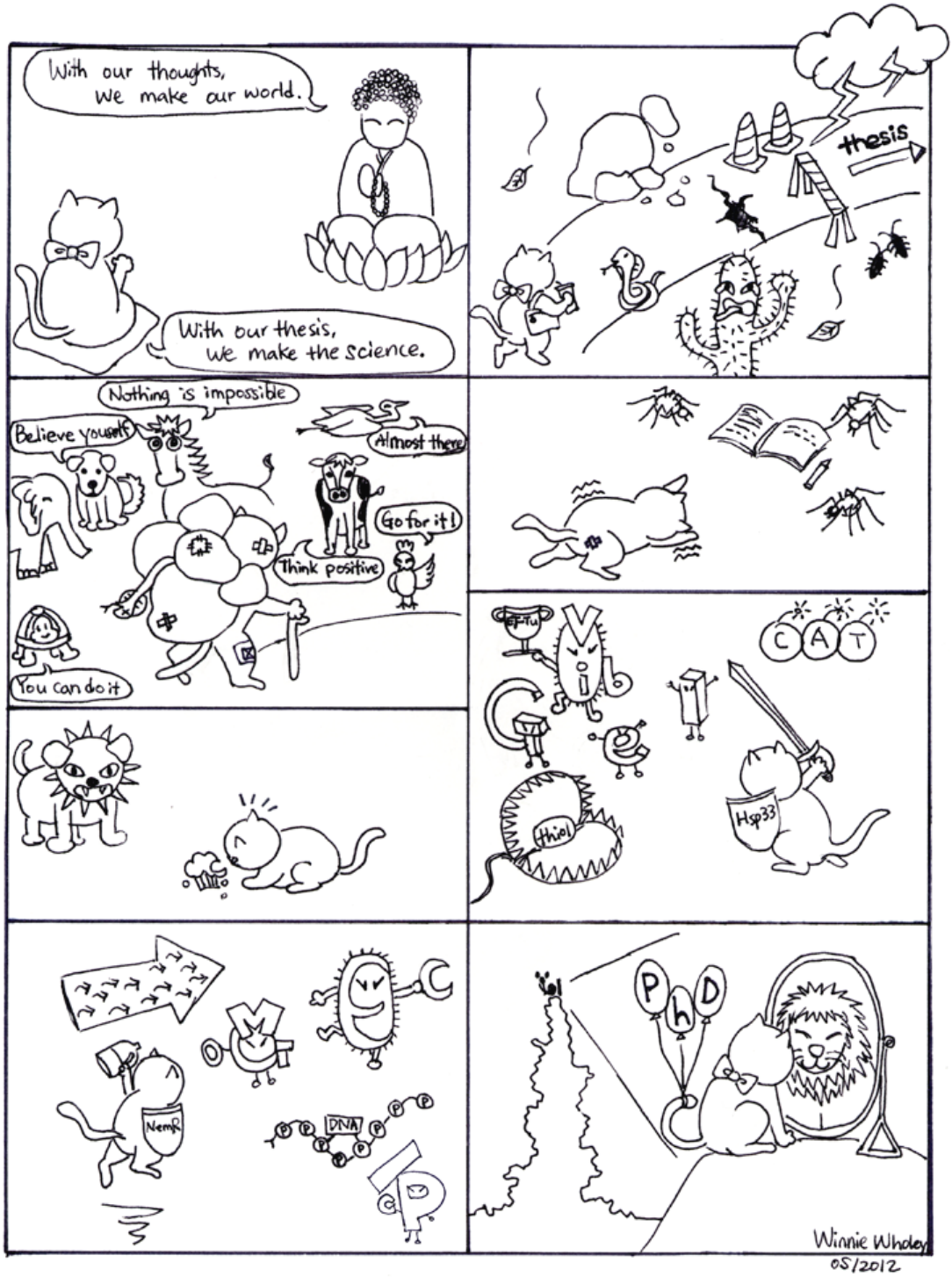
With our thoughts, we make our world.
With our thesis, we make the science.
thesis
Nothing is impossible
Believe yourself
Almost there
Go for it!
Think positive
You can do it
CAT
thiol
Hsp33
NemR
DNA
PhD
Winnie Wholey
05/2012

This thesis is dedicated

to my husband Kevin F. Wholey,
who always supports me with care and love

You made this dream possible and
never ever stopped believing in me

Well, and thanks for all the pressure

ACKNOWLEDGMENTS

Well, of course I want to express my super duper double stacker thanks to my professor Dr. Ursula Jakob, who gave me the opportunity to work in her lab and to pursue science. I received great support and training from her. Ursula inspired me with the art of teaching and supervising students. Thank you Ursula, for being such a great role model and leading me through my study here.

Many thanks to my thesis committee, Drs. James Bardwell, Victor DiRita, Robert Bender, and Matthew Chapman, for all the useful and constructive comments and suggestions along the way of my thesis. Without them, my project would not have moved as smooth. Thank you!! I would like to thank Dr. Michael Gray, who joined me on the bleach project and helped me on validating my microarray findings. From his testimony, an independent scientific observation, we all know that it is very difficult to work with the “highly reactive” HOCl oxidant.

I would like to thank the lab members of the Jakob lab for all the supports and for maintaining a cheerful working environment. I met a lot of great and crazy people here. Thanks to Caroline Kumsta and Marianne Ilbert for being the wonderful role models when I just joined the lab, and for teaching me “fun in the lab”. Thanks to Claudia Cremers, Daniela Knoefler, and Dana Reichmann for

support, encouragement, and the laugh!! Heather Tienson, Antje Mueller, Shu Quan who are wonderful friends to be around.

Many thanks to my husband Kevin Wholey for taking care of me when I was stressed frequently. Kevin supports my dream of pursuing a degree for every second tirelessly, with the hope that he will benefit when I get a tenure position. Well done, Kevin! We are getting there! I would like to also thank Kevin for providing me with a nice and relaxing home (… …) with kitties, chickens, ducks, deer and even uninvited raccoons. Thanks Kevin for building a nice house with me and showing me the tricks to become a weekend house construction worker. I am now well-prepared and equipped with an unusual wide range of skills, and I am ready to take on the next challenge of our lives. Well done, Kevin!

For everyone else that I didn't mention by name that helped me in the past 5.75 years, I appreciate you very much. Finally, I cannot forget all the bacteria that I killed during optimization of phenotypic assays and many other experiments. Without their sacrifice, this thesis is not possible.

終於苦盡甘來了, 完成悠悠長路的學業. 特別感謝我的媽媽, 姊姊和哥哥給我支持. 我有幾句話對我的媽媽說: 成為家裡的第一個博士, 我不會讓您失望的. 希望咱們家也是苦盡甘來, 可以臉上添光. 加油!

TABLE OF CONTENTS

LIST OF TABLES

LIST OF FIGURES

LIST OF ABBREVIATIONS

AKR	aldo-keto reductases
AMS	4-acetamido-4'-maleimidylstilbene-2,2'-disulfonic acid
AOPP	advanced oxidation products
ATP	Adenosine-5'-triphosphate
Ca	calcium
Cu	copper
DHAP	dihydroxyacetone phosphate
DHM	ehydromethionine
DNPH	2,4-dinitrophenylhydrazine
DuOx	dual oxidase
E. coli	*Escherichia coli*
EF-Tu	elongation factor Tu
EPO	eosinophil peroxidase
ESI	electrospray ionization
Fe	iron
FRET	Foerster resonance energy transfer
GAPDH	Glyceraldehyde 3-phosphate dehydrogenase
G6PDH	glucose-6-phosphate dehydrogenase

GSA	glutathione sulfonamide
GSH	reduced glutathione
GSSG	oxidized glutathione
H_2O_2	hydrogen peroxide
HDL	high-density lipoprotein
HOCl	hypochlorous acid
Hsp33	heat shock protein 33
IAM	iodoacetamide
LB	Luria Bertani medium
LC	liquid-chromatography
LDL	low-density lipoproteins
LPO	lactoperoxidase
m/z	mass-to-charge ratio
MALDI	matrix-assisted laser-desorption ionization
MetSO	methionine sulfoxide
$MetSO_2$	methionine sulfone
Mg	magnesium
MGO	methylglyoxal
Mn	manganese
MOPS	Neidhardt MOPS Minimal Medium
MPO	myeloperoxidase
MS	mass spectrometry
NADPH	Nicotinamide adenine dinucleotide phosphate

NCT	*N*-chlorotaurine
NEM	N-ethylmaleimide
NET	neutrophil extracellular trap
O_2•	superoxide
OH•	hydroxyl radical
PE	phosphatidylethanolamines
polyP	polyphosphate
PS	phosphatidylserines
ROS	reactive oxygen species
RSO_2H	sulfinic acid
RSO_3H	sulfonic acid
RSOH	sulfenic acid
TCA	trichloroacetic acid
ts	temperature sensitive
UV	Ultraviolet
V. cholerae	*Vibrio cholerae*
Zn	zinc

ABSTRACT

To kill invading bacterial pathogens, the antimicrobial hypochlorous acid (HOCl) is produced in high concentrations in the cells of the innate immune system. HOCl is also found to be produced at mucosal barrier epithelia, suggesting the importance of HOCl-induced responses for bacterial pathogenesis and colonization. Previous studies have demonstrated that the conserved *E. coli* Hsp33 chaperone has a major role in protecting bacteria against oxidative protein unfolding, a stress condition mediated by HOCl.

In an attempt to understand the function of Hsp33 in *Vibrio cholerae*, a causative agent of cholera, I characterized the *V. cholerae* Hsp33 deletion strain and discovered that it has temperature sensitive (*ts*) phenotype for growth when cultivated under aerobic conditions. Overexpression studies revealed that expression of the *E. coli* elongation factor EF-Tu is necessary and sufficient to rescue the *ts* growth defect as well as the severe HOCl-sensitivity of *V. cholerae* strains lacking Hsp33. Mechanistic studies revealed that Hsp33 protects *Vibrio* EF-Tu both from degradation at normal growth temperatures, and against aggregation under stress-conditions. These results suggest that Hsp33 protects bacteria against HOCl-mediated cellular death by preventing EF-Tu, an essential

component for protein biosynthesis, from oxidative protein unfolding and degradation.

To investigate the transcriptional changes in bacteria in response to sublethal HOCl treatment, Affymetrix microarray studies were performed on wild type *E. coli* cells. Our results confirmed previous observations that HOCl treatment leads to the accumulation of unfolded and aggregated proteins as many genes of the heatshock regulon were up-regulated. Protein unfolding is also the likely reason for increased intracellular level of free metals, which require the up-regulation of efflux systems to prevent intracellular damage. I identified the up-regulation of the transcriptional repressor NemR, which appears to be highly HOCl-specific, and whose gene product *gloA* facilitates methylglyoxal detoxification in HOCl-treated *E. coli* cells. The beneficial role of toxic methylglyoxal formation appears to be the replenishment of phosphates needed for ATP regeneration and other biological building blocks. This seems to be particularly important as HOCl treatment of cells was found to lead to a rapid accumulation of large quantities of inorganic polyphosphate crystals, which appear to play a strong protective role against macromolecular damage in cells. GloA-mediated methylglyoxal detoxification along with polyphosphate production, therefore appear to play major roles in cellular survival upon exposure to HOCl. Results of this study will help to reveal the molecular action of HOCl and elucidate the bacterium's strategy to counteract HOCl-stress in host defense.

CHAPTER I

Hypochlorous acid mediated oxidative stress and its physiological consequences

ABSTRACT

Hypochlorous acid (HOCl), the active component of household bleach, is generated in activated neutrophils during pathogenic infections. The highly potent oxidant HOCl, which reacts with all biological macromolecules, including proteins, DNA, and lipids can cause severe oxidative damage. The reactions of HOCl with cellular components give rise to a variety of secondary oxidative products, such as chloramines and aldehydes. These secondary oxidation products prolong the oxidation effects of the intrinsically short-lived oxidant. HOCl produced in neutrophils induces rapid bacterial death, and can cause tissue injuries and chronic diseases in cases when the production of HOCl becomes unmanageable. This chapter discusses both beneficial and detrimental roles of HOCl during the inflammation stage of the immune response. The current understanding on the rate of reactions, mechanisms involved, and the toxicity effects mediated by oxidative HOCl stress will also be summarized.

Introduction into redox biology

Oxygen is one of the main energy sources in aerobic eukaryotic organisms. Reactive oxygen species (ROS) is a collective term, describing activated oxygen derivatives, such as superoxide (O_2•), hydrogen peroxide (H_2O_2), hydroxyl radical (OH•), and hypochlorous acid (HOCl). Exogenous sources and environmental agents, including ionization, UV irradiation, atmospheric pollutants, and certain chemical compounds, contribute to the formation of intracellular ROS (Imlay, 2008).

Oxygen crosses cell membranes freely so that its intracellular concentration is as high as the surrounding extracellular environment (Ligeza *et al.*, 1998, Imlay, 2008). Transfer of one electron to molecular oxygen generates superoxide, which can spontaneously or enzymatically dismutate into molecular oxygen or harmful hydrogen peroxide. The enzyme catalase is then used to decompose the reactive hydrogen peroxide into harmless water and oxygen. Highly reactive hydroxyl radicals are generated from hydrogen peroxide in the presence of transition metals, particularly iron, through a process known as Fenton reaction (Fenton, 1894) Special enzymes, called myeloperoxidases, found in immune cells convert hydrogen peroxide into the highly reactive hypochlorous acid (Klebanoff, 1999). A schematic representation of the production of ROS is depicted in Figure 1-1.

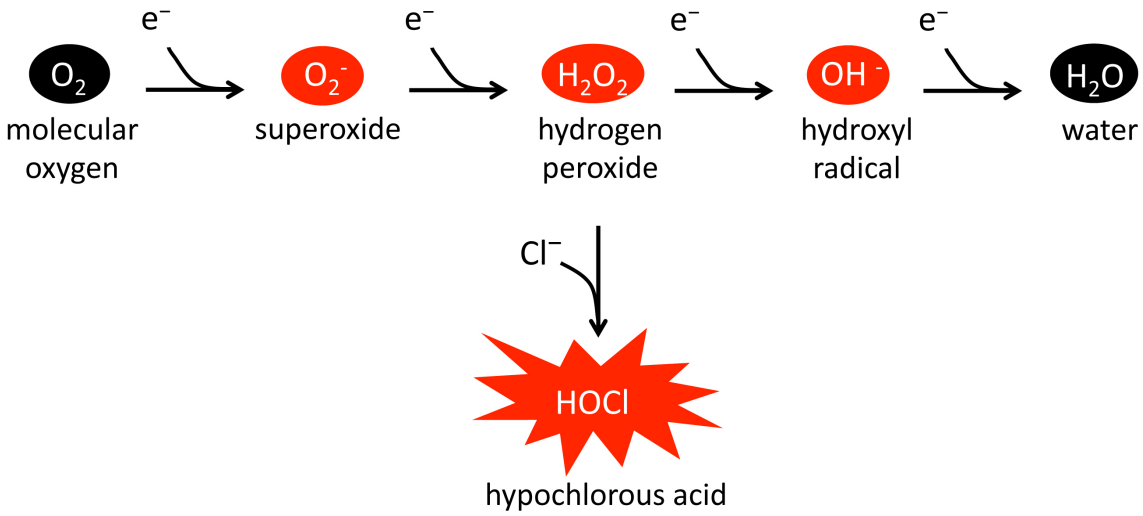

Figure 1-1. A schematic representation of oxygen reduction.
Reactive oxygen species (ROS) are labeled in red and they can be formed as byproducts of normal oxygen metabolism.

Under physiological conditions, ROS are constantly generated and eliminated in an effort to maintain redox homeostasis, which is essential for many cellular processes. When the equilibrium is shifted towards pro-oxidants, either by excess ROS production or by a reduced capacity of cells to eliminate the oxidants, cells experience a stress situation termed oxidative stress. For example, when an invading bacterium is engulfed by neutrophils, high levels of ROS, particularly the potent oxidant hypochlorous acid, are secreted as part of the host defense mechanism to kill the pathogen (Hampton *et al.*, 1998). The enzymatic and chemical reactions involved in HOCl stress were not fully solved until recently.

Oxidative burst as part of the innate immune response

HOCl earned its important position in non-physiological settings as the active and powerful ingredient in household bleach. There is no doubt that bleach is the most effective antimicrobial disinfectant used in many industrial and clinical settings (Okun, 2005, Rutala and Weber, 1997). One other significant role of HOCl is that it is part of an important antimicrobial strategy in the host defense system. Cells of the human innate immunity represent the first line of defense since they eliminate invading pathogens by phagocytosis. During the early phase of bacterial infection, neutrophils, which are circulating in the blood stream, are one of the first responders that arrive at infection sites. The receptors on the surface of neutrophils detect and recognize the bacteria as foreign particle; they then initiate a process called phagocytosis, in which bacteria are internalized forming an isolated phagosome compartment.

The respiratory burst, also called the oxidative burst, is a commonly known method used to destroy invading pathogens in cells of the human innate immunity. It involves activation of NADPH-oxidases, which are located on the phagosome membrane, and which reduce molecular oxygen to superoxide at the expense of intracellular NADPH. Peroxide, which is subsequently generated from superoxide, is used as a substrate by myeloperoxidases (MPO). These enzymes generate potent HOCl by catalyzing the reaction of H_2O_2 with physiological concentrations of chloride (Kettle, 1997, Klebanoff, 1999). High concentrations of HOCl along with myeloperoxidase are then released into the phagosome (Weiss and LoBuglio, 1982). Since HOCl has a very rapid toxic effect, it has long been

suspected that the antimicrobial effects in phagosomes are mediated by HOCl due to its high reactivity with bacterial components (McKenna and Davies, 1988, Hampton *et al.*, 1998, Klebanoff, 1999). After HOCl is formed within the phagosome, it reacts with an impressive array of biological molecules, including sulfur-containing amino acids, DNA, lipids, cholesterol and NADH, and eventually induces death of the ingested bacteria (Winterbourn and Brennan, 1997, Prutz, 1996 , Winterbourn *et al.*, 1992, Carr *et al.*, 1996). Other oxidants, such as O_2• and H_2O_2, appear to play only minor roles in neutrophils as these ROS require much higher concentrations and prolonged incubation times to kill bacteria (Klebanoff, 1980). The role of phagocyte-derived oxygen metabolites other than HOCl in microbicidal activity will not be subject of this thesis, and the reader is referred to recent comprehensive reviews (Klebanoff, 2005, van der Vliet, 2008, Imlay, 2008).

Very recent reports suggested that antimicrobial HOCl production might not be limited to the oxidative burst in phagocytes but is apparently also used as the first response in mucosal barrier epithelia of the airway and intestine (El Hassani *et al.*, 2005, Bae *et al.*, 2010). Because many trillions of bacteria are attempting to colonize the mucosal epithelia along the gastrointestinal track, the intestinal epithelial barrier is the first line of host defense against overpopulation of commensal microbiota, as well as against ingested food-borne bacterial infections. One strategy to limit bacterial colonization on mucosal barrier epithelia appears to involve the dual oxidase, DuOx, which contains both a NADPH oxidase and a peroxidase domain (Bae *et al.*, 2010). Using *Drosophila*

melanogaster as model system, it was recently described that DuOx plays a central role in the intestinal host defense (Ha *et al.*, 2005). Flies depleted of DuOx by RNAi show significantly increased levels of bacterial colonization in the intestine as compared to wild type *Drosophila* (Ha *et al*., 2005). Using HOCl-specific fluorescent probes, it has been shown that DuOx-mediated bacterial elimination in the intestine is greatly depended on HOCl production (Chen *et al.*, 2011). Intestinal bacterial colonization induces chronic inflammation which has been implicated in carcinogenesis and cancer, suggesting that generation of HOCl at mucosal barrier may have more roles than in host defense (Ullman and Itzkowitz, 2011).

The toxicity of HOCl, which so effectively eliminates invading pathogens, can also cause damage to the “bystanders”, the human tissues (Winterbourn and Kettle, 2000). Incorrect cellular trafficking and processing of myeloperoxidase (MPO) has led to the release of HOCl into extracellular compartments, where it has been shown to be involved in the progress of various human diseases, including atherosclerosis, chronic inflammation and some cancers (Weitzman and Gordon, 1990, Heinecke, 1999, Lau and Baldus, 2006, Wu and Yotnda, 2011). To elucidate the mechanism by which HOCl kills bacteria and destroys human tissue, a detailed understanding of the phagocyte-derived HOCl formation during pathogenic events and the biochemistry of HOCl reactivity are needed.

Myeloperoxidase generates HOCl in neutrophils

Myeloperoxidase (MPO) functions as a heme-containing haloperoxidase, which oxidizes halides to the respective hypohalous acids (i.e. Cl^- to HOCl) using hydrogen peroxide as substrate (Senthilmohan and Kettle, 2006). Although there are two additional haloperoxidases, lactoperoxidase (LPO) and eosinophil peroxidase (EPO) found in human immunity cells, MPO is the only peroxidase which produces HOCl. LPO and EPO have only very little affinity to chloride (Senthilmohan and Kettle, 2006). LPO is normally present in secreted fluids, such as tears, milk, and saliva while EPO is produced in eosinophils, a subtype of white blood cells. Both LPO and EPO produce hypothiocyanitie acid (HOSCN) as part of the antimicrobial defense (Davies *et al.*, 2008). The oxidant HOSCN is a weaker acid and only slowly reacts with thiol residues, suggesting that it causes less cellular damage (Ashby *et al.*, 2004, Arnhold *et al.*, 2006). A comparative study showed that the reaction of HOCl with thiols is 3 - 4 orders of magnitude faster than the corresponding reaction rates with HOSCN, demonstrating that HOCl is the most potent oxidant produced by those three haloperoxidases (Skaff *et al.*, 2009).

It has been documented that MPO catalyzes the reaction of Br^- to HOBr *in vivo* and has the ability to oxidize nitric oxide to nitrite *in vitro* (Senthilmohan and Kettle, 2006, Eiserich *et al.*, 1996). Because chloride is normally present at much higher concentration than other halides under *in vivo* physiological conditions, HOCl is most likely the specific product of the MPO enzyme. Neutrophils are the main producers of HOCl, as 5% of their proteins are comprised of MPOs

(Klebanoff, 1999). Other phagocytes synthesize MPO only during their progenitor development stages and no longer produce MPO once they have matured and became specialized white blood cells (Klebanoff, 2005).

HOCl enhances adaptive immunologic host defense

One important feature in the early phase of the innate immune response is the production of myeloperoxidase and HOCl in neutrophils (Klebanoff, 1999). However, there is now mounting evidence suggesting that HOCl also has a distinctive role in the human adaptive immune system (Prokopowicz *et al.*, 2010), which is a specialized systematic response between white blood cells to eliminate specific pathogens. The adaptive immunity is activated by innate immune responses and provides the ability to mount a stronger attack and to remember the pathogen (Litman *et al.*, 2010). An antiviral activity of HOCl in cultured human nasal epithelial cells has been documented, with low concentrations of HOCl being sufficient to reduce human rhinovirus (HRV) titers, the causative agent of 50-60% cased of the common cold (Yu *et al.*, 2011). Interestingly, HOCl treatment significantly decreased viral-induced secretion of interleukins in HRV infected cells (Yu *et al.*, 2011). As interleukins are groups of cytokines used as means of communication between white blood cells, these results suggest that HOCl might play a role as part of the adaptive response.

Early research has also shown that HOCl oxidation improves antigen processing and hence lowers the threshold of antigen required to trigger the humoral immune response (Marcinkiewicz *et al.*, 1992). It was postulated that

dityrosine-containing cross-linked proteins or advanced oxidation products, the products of HOCl-mediated damage, might act as superantigens, which cause non-specific activation of T-cells (Alderman *et al.*, 2002). Another piece of evidence came from recent studies, which showed that HOCl can work as a natural adjuvant of adaptive immunity by enhancing the T-cell response to the antigens, independently from the toll-like-receptor signaling pathway (Prokopowicz *et al.*, 2010). HOCl-modified antigens appear to be taken up more efficiently by T-cells and promote induction of the adaptive immunity. Moreover, HOCl-oxidized lipids trigger the maturation and enhance the processing of human dendritic cells, important antigen-presenting cells that interact with T-cells, providing additional evidence that HOCl plays an essential role in the adaptive immune response (Alderman *et al.*, 2002a, Prokopowicz *et al.*, 2010).

Another recently identified role of HOCl in adaptive immunity appears to be the involvement in the maturation of neutrophil extracellular traps (NETs). NETs are extracellular antimicrobial fiber complexes, comprised of chromatin and granule proteins, which are needed to immobilize and kill invading bacteria (Papayannopoulos and Zychlinsky, 2009). *In vitro* NET release assays using human peripheral neutrophils showed that HOCl is the dominant trigger of NET formation (Palmer *et al.*, 2012). Cells treated with myeloperoxidase inhibitors showed very little or no production of NETs, suggesting that MPO-mediated HOCl generation is necessary and sufficient for NET release (Palmer *et al.*, 2012).

An overview of HOCl-mediated toxicity on macromolecules

Proteins being the most abundant macromolecules within the cell are also the most common targets of HOCl, especially the sulfur containing amino acids cysteine and methionine as well as aromatic side chains. Oxidative modification of amino acid residues often results in conformational changes in the proteins that may alter their native functions, cross-link or unfold the proteins, or lead to toxic protein aggregates. Many different types of oxidative modifications have been documented, including thiol modifications, aldehyde formation, and protein-protein cross-linking through disulfide bond or di-tyrosine formation. Moreover, HOCl has been shown to cause covalent protein-DNA cross-links *in vitro* as well as *in vivo* (Kulcharyk and Heinecke, 2001).

A recent study compared the rate of HOCl-mediated amino acid oxidation using intact proteins and mixtures of N-acetyl amino acids that mimic the amino acid compositions of proteins being tested (Pattison *et al.*, 2007). Results showed that the local amino acid sequence and three-dimensional structure has a great impact on selectivity and reactivity of secondary chlorine transfer reactions mediated by chloramines during bleach stress.

HOCl also oxidizes nitrogen-containing groups and results in DNA fragmentation. Due to the highly reactive nature of HOCl, it also modifies poly-unsaturated double bonds in lipids and disrupts membrane fluidity and configuration. The initial oxidation products of HOCl may be chlorinated unstable intermediates, which can form other oxidation products. For example, chloramines are short-lived but can be further converted into long-lived N-

centered radicals or aldehydes, which are also reactive and cause downstream secondary oxidations. The effects of HOCl oxidation and its downstream biological reactants will be summarized below.

Kinetic reactions of HOCl with amino acids

It has been known for many years that HOCl reacts with proteins efficiently and rapidly. To determine the reaction rates of amino acids with HOCl, early biochemical studies and competitive kinetics assays were conducted. Using competitive reactions with monochlorodimedone, the relative reaction rates of selected free amino acids with HOCl were described as Cys > Met > Cystine > His > Ser > Leu (Winterbourn, 1985). Thiol-containing compounds, such as cysteine, GSH and methionine, showed significant 100-fold more reactivity than other amino acid tested (Winterbourn, 1985). Analysis of the reaction rate of HOCl with amino acids at different pH-values revealed that HOCl reacts most readily at pH values between 7.2-9.3, with a maximum around pH 8.5 (Armesto, 1993).

The second-order rate constants of HOCl reaction with various protein side-chains at physiological pH of 7.4 were later determined and found to be: Met > Cys >> Cystine ~ His ~ α-amino > Trp > Lys >> Tyr ~ Arg > Gln ~ Asn (Pattison and Davies, 2001). Depending on the charge environment, a variation of 4 orders of magnitude in the rate constant was observed for reactions of HOCl with peptide backbone amides (Pattison and Davies, 2001). Detailed rate constants

for reactions of HOCl with protein side chains, amines, and other functional groups are summarized in a recent review (Pattison *et al.*, 2012)

Sulfur-containing targets of HOCl modification

As proteins are the most abundant and major kinetic targets within the cell, it is not surprising that the consequences of protein damage by HOCl have been extensively studied. Chloramines and sulfenyl chlorides are initial reaction products, which are fairly unstable and form more stable oxidation products by means of chlorine transfers (Pitt and Spickett, 2008). The reaction of HOCl with sulfur-containing targets leads to higher oxidation states of sulfur, such as disulfide, sulfinic, and sulfonic acid.

Oxidation of methionines often leads to functional activity changes in proteins. For example, an *in vitro* activity assay using purified *E. coli* GroEL protein has shown that GroEL is rather insensitive to H_2O_2 but efficiently inactivated by HOCl through methionine oxidation (Khor *et al.*, 2004). Methionine is oxidized directly to form stable methionine sulfoxide (MetSO) or methionine sulfone ($MetSO_2$) (Hawkins *et al.*, 2003). It has been shown that oxidation of methionine to MetSO is reversible as cells are equipped with methionine sulfoxide reductase (MsrA) to repair these oxidation products. As a result, some studies have proposed that surface-exposed methionines play an important role as oxidant scavengers in the endogenous antioxidant defense (Levine *et al.*, 1996, Moskovitz *et al.*, 1998, Iwao *et al.*, 2012, Luo and Levine, 2009). In contrast, overoxidation to $MetSO_2$ is irreversible. It has also been shown that

HOCl can attack Met residues at the N-terminus of proteins to form dehydromethionine (DHM), which is specific to HOCl and might serve as a potential marker for MPO-mediated damages in cells and tissues (Beal *et al.*, 2009, Peskin *et al.*, 2009).

Methionine is typically the first translated amino acid and appears to be the crucial and limiting factor in protein translation. The sulfur-containing property of methionine makes it an important metabolite that affects redox homeostasis (reviewed in (Lee and Gladyshev, 2011). Interestingly, the oxidation of methionine plays an important role in MPO-mediated bacterial killing in neutrophils (Rosen *et al.*, 2009). It has been demonstrated that a linear correlation exists between methionine oxidation of bacterial proteins and the antimicrobial effect of HOCl. A methionine sulfoxide reductase (*msrA* or *msrB*) overexpressing *E. coli* mutant strain, which shows enhanced ability to repair HOCl-oxidized methionines, is more resistant towards HOCl-mediated killing than the corresponding deletion strains. This result suggests that maintaining reduced methionines in proteins might be important for cellular survival during HOCl stress. Using a carbon-containing analog of methionine, norleucine-substituted cells showed more protein damages and died more rapidly when stressed with HOCl; suggesting that methionine may play a role in antioxidant and redox homeostasis in *E. coli* (Luo and Levine, 2009).

Cysteine is another favorite target of oxidative modifications mediated by HOCl. The sulfenyl chloride, formed initially when HOCl reacts with cysteine, is a unstable compound that subsequently reacts with water to form sulfenic acid, or

with another cysteine group to form a disulfide bond (Hawkins *et al.*, 2003). Under strongly oxidizing conditions, such as persistent HOCl treatment, sulfenic acid (RSOH) can be further oxidized to form irreversible overoxidation products, such as sulfinic (RSO_2H) and sulfonic acid (RSO_3H). A schematic representation of cysteine oxidation is depicted in figure 1.2.

By using dimedone, a nucleophilic reagent that binds to thiol adducts, intermediates of the reaction of HOCl with a small regulatory protein were examined by mass spectrometry (Raftery *et al.*, 2001). Sulfenic acid was only detected if dimedone was added within 20 sec of HOCl treatment, illustrating its short-lived nature (Raftery *et al.*, 2001). Irreversible protein modifications mediated by HOCl may cause loss of protein function and likely contribute to inflammation and bacterial death, particularly as there is no known general sulfinic or sulfonic reductase identified to date (Kumsta and Jakob, 2009).

Reversible oxidative modifications on thiol-containing residues have been shown to play an important regulatory role in modulating the function of redox sensitive proteins (Jacob, 2011). Several studies have shown that the discriminating reactions of HOCl (i.e. by selective oxidation of thiol-containing amino aids) have inactivated many enzymes that themselves are important components of the inflammatory response. These enzymes are matrilysin MMP-7, tissue inhibitor of metalloproteinase I, the neutrophil proteinase cathepsin G, and lysozyme (reviewed in (Prokopowicz *et al.*, 2012). These results suggest that HOCl may be involved as part of an negative feedback loop, which might

contribute to switching off the regulation of inflammatory processes (Prokopowicz *et al.*, 2012).

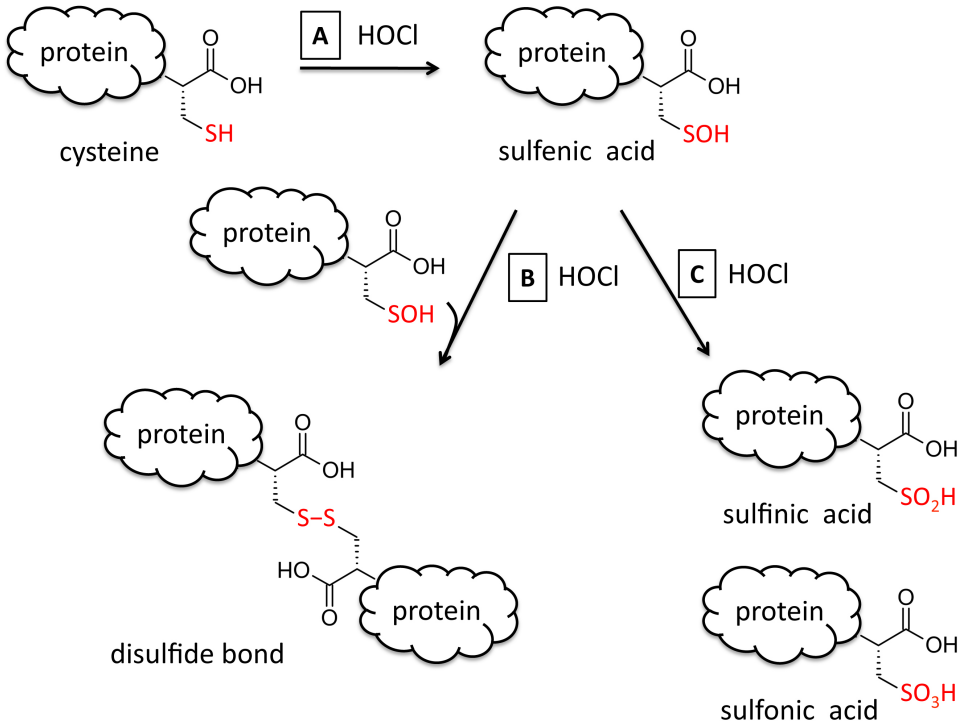

Figure 1.2. Oxidative cysteine modifications. (**A**) Formation of sulfenic acid. (**B**) Formation of reversible disulfide bond from two sulfenic acids. (**C**) Irreversible overoxidation of sulfenic acid to sulfinic acid or sulfonic acid.

Generation of protein carbonyls by HOCl

Protein carbonylations are oxidative modifications of the reactive carbonyl group on lysine, arginine or proline residues, which are irreversible *in vivo*. In some cases, the level of reactive carbonyls is used to measure the accumulation of oxidized proteins (Nystrom, 2005). The metal-catalyzed protein oxidations, particularly those mediated by iron, are believed to be one of the major pathways for carbonyl generation *in vivo*. Carbonyl groups can be labeled with 2,4-dinitrophenylhydrazine (DNPH) and subsequently measured using

spectrophotometric assays or antibodies specifically recognizing the DNPH-moiety (Nystrom, 2005).

To investigate the formation of carbonyls in oxidative reactions, *in vitro* studies were conducted with a variety of purified model proteins. Proteins incubated with HOCl alone showed significantly increased carbonyl formation as compared to non-treated controls (Adams *et al.*, 2001). Compared to other oxidants tested, HOCl-mediated carbonylation appeared to be extremely fast and unselective as it carbonylated all available amino acids within 10 sec (Adams *et al.*, 2001). These results demonstrated that HOCl is a potent carbonylation agent and most likely contributes to protein carbonyl formation *in vivo*. Irreversibly carbonylated proteins are toxic to living cells and form high molecular weight aggregates, which need to be degraded. Carbonyl formations are believed to play less role in HOCl toxicity because they only have modifications of the amine moieties, unlike the chlorine transfer from chloramines, which regenerate the parent amines and result in secondary damages to other molecules (Pattison *et al.*, 2012).

HOCl oxidation of aromatic side chains in proteins

It has been known for many years that tyrosine side chains can be attacked at their α-amino group to form ρ-hydroxyohenylacetaldehyde or at their aromatic ring to form 3-chlorotyrosine or the higher oxidized 3,5-dichlorotyrosine (Hawkins *et al.*, 2003). While the rapid and selective reaction between HOCl and sulfur containing amino acids produces products that are not specific for HOCl

and can be formed by other reactive oxygen species as well, oxidation of tyrosine appears to be a specific reaction product of HOCl. Hence, the product 3-chlorotyrosine is a well-validated HOCl-specific biomarker (reviewed in (Pattison *et al.*, 2012). 3-chlorotyrosine has been detected in specific HOCl-related inflammatory diseases as well as in purified *E. coli* GroEL protein in the presence of HOCl (Winterbourn, 2002, Mohiuddin *et al.*, 2006, Khor *et al.*, 2004).

The modification of tryptophan residue is another commonly found effect of HOCl-mediated protein oxidation. Formation of cyclic tryptophan-glycine cross-links has been demonstrated in the catalytic domain of HOCl-treated matrix metalloproteinases (Fu *et al.*, 2004). Using a small peptide library screen, it has been also shown that this product is sequence specific and only forms between tryptophans and glycines (Fu *et al.*, 2006). Other studies have shown that oxidative modification of tryptophan side chains lead to inactivation of enzymes and protein unfolding *in vivo* (reviewed in (Pattison *et al.*, 2012).

HOCl inactivates the trypsin inhibitor through the oxidation of Trp, Tyr and His, leading to protein unfolding and aggregation. In contrast, lysozyme is inactivated by the HOCl-mediated oxidation of Met residues (Hawkins and Davies, 2005). Extensive chloramine and carbonyl formation, rather than covalent interaction, can also lead to protein aggregation as demonstrated for HOCl-treated apomyoglobin (Chapman *et al.*, 2003).

The HOCl reaction product chlorotaurine is an effective antimicrobial

The most abundant amino acid found in the cytoplasm of neutrophils is taurine, which has a cellular concentration in the millimolar range (Marcinkiewicz *et al.*, 1995). Taurine is a derivative of cysteine with a naturally occurring sulfonic acid. It is well documented that taurine interacts with HOCl to form chlorotaurine at low pH, which is consistent with the pH-conditions of the phagosome (Marquez and Dunford, 1994). Chlorotaurine has well-recognized bactericidal properties, which play an important role in anti-inflammatory processes (Muz *et al.*, 2008). Although most chloramines react with thiol groups, their rate constants are 4 - 5 orders of magnitude less than HOCl, with the exception of chlorotaurine, which appears to react readily with thiols as well (Peskin and Winterbourn, 2001). There is good evidence that chlorotaurine is more selective in its reactions with essential cysteine thiols and is able to inactivate creatine kinase and Glyceraldehyde 3-phosphate dehydrogenase (GAPDH) more efficiently than HOCl (Peskin and Winterbourn, 2006).

Detection methods of protein oxidation

Protein oxidation research has greatly benefited from the recent development of new mass spectrometry techniques (Pitt and Spickett, 2008). As the side chains of protein are oxidatively modified, changes in their masses occur, which can be monitored by electrospray ionization (ESI) or matrix-assisted laser-desorption ionization (MALDI) mass spectrometry (MS) (Pitt and Spickett, 2008). For example, a well-characterized marker of protein oxidation, methionine

sulfoxide, shows a 16 Da mass increase as compared to the non-modified methionine. MS analyses have been used to identify specific oxidation products either with purified proteins *in vitro* or globally *in vivo*. The detection of 3-chlorotyrosine, the specific end product of HOCl, is either done using immunohistochemistry or biochemical techniques (Prokopowicz *et al.*, 2012). Several proteomic techniques, which characterize reactive cysteines and determine the oxidative thiol status of cysteine residues *in vivo* have been developed and are summarized in a recent review article (Thamsen and Jakob, 2011). For example, a quantitative mass spectrometry-based technique called OxICAT can analyze the oxidation state of cysteines in hundreds of different proteins in a single experiment (Leichert *et al.*, 2008).

HOCl-mediated oxidation effects on DNA

When HOCl is incubated with DNA, RNA or polynucleotides, the majority of initial products are unstable chloramines or chloramides, which subsequently decay by thermal or metal-catalyzed processes, forming nucleoside-derived nitrogen-centered radicals, aldehydes or dichlorinated species (Thomas *et al.*, 1986, Hawkins and Davies, 2002). As compared to HOCl, these reaction products are less reactive, yet longer-lived. Even at low concentrations, they can still act as catalysts to speed up DNA damage mediated by HOCl (Hayatsu *et al.*, 1971, Prutz, 1998b). Relatively more stable chloramines can be formed by the reaction of HOCl with the aromatic rings of nucleosides (Kawai *et al.*, 2004).

Studies conducted *in vitro* have shown that the HOCl-mediated chlorination reaction of thymine, which is believed to be the main cause of double strand dissociation, is much faster than chlorination of cytosine or adenosine (Prutz, 1998a, Prutz, 1998b). Chlorinated thymidine is more reactive towards GSH, disulfide and NADH as compared to cytosine, which only reacts with GSH (Prutz, 1998a). HOCl preferentially reacts with endocyclic nitrogens (thymidine, uridine and guanosine) than exocyclic nitrogen (adenosine, cytosine and quanosine) (Prutz, 1998a). Direct reaction of HOCl with plasmid DNA results in single and double-strand breaks through chloramine-mediated reactions (Hawkins and Davies, 2002). In addition to extensively fragmentized genomic DNA, precipitated protein-DNA complexes were found to be seven-fold increased after exposing *E. coli* cells to lethal doses of HOCl (Suquet *et al.*, 2010).

Lipid peroxidation caused by HOCl

When polyunsaturated fatty acids in membranes are oxidatively modified by HOCl, lipid peroxidations occur, which alter the integrity of membranes and decrease lipid fluidity. As a result, many membrane-bound proteins are disrupted and membrane properties change. Although HOCl reacts with lipids slower than with proteins, many phospholipids are modified and can be detected *in vivo* (Pattison *et al.*, 2003). Given that the breakdown products of lipids, such as aldehydes, are long-lived and very reactive with other molecules, the damages caused by lipid peroxidation are often significantly amplified (Humphries and Szweda, 1998).

It has been shown that HOCl attacks the acyl chains of polyunsaturated phospholipids and chlorinates the double bonds to form stable chlorohydrins *in vitro* (Winterbourn, 2002). When a phospholipid is extensively oxidized by HOCl, hydrolysis of the modified fatty acyl chains occurs, which results in smaller fragmented lysolipids (Arnhold *et al.*, 2002). Although other oxidation products of HOCl with alkenes and primary amines are possible *in vitro*, only chlorohydrin formation has been identified *in vivo* in atherosclerotic lesions (Ford, 2010). Early studies examining HOCl-mediated lysis of red blood cells have shown that phospholipid chlorohydrins introduce bulkier hydrophilic groups into the hydrophobic core of the membrane and disrupt the membrane (Carr *et al.*, 1997). In addition, the toxicity of fatty acid chlorohydrins accumulation has been observed in cultured endothelial cells (Vissers *et al.*, 2001). Antibodies against chlorohydrins have been developed in an effort to detect the presence of chlorohydrins in HOCl-treated red blood cells (Carr *et al.*, 1997). Fatty acid chlorohydrin and phospholipid chlorohydrin formations appear to contribute to the HOCl-mediated cellular ATP depletion as well as reduce viability of myeloid cells (Dever *et al.*, 2003, Dever *et al.*, 2006).

The amines in the head groups of phosphatidylserines (PS) and phosphatidylethanolamines (PE) are also favorite *in vivo* targets of HOCl and have been shown to form unstable chloroamines (Pattison *et al.*, 2003, Kawai *et al.*, 2006). Oxidization of the PS head group results in phosphatidylglycoaldehyde formation while oxidation of the PE head group causes an N-centered radical (Kawai *et al.*, 2006). A schematic representation of lipid oxidation is depicted in

figure 1.3. Reaction rates of HOCl with the head groups of PE or PS are much faster than the reaction rates with acyl chains (Pattison *et al.*, 2003).

Reaction of HOCl with glycerophospholipids causes the cleavage of the ether linkage and results in the formation of α-chloro fatty aldehyde and lysolipid (Albert *et al.*, 2001). The HOCl-mediated oxidation product of plasmalogens, abundant phospholipids found in tissues of the cardiovascular system, is also α-chloro fatty aldehyde. This end product appears to increase the level of activated monocytes and is detected both in atherosclerotic lesions and rat infracted myocardium, suggesting a link between HOCl-mediated lipid peroxidation and inflammatory diseases (Ford, 2010).

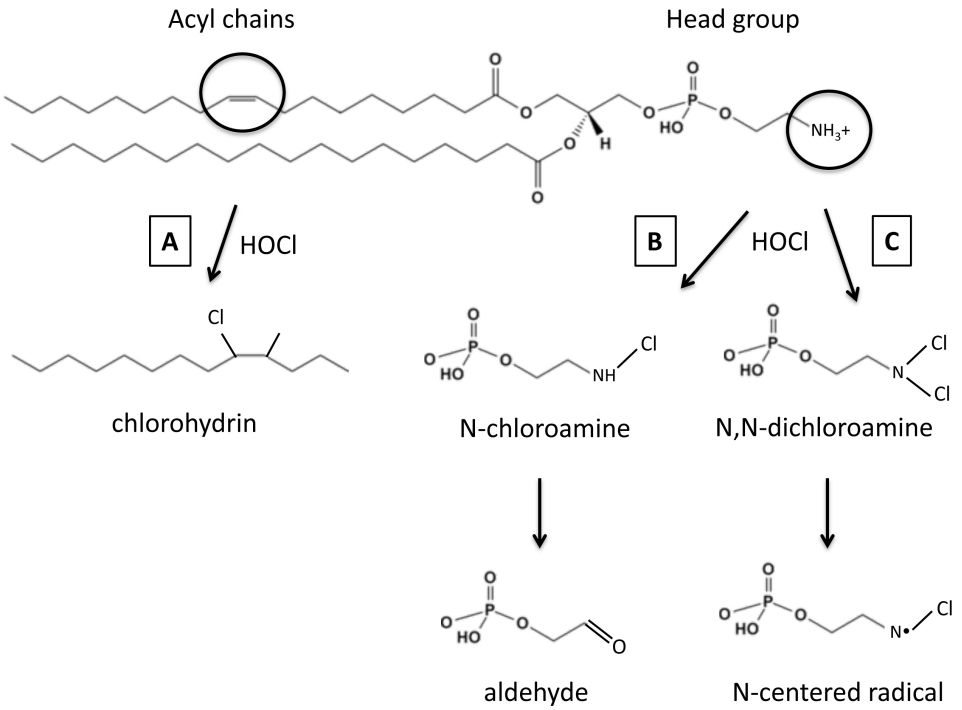

Figure 1.3. Examples of HOCl-mediated oxidation on a typical phospholipid. (**A**) Formation of chlorohydrin. (**B**) Formation of aldehyde. (**C**) Formation of N-centered radical.

HOCl oxidizes low-density lipoproteins (LDL) and converts them into pro-inflammatory lipoprotein particles, which in turn, trigger apoptosis in human T-cells (Resch *et al.*, 2011). It has been shown for many years that oxidation of LDL is an early event in atherogenesis as well as in other autoimmune diseases, and is the most important step of disease progression (Matsuura *et al.*, 2008). Many MPO-derived HOCl oxidation products accumulate at the lesion sites of inflammation (Ford, 2010). HOCl-modified LDL decreases the activity of the reverse cholesterol transport, an anti-atherogenic pathway that effluxes excess cholesterol from atherosclerotic cells by inhibiting the activity of an enzyme needed for high-density lipoprotein (HDL) maturation (McCall *et al.*, 2001).

Similarly, studies in endothelial cells revealed that a normally anti-atherogenic HDL can be converted into pro-inflammatory particles through HOCl-mediated oxidation, implicating the adverse effects of lipid peroxidation in cardiovascular diseases (Rossmann *et al.*, 2011). Interestingly, the effect of HOCl on HDL has two outcomes. When the concentration of HOCl is low, the modified HDL improves its anti-inflammatory properties and increases reverse cholesterol transport. However, these beneficial roles of HDL are lost when treated with high concentration of HOCl (Pirillo *et al.*, 2010). This result shows that low doses of HOCl can be beneficial to cells, suggesting that HOCl may play a regulatory role at early phases of inflammation.

Cholesterol is one of the most abundant molecules in the eukaryotic membrane, and is a precursor for hormone synthesis in eukaryotic cells. It can be oxidized by many free radical species. Similar to the reaction of HOCl with

lipids, *in vitro* studies have shown that HOCl reacts readily with the double bond in the second ring of cholesterol to from chlorohydrin, which is bulkier and has profound effects on the function and stability of the membrane (Heinecke *et al.*, 1994). Chlorohydrin formation of cholesterol has been detected in human red blood cells, neutrophils, mammary carcinoma cells, and in cultured myeloid cells upon treatment with HOCl (Carr *et al.*, 1996, Spickett *et al.*, 2001). These results suggested that HOCl oxidation plays an important role in pathological conditions. Indeed, there is emerging evidence that oxidized cholesterol has potential effects in several human diseases, including atherosclerosis, lung and liver diseases, cancers, and some neurodegenerative conditions (reviewed in (Iuliano, 2011).

To detect phospholipids, ESI or MALDI-MS methods can be used. Lipid oxidation is monitored by a change in mass-to-charge ratio (*m/z*) (Pitt and Spickett, 2008). For example, addition of chlorohydrin to any unsaturated phospholipid increases the *m/z* value by 52 Da. To analyze biological samples from cell lysates, given that oxidized or chlorinated lipids are often very similar in mass to their native lipids, liquid-chromatography (LC)-MS is used to assist in the separation (Pitt and Spickett, 2008). Based on the type of column used in LC-MS, lipids can be distinguished by their acyl chain length and degree of saturation. In this system, oxidized phospholipids typically elute earlier than their native lipids (Spickett *et al.*, 2001).

Effect of HOCl on carbohydrates, metals and glutathione

Very little is known about the extent that HOCl reacts with carbohydrates, which lack both sulfur or nitrogen. Early studies using purified compounds have shown that HOCl has very limited reactivity towards mannitol, ribose, deoxyribose, benzoate, dimethylsulphoxide or formate (Prutz, 1996, Winterbourn, 1985). HOCl does, however, react with glycosaminoglycans of bacterial extracellular matrix and causes subsequent fragmentation of the polysaccharide (Rees *et al.*, 2005).

Due to its high affinity for oxygen, Iron (Fe^{2+}) is used for oxygen transport and storage and hence plays an essential role in biology. Any reactive oxygen species can react with the Fe^{2+} of a heme group, causing heme destruction. It has been documented that the binding of HOCl to the heme moiety of hemoglobin damages the heme and leads to hemoglobin aggregation (Maitra *et al.*, 2011). Early studies using HPLC analysis and spin-trap experiments illustrated that the reaction of HOCl with Fe^{2+} yields very different reactive intermediates as compared to those generated in the reaction of hydrogen peroxide with Fe^{2+} (Folkes *et al.*, 1995). While the overall reaction between HOCl and the ferrous ion is similar to the Fenton reaction, it is apparently much faster, indicating that HOCl-mediated metal-catalytic reaction has the ability to generate free radicals (Folkes *et al.*, 1995).

To maintain a balanced reducing environment within the cytosol, high concentrations of reduced glutathione (GSH) are present to scavenge ROS. During oxidative stress, reduced glutathione, which is the most abundant peptide

in the cell, has the ability to exchange disulfide bonds with oxidized proteins, becoming oxidized in this process (GSSG). By doing so, GSH is able to keep proteins in their reduced state. The oxidized GSSG is then reduced to GSH at the expense of NADPH. Early studies conducted with human endothelial cells in the presence of HOCl have shown, however, that the cellular levels of GSH are irreversible depleted at sub-lethal doses of HOCl by forming glutathione sulfonamide (GSA) rather than GSSG (Pullar *et al.*, 1999, Pullar *et al.*, 2001, Harwood *et al.*, 2006). By blocking the GSH antioxidant pathway, HOCl interferes with the cells antioxidant defense and prevents the repair of oxidative protein modification. It has been shown that the generation of GSA is primarily mediated by HOCl and not by other ROS (Harwood *et al.*, 2006).

Other cellular responses to HOCl oxidation

A HOCl-resistant *Salmonella* strain was isolated from a poultry-processing plant, where HOCl was widely used to disinfect surfaces (Mokgatla *et al.*, 1998). To investigate possible protective mechanisms of this mutant strain, levels of several antioxidant enzymes were tested. This HOCl-resistant *Salmonella* isolate was found to have higher levels of peroxide-detoxifying catalase and glucose-6-phosphate dehydrogenase (G6PDH), an enzyme needed to maintain the NADPH pool and decrease DNA damage. These results suggested that HOCl disrupts cellular redox balance and damages DNA (Mokgatla *et al.*, 2002). Given that high level of catalases were needed for resistance toward to HOCl in the *Salmonella*

isolate, it was speculated that intracellular ROS might react with HOCl to form other toxic radicals that contribute to cell death (Mokgatla *et al.*, 2002).

Similarly, enhanced catalase levels were also found to assist *E. coli* in protecting against HOCl-stress (Dukan and Touati, 1996) while levels of reduced glutathione and G6PDH were found to be depleted or inactivated in HOCl treated *E.coli* (Dukan *et al.*, 1999). Mutation in DNA repair genes also increased *E. coli*'s sensitivity towards HOCl (Dukan and Touati, 1996).

Notably, the HOCl-resistant *Salmonella* isolate had more O-antigen side-chains of lipopolysaccharides (LPS) as compared to a HOCl-sensitive strain (Mokgatla *et al.*, 2002). It appears that tighter LPS structure with complete O-antigen side chains may protect cells against HOCl. In a transposon mutagenesis study, *E. coli* transposon mutants that resist oxidation mediated by lactoperoxidase (a close relative of myeloperoxidase) were isolated and tested for their sensitivity towards other oxidants. Mutants lacking membrane permeability due to reduced porin contents showed an increased resistance towards HOCl treatment (De Spiegeleer *et al.*, 2005). This result strongly suggests that HOCl enters the periplasmic space through porins. Studies conducted in HOCl-treated human endothelial cells have shown that HOCl increases cell permeability by causing cell shortening and retraction of cytoskeleton (Tatsumi and Fliss, 1994).

A recent genome–wide transcriptional analysis conducted in the pathogen *Staphylococcus aureus* in the presence of HOCl revealed that many amino acid biosynthesis genes are up-regulated while genes involved in cell wall formation

and nucleotide biosynthesis genes are repressed. Furthermore, they found genes associated with virulence, such as exotoxins, hemolysins, and surface adhesion proteins to be greatly induced by HOCl (Chang *et al.*, 2007). This result suggested that HOCl might trigger bacteria to “prepare themselves to fight” during active infection in host cells.

Glyceraldehyde-3-phosphate dehydrogenase (GAPDH) is particular susceptible to HOCl-mediated inactivation in human endothelial cells as well as in *E. coli* (Pullar *et al.*, 1999, Leichert *et al.*, 2008). HOCl treatment in endothelial cells also lead to ATP depletion and irreversible lost of glutathione (Pullar *et al.*, 1999). At chronic inflammation sites, myeloperoxidase activity and the HOCl specific biomarker, 3-chlorotyrosine, are commonly detected. Further analysis showed that the apoptosis-like cell death is induced by HOCl in human mesenchymal progenitor cells (Whiteman *et al.*, 2007).

Redox regulated Hsp33 chaperone protects against HOCl stress

Oxidation of the sulfur containing amino acids cysteine and methionine is usually reversible *in vivo* (Storz and Imlay, 1999). Some organisms have utilized these reversible thiol modifications as an on-and-off switch to regulate a protein’s activity. One example is the bacterial heat shock protein Hsp33, whose chaperone function is redox-regulated. It is specifically activated upon HOCl-mediated oxidation, and prevents the consequences of protein unfolding and aggregation during HOCl stress condition (Kumsta and Jakob, 2009, Winter *et al.*, 2008, Winter *et al.*, 2005). The Hsp33 chaperone is highly conserved in vast

majority of bacteria and some pathogenic eukaryotes (Jakob *et al.*, 1999). Hsp33 chaperone functions as a specialized holdase that binds to unfolded or partially unfolded proteins and prevents them from aggregation (Winter *et al.*, 2008, Winter *et al.*, 2005).

Under non-stress conditions, Hsp33 is inactive. Upon exposure of Hsp33 to oxidative protein unfolding conditions (i.e. H_2O_2 and heat or HOCl), Hsp33's chaperone function is rapidly activated (Winter *et al.*, 2005). The protective role of Hsp33 becomes appearent when wild type bacteria and mutant strains lacking Hsp33 are challenged with HOCl treatment. Both *E. coli* and *Vibrio cholerae* mutants showed severe HOCl sensitivity and failed to survive in the presence of HOCl (Winter *et al.*, 2008, Wholey and Jakob, 2012).

HOCl detection and probes

Excess of HOCl contributes to the tissue damage at sites of chronic inflammations and is involved in the progression of various chronic diseases (Winterbourn and Kettle, 2000). Many studies have been conducted to elucidate the usefulness of fluorescent probes that specifically detect and sense the presence of HOCl *in vivo*. Several rhodamine-based HOCl specific probes have been developed and shown to successfully detect a concentration range of 0.5-150 uM HOCl *in vitro* and HOCl production in cultured live cells (Kenmoku *et al.*, 2007, Sun *et al.*, 2008, Zhang *et al.*, 2011, Zhou *et al.*, 2012). Other types of probes, such as sulfonaphthoaminophenyl fluorescein and ferrocene-based fluorescent probes, have also been shown to be highly selective towards HOCl,

are cell membrane permeable and hence useful for live cell imaging (Shepherd *et al.*, 2007, Chen *et al.*, 2010). Biocompatible nanoparticles coated with oxazine fluorophores provide another way to assess HOCl generation in phagocyte *in vivo* (Panizzi *et al.*, 2009). A HOCl-sensing probe using quantum-dot conjugated microbeads has recently been developed to measure absolute concentrations of endogenous HOCl produced in phagocytes upon stimulation with bacterial particles (Yang *et al.*, 2011).

The first HOCl probe used in whole organism was R19-S, a rhodamine fluorophore derivative-based probe, which shows high selectivity and sensitivity towards HOCl (Chen *et al.*, 2011). R19-S has a linear detection range between 0-12 μM HOCl, and is saturated above 20 μM. Given that it is able to detect the DuOx-dependent HOCl production in the fruit fly *Drosophila* intestine when stimulated with bacteria, R19-S has the potential to provide novel insights into the innate immunity at the mucosal barrier (Chen *et al.*, 2011).

A major drawback of these fluorescent probes is that the detection is intensity-based and not ratiometric. Slight variations in sample environment or probe uptake and distribution leads to different outcomes. Ratiometric fluorescent probes with two different wavelength measurements of emission intensities have recently developed (Lin *et al.*, 2009, Yuan *et al.*, 2012). The first ratiometric highly selective HOCl probe was designed based on a deoximation reaction, where an aldehyde group is oxidized by HOCl (Lin *et al.*, 2009). Although the probe is stable between pH 2.5-10.5, it is much more sensitive at pH 9, making it unsuitable for many biological samples. Intramolecular Foerster resonance

energy transfer (FRET) probes were then used to design a dual-emission ratiometric fluorescent probe that is specific to HOCl and can be used in the imaging of live cells (Yuan *et al.*, 2012). Upon exposure to HOCl, this probe changes its structure from rhodamine-thiosemicarbazide to rhodamine-oxadiazole, which significantly alters the emission wavelength peak. This probe has been successfully tested in macrophages and other live cells and allows a quantitative assessment of endogenous HOCl production, independent of sample variations and probe distributions, in immune systems and pro-inflammatory damaged tissues (Yuan *et al.*, 2012).

Specific monoclonal antibodies recognizing advanced oxidation products (AOPP) (Witko-Sarsat *et al.*, 1996) have been developed to detect the localization of HOCl-damaged proteins, which will reveal information about the mechanism of pathogenesis or provide therapeutic strategies for HOCl-related diseases in clinical evaluations (Liu *et al.*, 2011). Using *in vitro* serum albumin incubated with HOCl, AOPP were generated. These served as epitopes to develop antibodies, which successfully detected AOPP in rat tissues treated with HOCl as well as patient samples with chronic kidney diseases (Liu *et al.*, 2011). This result suggests the broad implication of this antibody in the research of HOCl-related chronic diseases. However, by using HOCl-modified serum albumin as immunogen, this antibody may not be useful for detect oxidized bacterial proteins in studies conducted to understand bacterial response in host defense.

Another antibody developed to detect the effects of HOCl stress in vivo was targeted at oxidatively modified low-density lipoprotein (LDL) (Malle *et al.*, 1995). This antibody recognize epitopes that appeared to be specific for HOCl-LDL and depends on the tertiary structure of the lipoprotein, as judged by a lack of cross-reactivity with HOCl-modified serum albumin and a loss of reactivity associated with denatured lipoprotein (Malle *et al.*, 1995, Malle *et al.*, 2000). This antibody might be a useful tool for the investigation of a possible role for HOCl-mediated damage to lipoproteins in atherosclerosis and other inflammatory diseases.

Conclusion and perspective

There is no doubt that the potent oxidant HOCl leads to significant oxidative damage of all kinds of macromolecules in cells and tissues. This activity can be beneficial when used as part of an antimicrobial killing mechanism in neutrophils during host defense, but is otherwise detrimental when misplaced as seen in the many non-infectious human chronic inflammatory diseases associated with HOCl toxicity. Exposure to excess levels of HOCl causes protein unfolding and aggregation, irreversible thiol oxidations, severe DNA fragmentation, depletion of GSH, and ultimately cell lysis and apoptosis. The identification and detection of HOCl-specific biomarkers using antibodies in HOCl-stressed cells provide a direct method to assess the role of this powerful oxidant in many biologically relevant conditions. Quantitative measurement of endogenous HOCl generation in real-time using ratiometric probes offers a new

way to monitor the onset of HOCl stress in physiological and pathological processes.

Although our knowledge about HOCl stress response is gradually increasing, there are still many questions that remain unsolved. For instance, little is known how bacteria defend themselves against HOCl stress. The goal of this thesis is to elucidate the specific bacterial strategies that allow bacteria to respond and survive in HOCl treatment. This thesis is aimed to answer some of these fundamental questions. Its outcome has the clear potential to form the basis for novel antimicrobial strategies, which will target the ability of bacteria to respond to HOCl-stress as early as during bacterial colonization.

CHAPTER II

Hsp33 confers bleach resistance by protecting elongation factor Tu against oxidative degradation in *Vibrio cholerae*[1]

ABSTRACT

The redox-regulated chaperone Hsp33 protects bacteria specifically against stress conditions that cause oxidative protein unfolding, such as treatment with bleach or exposure to peroxide at elevated temperatures. To gain insight into the mechanism by which expression of Hsp33 confers resistance to oxidative protein unfolding conditions, we made use of *V. cholerae* strain O395 lacking the Hsp33 gene *hslO*. We found that this strain, which is exquisitely bleach-sensitive, displays a temperature-sensitive (*ts*) phenotype during aerobic growth, implying that *V. cholerae* suffers from oxidative heat stress when cultivated at 43°C. We utilized this phenotype to select for *E. coli* genes that rescue the *ts* phenotype of *V. cholerae* Δ*hslO* when overexpressed. We discovered that expression of a single protein, the elongation factor EF-Tu, was

[1] This chapter has been published in: W.-Y. Wholey and U. Jakob (2012) Hsp33 confers bleach resistance by protecting elongation factor Tu against oxidative degradation in *Vibrio cholerae*. *Molecular Microbiology* **83**: 981-991.

sufficient to rescue both the *ts* and bleach-sensitive phenotypes of *V. cholerae* Δ*hslO*. *In vivo* studies revealed that *V. cholerae* EF-Tu is highly sensitive to oxidative protein degradation in the absence of Hsp33, indicating that EF-Tu is a vital chaperone substrate of Hsp33 in *V. cholerae*. These results suggest an "essential client protein" model for Hsp33's chaperone action in *Vibrio* in which stabilization of a single oxidative stress-sensitive protein is sufficient to enhance the oxidative stress resistance of the whole organism.

INTRODUCTION

The heat shock protein Hsp33 is a highly conserved, redox-regulated chaperone, which has been shown to specifically protect bacteria against a variety of different oxidative stress conditions that are accompanied by protein unfolding. These stress conditions include exposure to hypochlorous acid (HOCl), the active ingredient of household bleach and a known physiological antimicrobial, produced by cells of the innate immune response to kill invading microorganisms (Miller and Britigan, 1997). HOCl is a fast acting oxidant, which directly induces protein unfolding both *in vitro* and *in vivo* (Winter *et al.*, 2008). Other physiological oxidants, such as peroxide or nitric oxide, do not cause widespread protein unfolding in organisms and induce activation of Hsp33 only when combined with protein unfolding conditions, such as heat shock treatment (i.e., oxidative heat stress) (Winter *et al.*, 2005).

The reason why bacteria require Hsp33 particularly under oxidative protein unfolding conditions is likely due to the fact that enzymes involved in ATP-

generation fall victim to oxidative inactivation (Hyslop *et al.*, 1988) causing ATP-dependent chaperones, commonly used to protect against protein aggregation, to lose their *in vivo* function (Winter *et al.*, 2005). Hsp33, which functions as an ATP-independent chaperone and is activated by oxidative unfolding apparently compensates for this loss of ATP-dependent chaperone activity by protecting hundreds of different proteins against protein aggregation in *E. coli* (Ilbert *et al.*, 2007, Winter *et al.*, 2008). At this point, it is still unresolved whether the protective role of chaperones such as Hsp33 results from the general decrease in the pool of aggregated proteins, from the protection of a single essential protein whose stress sensitivity dictates the stress sensitivity of the organism, or from something in between.

To investigate how expression of the chaperone Hsp33 confers resistance to oxidative protein unfolding conditions in bacteria, we made use of *V. cholerae* strain O395 lacking the Hsp33 gene *hslO*. We found that this strain, which has been previously shown to be highly HOCl-stress sensitive, displays a temperature-sensitive phenotype under aerobic growth conditions, implying that cultivation of *V. cholerae* at 43°C causes oxidative protein unfolding. We utilized this phenotype to select for *E. coli*-specific system(s) that compensate for the deletion of *Vibrio hslO*. We discovered that expression of the *E. coli* elongation factor EF-Tu fully rescues the temperature-sensitive phenotype of *V. cholerae hslO* deletions and restores bleach resistance to wild-type levels. *In vivo* studies revealed that *V. cholerae* EF-Tu is rapidly degraded in the absence of Hsp33. Expression of *E. coli* EF-Tu compensates for the lack of Hsp33, suggesting that

the cytoprotective effect of the general chaperone Hsp33 in *Vibrio* comes from guarding a single stress-sensitive protein, EF-Tu, whose presence is essential for the survival of the organism.

RESULTS

V. cholerae Hsp33 null mutants reveal a temperature-sensitive (*ts*) phenotype

In vitro studies showed that the highly specialized bacterial chaperone Hsp33 contains a dual stress-sensing mechanism, which mediates activation of the chaperone function specifically under oxidative stress conditions that lead to protein unfolding (Ilbert et al., 2007, Winter et al., 2008). *In vivo* studies confirmed these results and showed that absence of the Hsp33 gene *hslO* significantly decreases *E. coli*'s resistance to HOCl stress or oxidative heat stress treatment but does not affect *E. coli*'s survival at high concentrations of peroxide or at elevated temperatures alone (Winter *et al.*, 2005). It thus came as a surprise when we tested the *hslO* deletion phenotype in *V. cholerae* O395 and found this strain to be severely temperature-sensitive (*ts*) for growth. As shown in Figure 2.1A and 2.1B, compared to wild-type cells, *V. cholerae ΔhslO* forms significantly smaller colonies on LB plates and fails to form any colonies on MacConkey plates after 24 h of incubation at 43°C. The temperature sensitivity of *hslO* null mutants in *Vibrio* and the finding that Hsp33 functions as an oxidative stress-regulated chaperone in *E. coli* suggested that heat treatment of *V. cholerae* either causes or exacerbates oxidative stress conditions that induce the

activation of Hsp33, which in turn enhances the survival of *V. cholerae* at high temperatures.

To investigate whether reactive oxygen species (ROS) indeed affect *Vibrio*'s survival at elevated temperatures, we compared the growth of *V. cholerae* wild type with that of the *hslO* deletion mutant in liquid media under both aerobic and anaerobic growth conditions (Figure 2.1C). When cultivated under aerobic conditions, we observed a slight growth disadvantage in *ΔhslO* strains at 37°C and a significant reduction in growth rate at 43°C when compared to the growth of wild type O395. This result was fully consistent with the *ts* phenotype of this mutant strain on plates. In contrast, however, when we cultivated the same strains under anaerobic conditions, the growth rates of wild type and *ΔhslO* mutants strains were not significantly different at either 37°C or 43°C (Figure 2.1C). These results suggest that at elevated temperatures *V. cholerae* suffers from oxidative heat stress, which requires activation of Hsp33's chaperone function for survival. Expression of *E. coli* Hsp33 in the *V. cholerae ΔhslO* deletion strain was able to fully complement the *ts* phenotype of this strain (Figure 2.1A and 2.1B), excluding significant differences in the activation requirements between the two Hsp33 homologues.

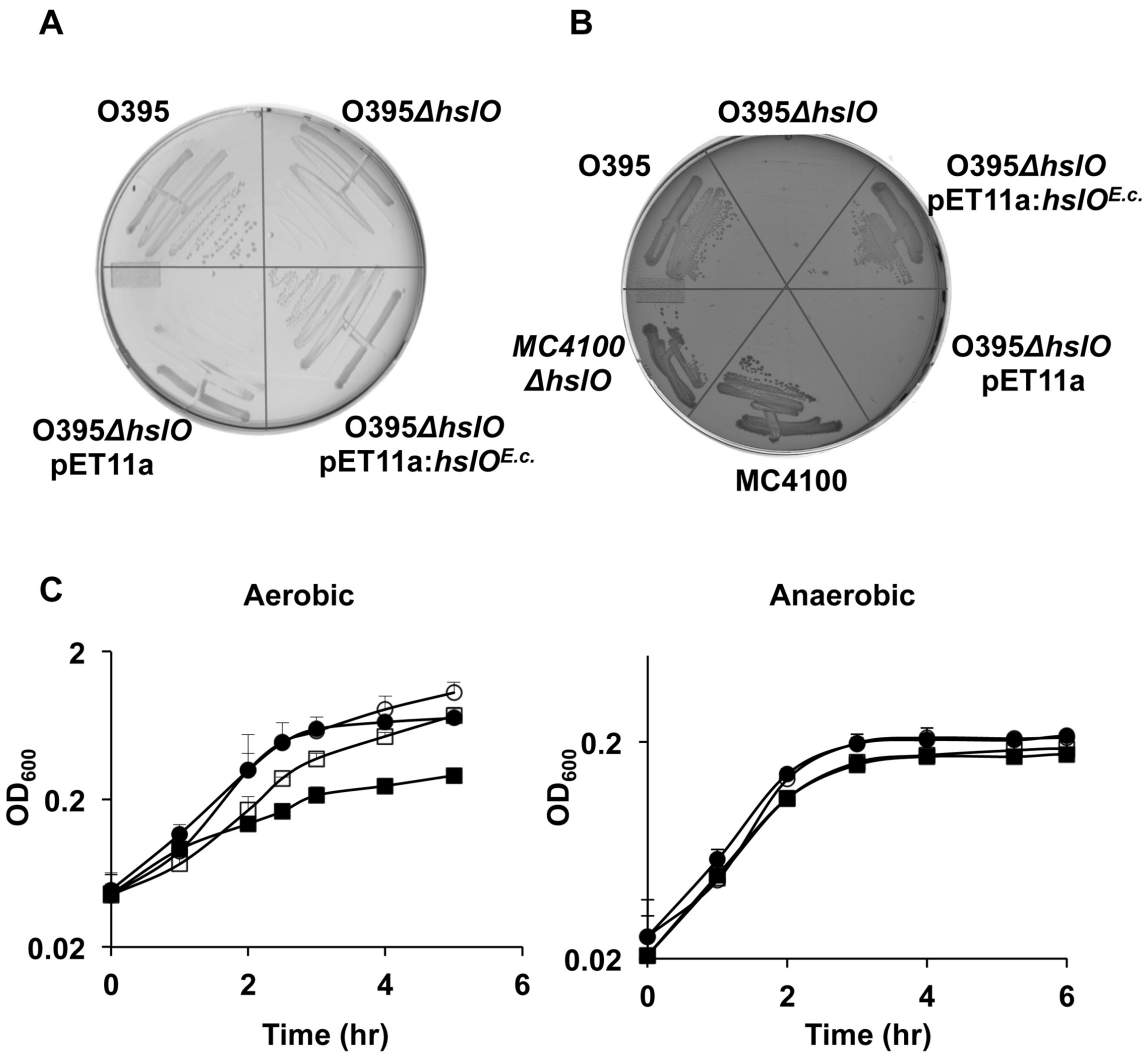

Figure 2.1. Aerobically grown *V. cholerae* Δ*hslO* strain has *ts* phenotype. (**A** and **B**). Wild-type *V. cholerae* O395, O395 Δ*hslO*, or O395 Δ*hslO* expressing either the empty pET11a plasmid or *E. coli* Hsp33 from a pET11a plasmid were grown on LB plates (**A**) or MacConkey plates (**B**) for 24 h at 43°C. Wild-type *E. coli* MC4100 and the corresponding MC4100 Δ*hslO* mutant strain are shown as controls. **(C**). *V. cholerae* O395 (circles) or O395 Δ*hslO* (squares) were cultivated in LB growth medium at either 37°C (open symbols) or 43°C (filled symbols) in the presence (left panel) or absence (right panel) of air oxygen. Bacterial growth was monitored by optical density measurements at 600 nm.

Identification of *E. coli* genes that rescue the *ts* phenotype of *O395 ΔhslO*

We reasoned that the severe *ts* phenotype of the O395 *ΔhslO* mutant strain on MacConkey plates might serve as an *in vivo* selection system to identify *E. coli* proteins that, when overexpressed in *V. cholerae*, protect against oxidative heat stress and, by extension, against HOCl-mediated protein damage. The complementing *E. coli* gene could encode Hsp33 itself or proteins that function in a way analogous to Hsp33 in parallel pathways. Alternatively, rescuing genes could encode *E. coli* homologues for important *Vibrio* Hsp33 substrates, which are either Hsp33-independent in *E. coli* or become Hsp33-independent in *Vibrio* simply by increasing their steady state concentrations.

Since we were searching for proteins that are potent in rescuing *hslO* null mutants at relatively low levels of expression, we constructed genomic expression libraries from wild type *E. coli* MG1655 using either pBR322 (15-20 copies per cell) or pET11a plasmids as expression vectors. We had previously observed that pET11a mediated expression of *E. coli* Hsp33 in *hslO* null strains lacking the T7 DNA polymerase provides sufficient Hsp33 levels to allow complementation (Figure 2.1A and 1.1B). We transformed the genomic library into the O395*ΔhslO* mutant strain and selected for transformants showing robust growth on MacConkey plates after 24 h incubation at 43°C. All six investigated transformants encoded the *E. coli hslO* gene. To avoid repeated cloning and identification of the *hslO* gene, we next constructed a genomic library using chromosomal DNA of the MG1655 *ΔhslO* deletion mutant WC126, and performed the same selection procedure.

We found two independent clones, clone 5 from the pBR322 library and clone 12 from the pET11a library, which conferred a high degree of complementation (Figure 2.2A). Cultivation of *V. cholerae ΔhslO* strain mutants expressing either clone 5 or 12 on MacConkey plates at 43°C yielded colonies that were similar in size to colonies formed by *V. cholerae* wild-type or by *V. cholerae ΔhslO* strains expressing *E. coli* Hsp33 from either pBR322 or pET11a plasmid (Figure 2.2A). In contrast, a *V. cholerae ΔhslO* mutant strain expressing the empty vector failed to form colonies under these conditions. As mentioned previously, Hsp33 protects bacteria against oxidative protein unfolding conditions induced by either high concentrations of peroxide at elevated temperatures (Winter *et al.*, 2005) or by low concentrations of HOCl (Winter *et al*., 2008).

To test whether expression of either one of the two identified *E. coli* clones rescues the HOCl-sensitive phenotype of the O395 *ΔhslO* mutant as well, we exposed O395 wild-type, O395 *ΔhslO*, or the O395 *ΔhslO* mutant strains expressing either clone 5 or clone 12 to a 10 μM HOCl treatment for 20 min and tested their survival (Figure 2.2B). Consistent with earlier studies (Winter *et al*., 2008), O395 *ΔhslO* was significantly more sensitive to HOCl treatment than wild type. Importantly, O395 *ΔhslO* mutant strains expressing either clone 5 or 12 were resistant to HOCl treatment. These results indicate that the gene(s) encoded on these plasmids are capable of protecting O395 *ΔhslO* against a variety of different stress conditions that cause oxidative protein unfolding.

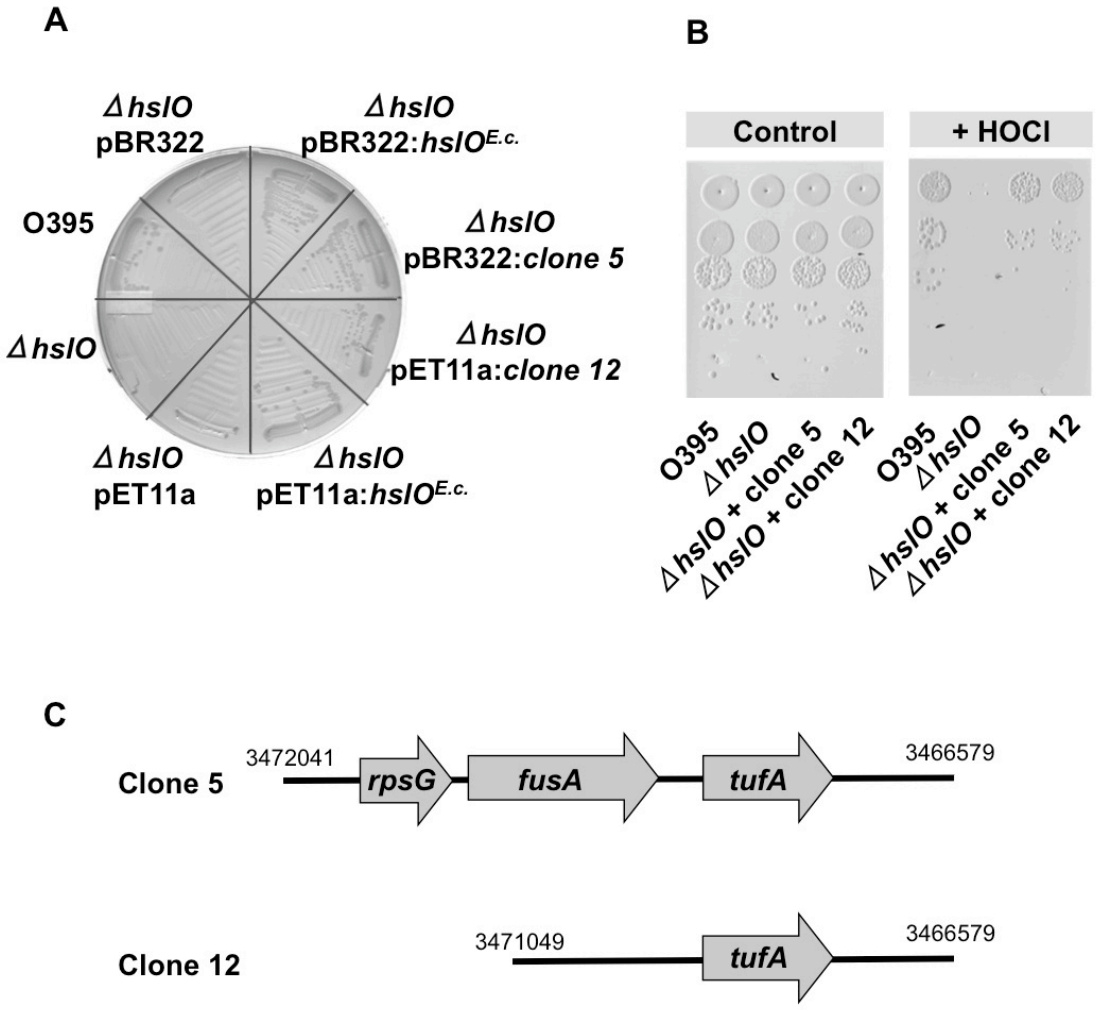

Figure 2.2. *E. coli* expression library contains clones that rescue *ts* and HOCl-sensitive phenotypes of O395 *ΔhslO* mutant.
(**A**) *E. coli* gene expression library from MG1655 *ΔhslO* mutant strain was constructed in either pET11A or pBR322 plasmids and transformed into the *V. cholerae* O395 *ΔhslO* mutant strain. Transformants were cultivated on MacConkey plates for 24 h at 43°C. Two independently identified transformants, clone 5 from the pBR322 library and clone 12 from the pET11a library, were selected for further analysis. Growth of these two strains was tested on MacConkey plates for 24 h at 43°C and compared to O395 wild type, O395 *ΔhslO*, and O395 *ΔhslO* expressing the respective empty plasmids. (**B**) To test the bleach sensitivity of these strains, wild type O395, O395 *ΔhslO*, or O395 *ΔhslO* expressing either clone 5 or clone 12 were cultivated in LB medium until mid-log phase was reached. Cells were washed, resuspended in phosphate buffer, and treated with 10 μM HOCl for 20 min. Cell viability was analyzed by preparing serial dilutions of the cultures and spotting them onto LB plates. (**C**) Schematic presentation of *E. coli* genomic sequences with indicated chromosomal positions that were inserted into clone 5 or clone 12.

E. coli EF-Tu expression rescues the *ts* phenotype of *V. cholerae ΔhslO*

To investigate which *E. coli* genes are responsible for rescuing the temperature- and HOCl-sensitive phenotype of the *V. cholerae* O395 *ΔhslO* mutant, we sequenced the inserts in clones 5 and 12. While the pBR322:clone 5 contained a sequence spanning three separate genes (*rpsG*, *fusA,* and *tufA*), the pET11a:clone 12 contained only one complete gene (*tufA*) that encodes elongation factor Tu (EF-Tu) (Figure 2.2C). Phenotypically analysis of O395 *ΔhslO* expressing subclones of pBR322:clone 5 with either *rpsG* or *rpsG* / *fusA* deleted verified that the presence of the *E. coli tufA* gene, including its upstream regions, is sufficient to rescue the *ts* phenotype of the O395 *ΔhslO* mutant strain.

Erase-A-Base (Promega) was used to identify the minimal sequence sufficient to complement the *ts* phenotype of O395 *ΔhslO*. The shortest sequence capable of rescuing the *ts* phenotype contained 405 bases upstream of the *tufA* gene as well as the complete *tufA* gene. This result is in excellent agreement with previous studies showing that the promoter region of *tufA* is about 400 bases upstream of the start codon (Zengel and Lindahl, 1990). We concluded from these studies that expression of a single protein, *E. coli* EF-Tu, is necessary and sufficient to rescue the *ts* phenotype and, by extension, the HOCl-sensitive phenotype of a *V. cholerae* mutant strain lacking Hsp33. We noted that *E. coli* EF-Tu was not massively overexpressed; rather, its expression levels were comparable to the endogenous level of EF-Tu in wild-type *V. cholerae* (see below).

Hsp33 is essential for maintaining high levels of soluble EF-Tu in *V. cholerae*

The elongation factor EF-Tu is one of the most abundant proteins in the bacterial cytosol and is essential for cell growth (Pedersen *et al.*, 1978). To begin to understand how overexpression of *E. coli* EF-Tu can rescue the temperature-sensitive growth defect of the O395 *ΔhslO* mutant strain on plates and in cultures, we compared the levels of endogenous EF-Tu in *V. cholerae* and O395 *ΔhslO* mutant strains under both non-stress and heat shock conditions in the absence of additional *E. coli* EF-Tu. We found that lack of Hsp33 did not cause a noticeable change in the steady state concentration of endogenous *Vibrio* EF-Tu at 30°C, but led to a reproducible decrease in EF-Tu levels at 37°C and a very substantial decrease at 43°C when compared to EF-Tu levels in either wild type or the O395 *ΔhslO* mutant expressing *E. coli* Hsp33 from a plasmid (Figure 2.3).

When we cultivated the strains anaerobically, however, no difference in the steady state levels of EF-Tu was detected at any temperature (Figure 2.3). This result is entirely consistent with the lack in phenotype of *hslO* null mutants in *Vibrio* under anaerobic growth conditions (Figure 2.1C) and serves to show that elevated temperatures alone do not affect EF-Tu levels in *V. cholerae*. These results suggest that under aerobic heat shock conditions, presence of the redox-regulated chaperone Hsp33 is necessary to maintain EF-Tu at cellular levels that are sufficient for cell growth. Note that we saw no differences in the steady state levels of EF-Tu in *E. coli* wild-type vs. *E. coli ΔhslO* strains at 43°C, which is

consistent with the fact that the *E. coli ΔhslO* deletion strains are not temperature-sensitive for growth (Winter *et al*., 2005).

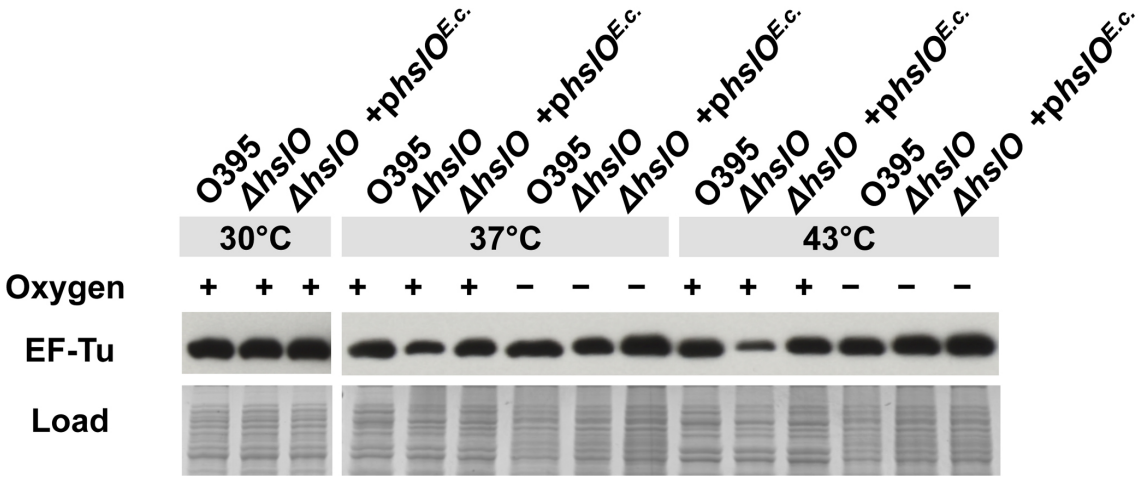

Figure 2.3. Hsp33 protects *V. cholerae* EF-Tu against protein degradation. Wild-type O395, O395 *ΔhslO* mutant, or O395 *ΔhslO* mutant encoding *E. coli hslO* on a pBR322 plasmid (*ΔhslO* + p*hslO*$^{E.c.}$) were cultivated in LB medium at the indicated temperature in the presence and absence of air oxygen. Cells were harvested at mid-log growth and lysed. Steady state levels of EF-Tu were visualized using Western blot analysis with polyclonal antibodies against *E. coli* EF-Tu.

Absence of Hsp33 leads to accelerated degradation of EF-Tu

Changes in the steady state levels of a protein are either the result of decreased rates of transcription and translation and/or are caused by increased rates of proteolysis. To assess the mRNA levels of *tufA* in *V. cholerae* and *V. cholerae ΔhslO* strains, we performed RT-PCR under aerobic conditions at three different temperatures: 30°C, 37°C, and 43°C. No significant difference in *tufA* transcript levels was observed (Figure 2.4), arguing against the possibility that Hsp33 either directly or indirectly affects the expression of *tufA*. Our results strongly suggested that Hsp33 acts at the post-transcriptional level, presumably by protecting EF-Tu against premature degradation.

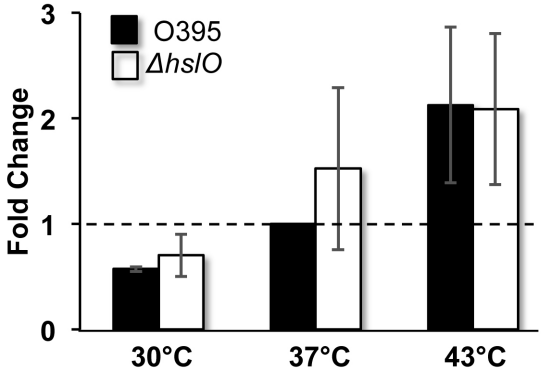

Figure 2.4. RT-PCR analysis of *tufA* transcript level. *V. cholerae* O395 wild type and O395 *ΔhslO* mutant were cultivated in LB medium at the indicated temperatures until OD_{600}=0.45 was reached. Total RNA was isolated and RT-PCR experiments were performed to determine the mRNA levels of EF-Tu (encoded by *tufA* and *tufB*). rRNA levels of the ribosomal gene *rrsD* were used as an internal standard. The mRNA levels of EF-Tu are expressed relative to the mRNA levels present in wild-type O395 at 37°C. The error bars represent the standard deviation of four independent experiments.

To determine the proteolytic stability of endogenous EF-Tu in the presence and absence of Hsp33, we conducted pulse-chase experiments combined with 2D gel electrophoresis. We performed these experiments at non-stress temperatures to exclude that major differences in the growth rates of *V. cholerae* wild-type and *ΔhslO* deletion strains affect our data analysis. We reproducibly identified the same 300 protein spots on 2D gels and autoradiographs and used them as reference spots for our analysis (see Figure 2.5 *Experimental procedures* for details). Analysis of the Coommassie stained 2D gels confirmed our previous observations and showed a 26% reduction in EF-Tu steady state levels in the O395 *ΔhslO* mutant strain as compared to wild-type O395 at non-stress temperatures (Figure 2.6A, left panel). Westernblot analysis failed to detect any fragments of EF-Tu. When we compared the ratio of EF-Tu steady state levels in O395 wild type and the corresponding *ΔhslO* deletion mutant to the 40 most abundant protein spots (Figure 2.7A), we found the ratio of EF-Tu to be significantly below the mean (Figures 2.6A, right panel), suggesting that Hsp33 affects EF-Tu-levels rather specifically.

Analysis of the autoradiographs revealed that EF-Tu translation was not significantly different in wild-type and mutant cells, confirming that Hsp33 has no effect on transcription or translation of EF-Tu (Figure 2.6B and Figure 2.7B). In contrast, we found that the rate of EF-Tu degradation in wild-type and *ΔhslO* mutant strains was dramatically different. We detected almost 50% of the original ^{35}S-label after 4 h of pulse in EF-Tu isolated from wild-type cells, whereas only 20% of the original label was detected in EF-Tu isolated from cells lacking

Hsp33. These results indicate that EF-Tu was degraded 2.5-fold faster in the *hslO* deletion strain than in wild-type cells (Figure 2.6C and Figure 2.7C). Compared to the 40 most abundant protein spots on the 2D gel, EF-Tu showed again the largest difference in degradation rates between wild type and the *hslO* deletion mutant (Figure 2.6C, right panel, and Figure 2.7C). These results strongly suggest that EF-Tu is a key Hsp33 client protein, a conclusion, which is consistent with global protein-protein interaction studies in *E. coli* that showed that Hsp33 is an interaction partner of EF-Tu (Butland *et al.*, 2005).

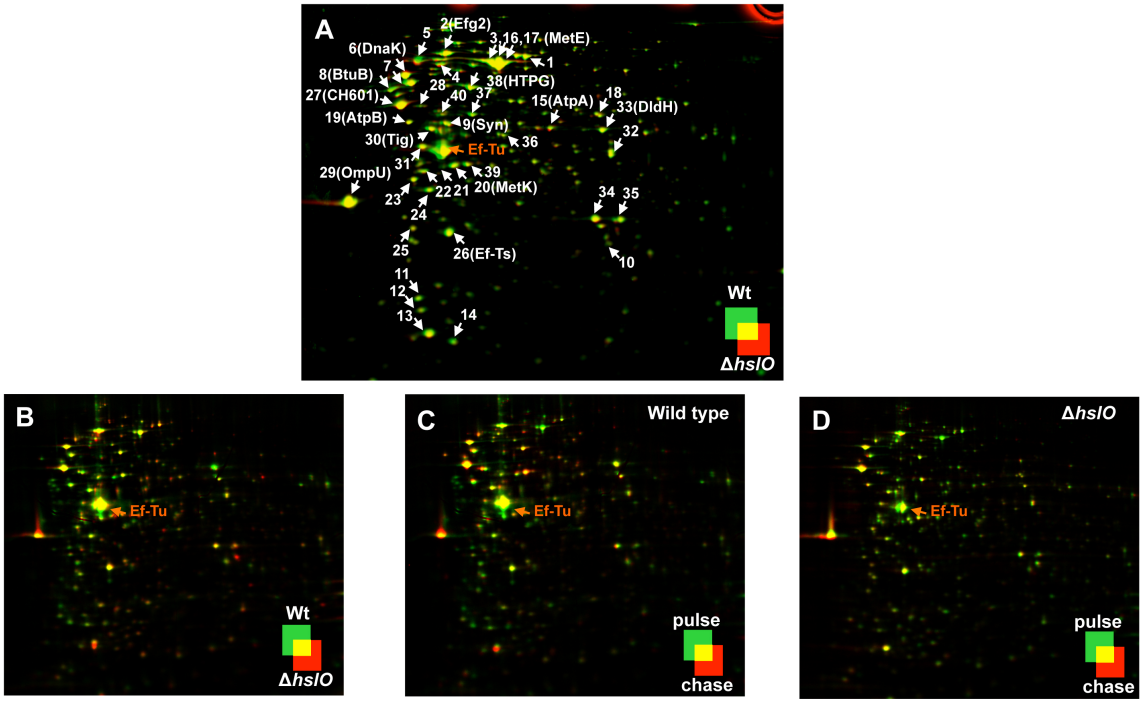

Figure 2.5. Analysis of the *V. cholerae* proteome by pulse chase labeling and 2D gels. (**A**) Comparison of steady state protein levels and (**B**) newly translated proteins in *V. cholerae* O395 wt and *ΔhslO* mutant. Representative false-colored overlays of either Coommassie-stained 2D-gels in **A** or autoradiographs after 2 min pulse with ^{35}S-Met in **B** of wt (green) and *ΔhslO* mutant (red) are shown. Arrows indicate the positions of the 40 most abundant protein spots, which were used for data analysis**.** (**C**) Extent of protein degradation within a 4 h chase in wt or (**D**) *ΔhslO* mutant. Representative false-colored overlays of autoradiographs after 2 min pulse (green) and 4h chase (red) are shown.

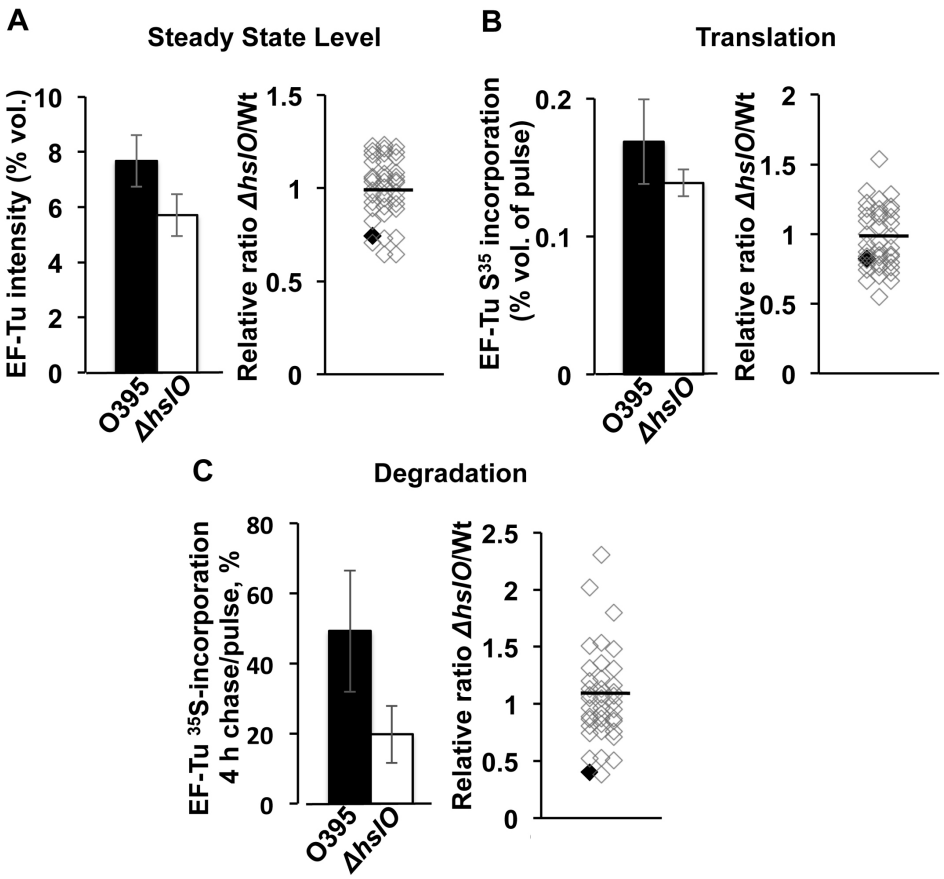

Figure 2.6. EF-Tu is degraded in the *V. cholera ΔhslO* mutant strains. *V. cholerae* wild-type and *V. cholerae ΔhslO* mutant strains were cultivated in minimum MOPS medium supplemented with all amino acids except methionine and cysteine. Cells were pulsed for 2 min with radioactive ^{35}S-methionine, flushed with cold unlabeled methionine, and chased for 4 h. The cell lysates were prepared and proteins were separated by 2D PAGE and scanned for ^{35}S incorporation. The error bars represent standard errors from 4 individual experiments. (**A**) Left Panel: To compare the steady state EF-Tu levels in *V. cholerae* wild type (black bar) and *ΔhslO* mutant (white bar), the relative spot intensity of EF-Tu on Coommassie-stained 2D gels was determined for both strain backgrounds. Right Panel: The relative spot intensity of the 40 most abundant protein spots (see Figure 2.7) was determined in both *ΔhslO* and wild type *V. cholerae* and compared. Individual proteins are represented by open diamonds. EF-Tu is indicated as black diamond. (**B**) Left Panel: To compare the ^{35}S incorporation into EF-Tu from *V. cholerae* wild type and *ΔhslO* mutant, the relative spot intensity of EF-Tu on the respective autoradiographs was determined. Right Panel: The relative ratio of ^{35}S-incorporation into the 40 most abundant protein spots in *ΔhslO* and wild type *V. cholerae* was determined. Individual proteins are represented by open diamonds. EF-Tu is indicated with a black diamond. (**C**) Left Panel: To determine the rates of protein degradation, ^{35}S incorporation after 4 h of chase relative to ^{35}S incorporation after 2 min pulse was calculated for EF-Tu in *V. cholerae* wild type and *ΔhslO* mutant. Right Panel:

Protein degradation rates were determined for the 40 most abundant protein spots in both *ΔhslO* and wild type *V. cholerae* and compared. Individual proteins are represented by open diamonds. EF-Tu is indicated with a black diamond.

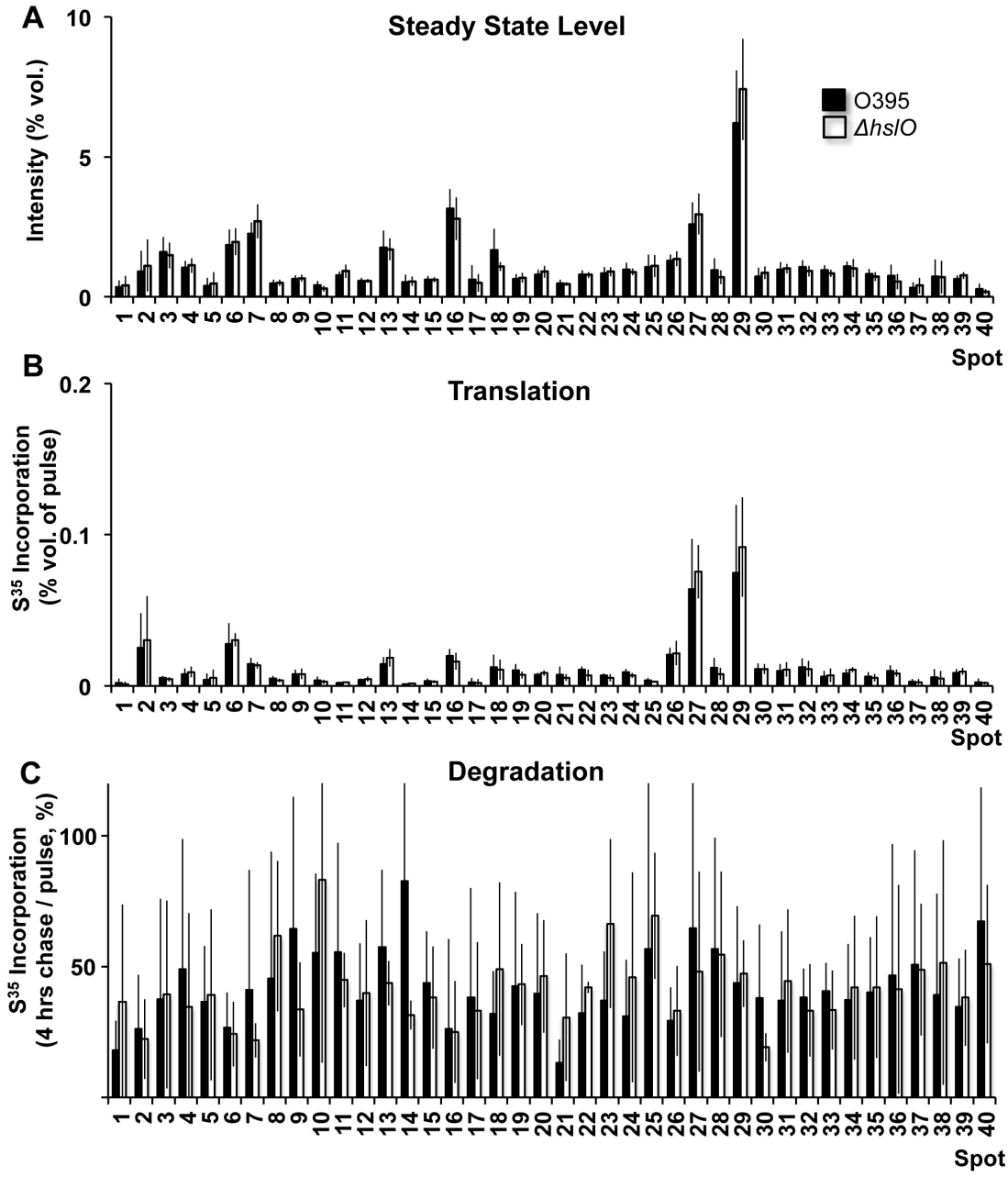

Figure 2.7. Analysis of the 40 most abundant proteins in *V. cholerae* by pulse chase labeling (**A**) Analysis of steady state levels, (**B)** translation levels, and (**C**) percentage degradation of 40 most abundant proteins in *V. cholera* O395 wild type (black bars) and O395 Δ*hslO* mutant (white bars). The error bars represent the standard deviation of four idependent experiments. The corresponding data for EF-Tu can be found in Figure 2.6.

V. cholerae EF-Tu is exquisitely sensitive to oxidative stress treatment

Our studies demonstrated that during aerobic growth of *V. cholerae*, presence of Hsp33 is required to maintain the stability of the EF-Tu protein. The fact that plasmid-driven expression of *E. coli* EF-Tu is sufficient to complement the *ts* phenotype of the O395 *ΔhslO* mutant furthermore suggested that *V. cholerae* EF-Tu might exhibit higher oxidative stress sensitivity than *E. coli* EF-Tu. It has been previously shown that *E. coli* EF-Tu, although apparently insensitive to peroxide-mediated thiol modifications, quickly responds to HOCl stress treatment with the reversible modification of at least one of its three cysteine residues (Leichert *et al.*, 2008). To compare the *in vivo* redox status of *E. coli* and *V. cholerae* EF-Tu before and after HOCl treatment, we performed differential thiol-trapping experiments using MC4100 and O395 strains. Both strains were cultivated in LB medium at 37°C to mid-log phase. Cell aliquots were removed before and 20 min after HOCl treatment, and lysed in the presence of 10% TCA to prevent any further thiol oxidation (Zander *et al.*, 1998). All reduced cysteine thiols were irreversibly alkylated with N-ethylmaleimide (NEM), whereas all reversibly oxidized cysteines were reduced with DTT and subsequently labeled with the 500 Da thiol-specific alkylation reagent 4-acetamido-4'-maleimidylstilbene-2,2'-disulfonic acid (AMS). The latter labeling step introduces a 500 Da molecular mass to every cysteine residue that was originally oxidized *in vivo*. This mass addition significantly slows the migration of AMS-labeled proteins and allows direct visualization of the *in vivo* redox status of proteins on one-dimensional SDS-PAGE.

We observed a striking difference in the *in vivo* redox status of *V. cholerae* and *E. coli* EF-Tu, particularly in exponentially growing bacteria. While *E. coli* EF-Tu was almost completely reduced during logarithmic growth, the majority of *V. cholerae* EF-Tu was already partially oxidized (Figure 2.8, compare lanes 5 and 7). Treatment of *V. cholerae* with sublethal concentrations of HOCl shifted almost all of the endogenous EF-Tu into the fully oxidized species. Comparative analysis of NEM-trapped samples on reducing and non-reducing gels suggested the formation of both inter- and intramolecular disulfide bonds in HOCl-treated *V. cholerae* EF-Tu (Figure 2.9). In contrast, the same treatment of *E. coli* cells led only to a partial oxidation of *E. coli* EF-Tu and no visible intermolecular disulfide bond formation (Figure 2.8 and Figure 2.9). These results suggest that *V. cholerae* EF-Tu is highly susceptible to oxidation and appears to be exposed to substantial levels of reactive oxygen species during aerobic exponential growth even at non-stress temperatures.

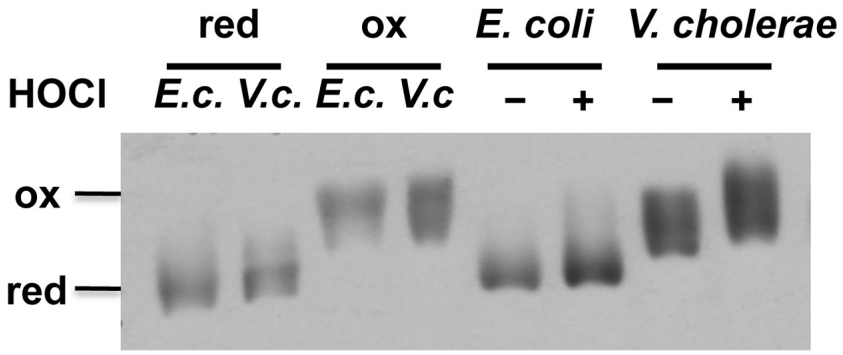

Figure 2.8. *V. cholerae* EF-Tu is exquisitely sensitive to oxidative thiol modifications.
To determine the redox status of EF-Tu *in vivo*, *E. coli* MC4100 and *V. cholerae* O395 were grown in LB medium at 37°C under aerobic conditions until mid-log phase was reached. Cells were either left untreated or were treated with 3 mM HOCl for 20 min. Samples were taken and cysteines were labeled with NEM, followed by the reduction of all oxidized thiols and the labeling of all newly reduced cysteines with the 500 Da thiol-alkylating molecule AMS. Addition of AMS molecules is visualized as migration difference on SDS-PAGE, whose extent directly reflects the number of *in vivo* oxidized cysteines. To define the migration behavior of fully NEM-labeled EF-Tu (equivalent to reduced species) and fully AMS labeled EF-Tu (equivalent to completely oxidized species), aliquots of non-stressed MC4100 or O395 cells (indicated by *E.c*. and *V.c*., respectively) were reduced with DTT and labeled exclusively with either NEM (lanes 1 and 2) or AMS (lanes 3 and 4). Proteins were separated on SDS-PAGE and EF-Tu was visualized with Western blot analysis using antibodies against *E. coli* EF-Tu.

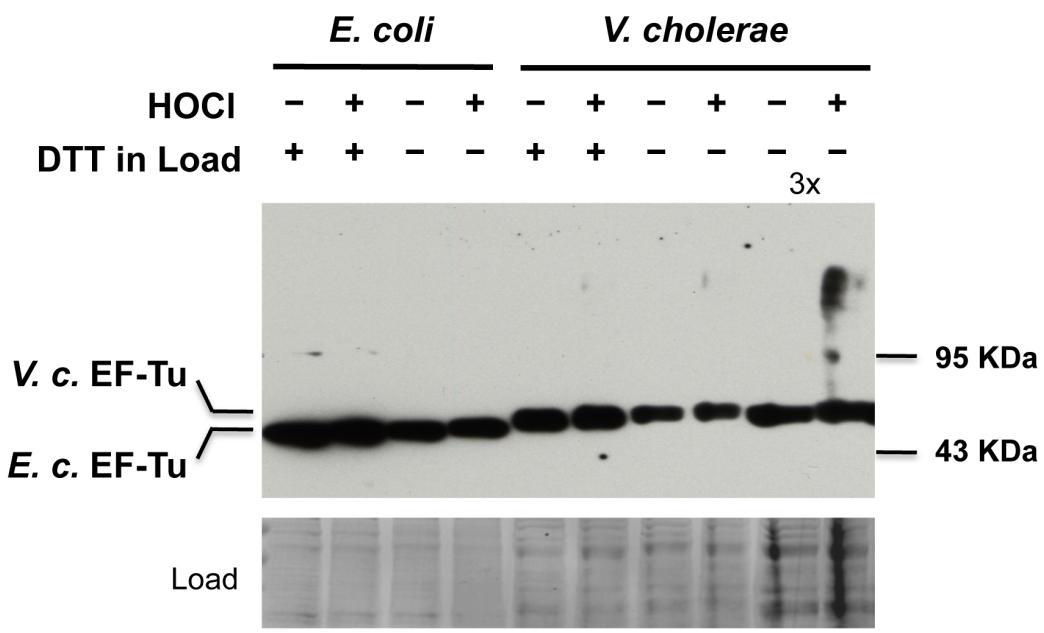

Figure 2.9. *V. cholerae* EF-Tu forms oligomers. Monitoring disulfide bond formation in EF-Tu. *E. coli* MC4100 and *V. cholerae* O395 were grown in LB medium at 37°C under aerobic conditions until mid-log phase was reached. Cells were treated with 3 mM HOCl for 20 min. Samples were taken and cysteines were labeled with NEM while all oxidized cysteines were left untreated. Protein samples were then split into two aliquots and resuspended in either reducing or non-reducing loading buffer prior to SDS-PAGE analysis. To enhance transfer efficiency of higher molecular weight EF-Tu complexes, proteins were reduced in gel immediately before the westernblot using β-mercaptoethanol. Without in-gel reduction, no higher molecular weight complexes were detected and only very faint bands were visible in the *V. cholerae* samples prepared under non-reducing conditions. These results suggest that *V. cholerae* EF-Tu forms reversible inter- and intramolecular disufide bonds.

Expression of *E. coli* EF-Tu affects *V. cholerae* EF-Tu levels *in vivo*

Our results suggested that *V. cholerae* EF-Tu is a highly oxidative stress-sensitive protein whose loss in steady state levels in the absence of Hsp33 is compensated by expressing the potentially more oxidative stress-resistant *E. coli* EF-Tu homologue. Amino acid sequence comparison between *E. coli* and *V. cholerae* EF-Tu revealed that in addition to the three cysteine residues that are present in the two EF-Tu homologues, *V. cholerae* EF-Tu encodes one additional cysteine residue that is located at position 33 (Cys33) (Figure 2.10). To elucidate whether this cysteine is responsible for the increased oxidative stress sensitivity of *V. cholerae* EF-Tu, we generated a variant of *E. coli* EF-Tu that carries an additional cysteine residue at this position. For these experiments we used *E. coli* EF-Tu since we were unable to express detectable levels of *V. cholerae* EF-Tu from plasmid constructs in either *V. cholerae* or *E. coli* despite the use of various expression vectors. We expressed the *E. coli* EF-Tu^{T33C} variant in the *Vibrio* O395 *ΔhslO* mutant strain to test its ability to rescue its *ts* phenotype. We expected that any increase in oxidative stress sensitivity or overall decrease in EF-Tu stability caused by introducing the T33C mutation into *E. coli* EF-Tu should lead to lower steady state levels of EF-Tu and thus to a lower capacity of this mutant protein to rescue the *ts* or bleach-sensitive phenotype of the *V. cholerae* O395 *ΔhslO* mutant. As shown in Figure 2.11A, the O395 *ΔhslO* mutant expressing *E. coli* EF-Tu^{T33C} formed slightly smaller colonies on MacConkey plates at 43°C than O395 wild-type or O395 *ΔhslO* mutant strains expressing wild-type *E. coli* EF-Tu from the same plasmid.

Moreover, monitoring the aerobic growth of these strains in LB medium at 43°C revealed that expression of the *E. coli* EF-Tu^{T33C} variant was only partially able to rescue the growth defect of O395 *ΔhslO* (Figure 2.11B). We then decided to analyze the levels of soluble *E. coli* EF-Tu and *E. coli* EF-Tu^{T33C} variant upon plasmid-mediated expression in O395 *ΔhslO* at 43°C, which was made possible by the fact that *V. cholerae* EF-Tu and *E. coli* EF-Tu differ significantly in their migration behavior on SDS-PAGE and hence can be distinguished even when co-expressed (Figure 2.11C). We did not find any significant difference in the cellular levels of the two *E. coli* EF-Tu variants, suggesting that the simple presence of additional EF-Tu might not be sufficient to rescue the *ts* phenotype of O395 *ΔhslO* (Figure 2.11C). What we did notice, however, was a significant difference in the levels of endogenous *Vibrio* EF-Tu. Whereas expression of wild type *E. coli* EF-Tu in O395 *ΔhslO* mutant strains raised the endogenous EF-Tu levels to those observed in wild-type O395 at both 37°C and 43°C, expression of the *E. coli* EF-Tu^{T33C} variant did not affect the endogenous levels of *V. cholerae* EF-Tu (Figure 2.11C).

These results suggested that wild-type *E. coli* EF-Tu but not *E. coli* EF-Tu^{T33C} confers stability to *Vibrio* EF-Tu, thus increasing its steady state levels and potentially contributing to the enhanced stress survival observed in these bacteria. We obtained very similar results when we analyzed the steady state levels of *V. cholerae* EF-Tu in response to bleach treatment at 37°C. While expression of either Hsp33 or *E. coli* EF-Tu significantly stabilized the levels of endogenous EF-Tu in the presence of HOCl, absence of Hsp33 or presence of

the *E. coli* EF-Tu^{T33C} mutant led to substantially increased bleach-mediated degradation of endogenous EF-Tu. These results thus suggest that expression of *E. coli* EF-Tu functionally replaces Hsp33 at least in part by protecting *V. cholerae* EF-Tu against oxidative protein degradation. Furthermore, our study demonstrates that the oxidative stress sensitivity of the single bacterial protein EF-Tu is sufficient to determine the cellular survival of *V. cholerae* at elevated temperatures and in the presence of the physiological antimicrobial bleach.

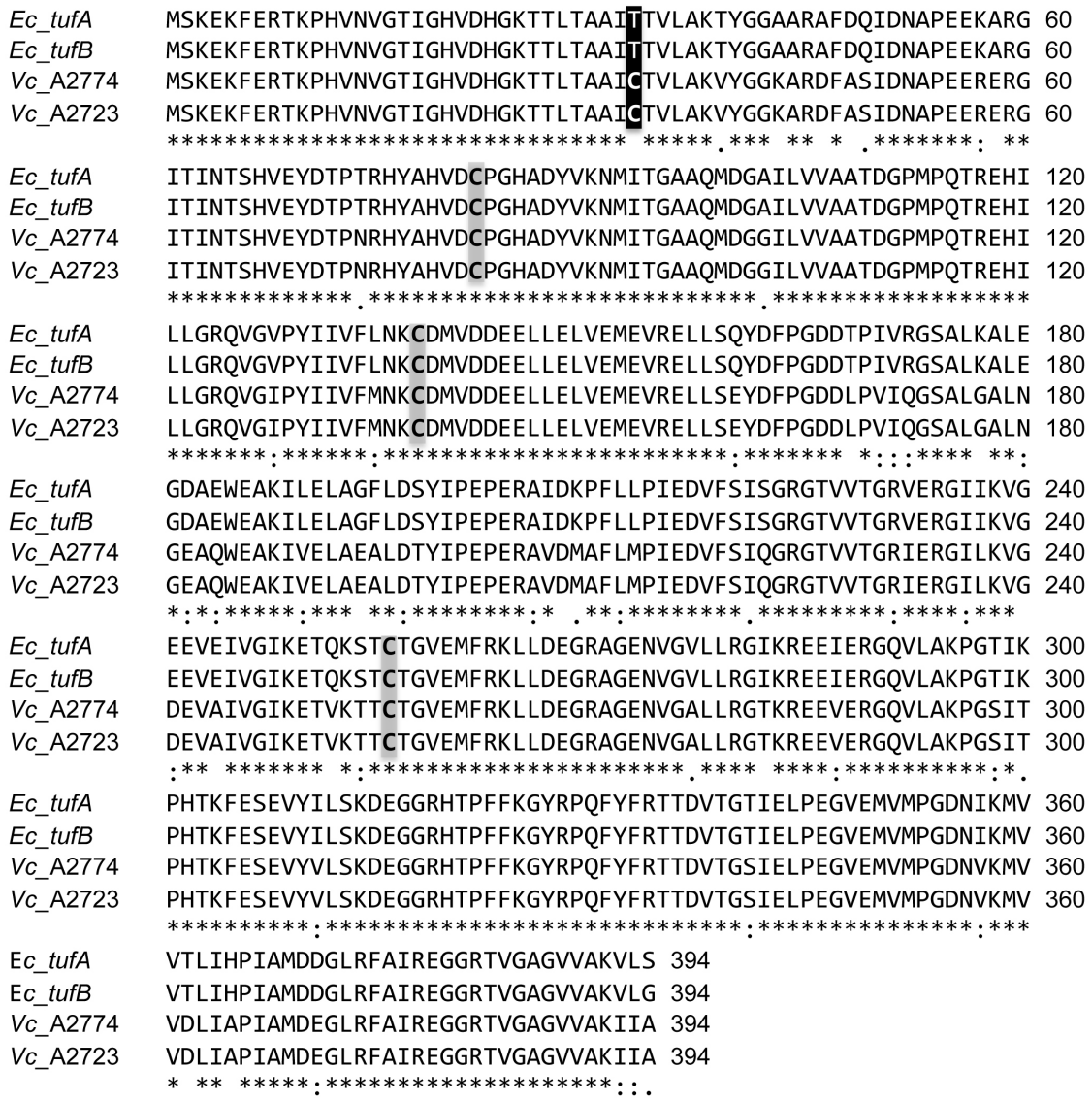

Figure 2.10. EF-Tu sequence aligment. Sequence comparison between *E. coli* EF-Tu (encoded by *tufA* and *tufB* genes) and *V. cholerae* EF-Tu (encoded by A2774 and A2723 genes). Cysteine residues are highlighted.

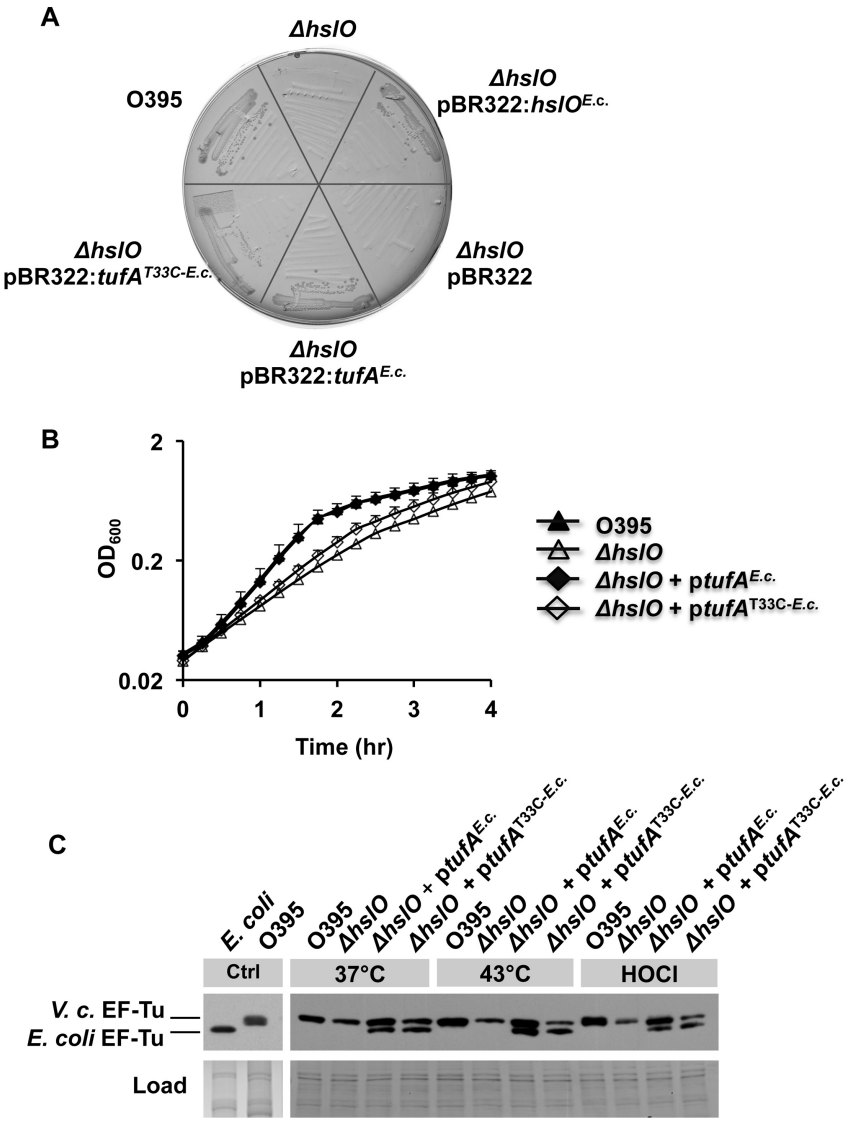

Figure 2.11. *E. coli* EF-Tu compensates for lack of Hsp33 by protecting *V. cholerae* EF-Tu against oxidative protein degradation. (**A**) *V. cholerae* O395 wild type, O395 *ΔhslO* mutant, or O395 *ΔhslO* expressing the empty pBR322 vector, *E. coli* Hsp33, *E. coli* EF-Tu, or the *E. coli* EF-Tu^{T33C} variant were cultivated on MacConkey plates for 24 h at 43°C. (**B**) *V.* O395 wild type (black triangles), O395 *ΔhslO* mutant (white triangles), and O395 *ΔhslO* expressing either *E. coli* EF-Tu (black diamonds) or the *E. coli* EF-Tu^{T33C} variant (white diamonds) were cultivated in LB medium at 43°C aerobically. Bacterial growth was monitored by optical density at 600 nm. (**C**) To analyze the steady state levels of EF-Tu in these bacterial strains, the different strains were cultivated in LB medium at either 37°C or 43°C until mid-log phase was reached. To evaluate the effects of HOCl on cellular EF-Tu levels, the 37°C cultures were split and either left untreated or incubated with 3 mM HOCl for 20 min. Cell aliquots were taken and the proteins were separated by SDS-PAGE. EF-Tu was visualized by Western blot using antibodies against *E. coli* EF-Tu.

DISCUSSION

Hsp33 is a highly specialized chaperone, which appears to be selectively activated by protein unfolding conditions in the presence of elevated ROS levels, such as experienced by organisms during hypochlorous acid stress or oxidative heat stress (Winter *et al.*, 2008). Absence of Hsp33 in bacteria exposed to these specific stress conditions causes a substantial growth disadvantage, allowing us to use the *hslO* deletion phenotype as an indicator for oxidative protein unfolding *in vivo*. Here we report the surprising finding that deletion of the Hsp33 gene *hslO* in *V. cholerae*, a mutant strain with a high sensitivity to HOCl stress (Winter *et al.*, 2008), displays a temperature-sensitive (*ts*) growth defect. Importantly, we found that the *ts* phenotype was fully abrogated when the mutant bacteria were cultivated under anaerobic conditions. One reasonable explanation is that *V. cholerae* is exposed to significant ROS production during aerobic growth and requires Hsp33 as an alternative chaperone once it encounters protein unfolding induced by stress conditions, such as elevated temperatures.

The severe *ts* phenotype of *V. cholerae hslO* deletion mutants provided us with the opportunity to use a genetic approach to shed light on the *in vivo* mechanism of Hsp33's chaperone action. We reasoned that by searching for genes in addition to *hslO* that are capable of rescuing the *ts* phenotype of *V. cholerae* ∆*hslO* mutants, we might discover alternative *E. coli* chaperones or antioxidant systems that are able to replace Hsp33 under oxidizing protein unfolding stress conditions. Alternatively, we might identify bacterial proteins whose high sensitivity to oxidative protein unfolding causes the observed

phenotype and can be compensated by an increase in their steady state levels. We independently selected two EF-Tu clones that rescued both the temperature-sensitive and bleach-sensitive phenotypes of *V. cholerae* lacking Hsp33. EF-Tu promotes binding of aminoacyl-tRNA to the ribosome and therefore allows peptide chain elongation during protein biosynthesis (Thompson *et al.*, 1986). Previous *in vivo* studies provided evidence that *E. coli* EF-Tu is a redox-sensitive protein that shows elevated levels of thiol oxidation during aerobic growth and undergoes additional oxidative thiol modifications in response to HOCl treatment (Leichert *et al.*, 2008).

Moreover, exposure of *E. coli* cells to near-lethal HOCl stress conditions or oxidative heat shock caused EF-Tu's aggregation, suggesting that excessive thiol modifications might induce protein unfolding (Winter *et al.*, 2008). Finally, it was found that decreasing the levels of EF-Tu by deleting the *tufA* gene increased *E. coli*'s bleach sensitivity (Leichert *et al.*, 2008). Our studies in *V. cholerae* were fully consistent with the results in *E. coli.* Yet, our finding that EF-Tu's cysteines become oxidized simply by growing *Vibrio cholerae* under aerobic conditions suggested an even higher oxidation sensitivity of *Vibrio* EF-Tu as compared to *E. coli* EF-Tu. Absence of the redox-regulated chaperone Hsp33 then leads to the premature degradation of EF-Tu, which causes a decrease in growth rates and, by a yet to be defined mechanism, a significant increase in bleach-sensitivity.

At this point, it is unclear how expression of *E. coli* EF-Tu confers enhanced bleach resistance to *V. cholerae*. The simplest and most straightforward explanation of our results would be that *E. coli* wild-type EF-Tu

has increased oxidative stress resistance, hence functionally replacing *V. cholerae* EF-Tu in protein translation and promoting *E. coli*'s recovery after bleach stress by rapidly resuming protein translation. Introduction of the additional Cys33 would increase EF-Tu's oxidative stress sensitivity and hence abrogate this protective function. However, our studies led to a very unexpected finding: we showed that presence of *E. coli* EF-Tu not only increased the steady-state levels of *V. cholerae* EF-Tu during aerobic growth but significantly stabilized *Vibrio* EF-Tu both during heat stress and upon short-term treatment with bleach. Hence the beneficial effects of *E. coli* EF-Tu expression were less likely simply due to an increase in the translation rate of *V. cholerae* EF-Tu but appeared to involve stabilization of *Vibrio* EF-Tu towards oxidative protein degradation.

This conclusion was also consistent with our analysis of protein translation in *V. cholerae* strains lacking Hsp33, which appeared to not be affected by the decreased EF-Tu levels. It has long been known that even during exponential growth EF-Tu molecules outnumber ribosomes by a factor of seven (Furano, 1975, Pedersen *et al.*, 1978). This finding has fueled the idea that EF-Tu plays more than one role in the cell. For instance, it has been demonstrated that EF-Tu polymerizes with other proteins to form filamentous, actin-like structure that function to maintain cell shape in *E. coli* and *Bacillus subtilis* (Beck, 1979, Defeu Soufo *et al.*, 2010). Moreover, previous *in vitro* studies showed that purified elongation factor EF-Tu protects thermally unfolding citrate synthase, a commonly used *in vitro* chaperone substrate, against protein aggregation and supports the refolding of citrate synthase upon return to non-stress temperatures

(Caldas *et al.*, 1998, Kudlicki *et al.*, 1997). This potential chaperone function of *E. coli* EF-Tu might compensate for the lack of Hsp33 and hence stabilizes *V. cholerae* EF-Tu. We were unable to find increased stabilization or decreased aggregation in response to heat or bleach stress for any other *Vibrio* protein(s) in *hslO* deletion mutants expressing *E. coli* EF-Tu, suggesting that EF-Tu might act specifically with the *Vibrio* EF-Tu pool, for instance by forming intermolecular dimers (Weijland and Parmeggiani, 1994). Another proposed function of EF-Tu includes an antioxidant scavenger role to buffer oxidants through the use of its ten methionine residues (Luo and Levine, 2009). This scavenging function of EF-Tu has been proposed to decrease the levels of ROS *in vivo* and hence protect oxidation-sensitive proteins against oxidative damage. As the *E. coli* EF-Tu^{T33C} variant has the same number of methionines and is expressed to the same extent, this non-specific antioxidant function appears to play only a minor role in conferring bleach resistance in *V. cholerae*. Future studies are clearly needed to address these fundamental questions regarding EF-Tu's alternative *in vivo* functions.

In summary, our study revealed that the stress sensitivity of a whole organism is determined in large part by the stress sensitivity of a single essential protein. In the case of *Vibrio*, this single essential protein appears to be EF-Tu. The stabilization of ET-Tu by the chaperone Hsp33 is sufficient to significantly enhance the stress resistance of the whole organism. It remains now to be determined what essential protein(s) are the "weakest links" in other organisms under the same or other stress conditions. Given the many known stress

conditions, which vary in effects and biological targets, it is likely to be different proteins for different stress conditions, justifying the wide substrate specificity of molecular chaperones.

EXPERIMENTAL PROCEDURES

Strain and growth condition

The *V. cholerae* and *E. coli* strains used in this study can be found in Table 1. Strains were cultivated in Luria-Bertani (LB) medium at the indicated temperatures. Ampicillin (100 μg/ml) was added to those cultures that contained pET11a or pBR322 plasmids. Growth on MacConkey agar at 43°C was used to select for temperature-sensitive phenotypes.

Table 1.1. Bacterial strains and plasmids used in Chapter II

Strain	Relevant genotype	Plasmid	Reference
JW370	*V. cholerae* O395 WT		Winter *et al.* (2008)
JW371	O395 *ΔhslO*		Winter *et al.* (2008
WC022	JW371	pET11a	This study
WC025	JW371	pET11a:*hslO*$^{E.c.}$	This study
WC038	JW371	pET11a:clone 12	This study
WC028	JW371	pBR322	This study
WC159	JW371	pBR322:*hslO*$^{E.c.}$	This study
WC037	JW371	pBR322:clone 5	This study
WC157	JW371	pBR322:*tufA*$^{E.c.}$	This study
WC187	JW371	pBR322:*tufA*$^{T33C\text{-}E.c.}$	This study
WC126	MG1655		Lab collection
WC127	WC126 *hslO*::kan		Lab collection
BB7222	MC4100		Winter *et al.* (2008)
JW176	BB7222 *hslO*::kan		Winter *et al.* (2008)

Preparation of genomic overexpression library

Genomic DNA from the *E. coli* wild-type strain MG1655 or the Δ*hslO* deletion strain JW176 was prepared using the GenElute Bacterial Genomic DNA kit (Sigma-Aldrich). The genomic DNA (2 µg) was partially digested with 0.05-0.2 units of BfuCI (New England Biolabs) in a total volume of 50 µl for 10 min at 37°C. Digested products were analyzed on 1% agaroase gels and showed fragment sizes ranging between 1 and 8 kb. After heat inactivation of enzyme, the DNA fragments were ligated into linearized pBR322/BamH1 or pET11a/BamH1 plasmid vectors using T4 ligase (New England Biolabs). The overexpressing plasmids were transformed into ultracompetent XL10-Gold cells (Stratagene) following the manufacturer's protocol. Colony forming units of transformants were counted the next day to calculate the size of the libraries ($1x10^5$ colonies for pBR322:Δ*hslO* library; $5x10^4$ colonies for pET11a:Δ*hslO* library). The transformants of each library were combined and the plasmids were purified using Wizard Plus SV Minipreps kit (Promega). The plasmids were then transformed into *V. cholerae ΔhslO* mutant strain. The transformants were plated on MacConkey agar and incubated for 24 h at 43°C to select for clones that rescue the *ts* phenotype of the *V. cholerae ΔhslO* mutant strain. Transformants that formed healthy looking colonies on plates were re-streaked on MacConkey plates and grown at 43°C. Plasmids of 12 transformants per library were purified and re-transformed into *V. cholerae ΔhslO* mutant to eliminate the possibility of mutations in the strain background.

HOCl survival assay

To determine the HOCl stress resistance, bacterial stains were cultivated in LB media at 37°C until OD_{600} of 0.4–0.5 was reached. Due to the reactivity of HOCl, cells were harvested, washed twice with 83 mM sodium phosphate buffer, pH 7.0, and resuspended in the same buffer. The cell density in each sample was normalized to $2x10^8$ cells per ml and treated with the indicated concentrations of sodium hypochlorite (Sigma-Aldrich). After 20 min incubation at room temperature, the treated cells were diluted 1:10 into 5-fold concentrated LB medium to quench the remaining HOCl (Winter *et al*., 2008). Serial 10-fold dilutions of treated cells were prepared and spotted onto LB plates. The colony-forming units after overnight incubation at 37°C were counted and used for determination of cell survival.

Pulse-chase labeling and 2D gel electrophoresis

V. cholerae O395 wild type and *V. cholerae* Δ*hslO* were cultivated in MOPS minimal medium supplemented with 0.2% glucose and all amino acids except methionine and cysteine for 24 h at 37°C. Cells were then diluted 1:80 into fresh media and grown at 35°C until OD_{600} = 0.4 - 0.5 was reached. Then, 15 µCi/ml radioactive ^{35}S-methionine (Easytag Expre^{35}S Protein Labeling Mix, PerkinElmer) was added to each culture for 2 min (i.e., pulse) followed by the addition of 2.7 mM unlabeled methionine (i.e., chase). Aliquots of 1.8 ml cells were collected immediately after the pulse as well as 1, 2, and 4 h during the chase. All samples were washed twice with ice-cold 60 mM KCl buffer and lysed

in DAB buffer (6 M Urea, 200 mM Tris-HCl pH8.5, 10 mM EDTA, and 0.5% w/v SDS). To determine the protein amount in the cell lysates, the D_C Protein Assay Kit (Bio-Rad) was applied using BSA as standard. 90 µg of protein from each sample were then pelleted using trichloroacetic acid precipitation and re-dissolved in 450 µl of loading buffer (7 M urea, 2 M thiourea, 1% [w/v] Serdolit MB-1, 1% [w/v] dithiothreitol, 4% [w/v] Chaps, and 0.5% [v/v] Pharmalyte 3–10). The 2D gel electrophoresis, staining of the gels and autoradiography were performed as previously described (Leichert and Jakob, 2004).

Image and data analysis

The protein pattern on the stained 2D gels and autoradiographs were compared and analyzed using the Delta2D 3.6 Software (Decodon). Spot detection, background correction and normalization were performed according to the software's instructions. Spot matching and alignments across the autoradiographs and stained gels of at least 4 independent pulse-chase experiments were performed. A master fusion gel, which retained all spots located on all individual images (Figure 2.5) was generated for spot labeling, visualization and cross-reference between gels. With the built-in settings of Delta2D, the spot quality, pixel intensity (i.e., volume) and % volume (volume of individual spot over total volume of all spots) for each protein spot was determined and exported as a spreadsheet table.

To compare the steady state concentration and translation of EF-Tu within a 2 minute time frame in *V. cholerae* and *V. cholerae* Δ*hslO*, we calculated the

mean % volume of EF-Tu as well as of the 40 most abundant protein spots on the Coomassie-stained 2D gels or autoradiographs (Figure 2.6). To analyze the protein degradation rates in *V. cholerae* and *V. cholerae* Δ*hslO*, we divided the % volume of each spot on the autoradiograph by the % volume of the respective spot on the Coommassie stained 2D gel and determined the fold decrease of ^{35}S incorporation from the 2 min pulse to 4 h of chase. The mean degradation rate for EF-Tu and the each of the 40 pre-selected spots was calculated from four independent pulse-chase experiments (Figure 2.7). Standard errors were calculated and are shown in the Figures.

Protein identification by mass spectrometry

The identification of protein spots from 2D gels was conducted as described with only minor modifications. Spot analysis was performed by MS/MS analysis using MALDI TOF. Peptide identification was conducted using the Mascot software with default parameters. The search was done against the Swiss-Prot database.

E. coli EF-Tu^{Q97P} mutagenesis

The *E. coli* EF-Tu^{Q97P} variant was generated by site-specific mutagenesis using the forward primer 5' CCGGTGCTGCTCCGATGGACGGCGC and the reverse primer 5' GCGCCGTCCATCGGAGCAGCACCGG. Plasmid pBR322:*tufA*$^{E.c.}$ (see Table 1) was used as DNA template. A typical 50 µl reaction contained 0.3 ng/µl DNA template, 0.2 mM dNTPs, 3% DMSO, 1 U Phusion

polymerase and 25 pmole/µl of each primer in HF buffer supplied by the Phusion polymerase kit (Finnzymes). The PCR program consisted of 1 cycle of 30 sec at 98°C, 30 cycles of 1) 30 sec at 98°C, 2) 30 sec at 70°C, and 3) 3 min 45 sec at 72°C, followed by 1 cycle of 10 min at 72°C, and hold at 4°C. The parental plasmid was digested by adding 40 U DpnI restriction enzyme (NEB) to the PCR products. The reaction was incubated at 37°C for 3 h. The DNA was concentrated to 5 µl using Pellet Paint (Novagen) and transformed into XL-10 Gold Ultracompentent cells (Stratagene). The transformants were streaked twice on selective growth plates and the plasmid was purified using Wizard Plus SV Minipreps kit (Promega). DNA sequencing was performed and correct clones were transformed into O395 and O395Δ*hslO* strains.

Differential in vivo thiol trapping with NEM and AMS

Bacterial strains were cultivated in LB media at 37°C until OD_{600} of 0.4–0.5 was reached. Then, 3 mM HOCl was added to the medium directly and incubation was continued for 20 min. Before and after the stress treatment, aliquots of 1 ml were taken and acidified with trichloroacetic acid (TCA) to a final concentration of 10%. After 30 min of incubation on ice, precipitated proteins were pelleted by centrifugation (13, 000 rpm, 20 min, 4°C). The protein pellet was resuspendend in DAB buffer (6 M Urea, 200 mM Tris-HCl pH8.5, 10 mM EDTA, and 0.5% w/v SDS) supplemented with 100 mM N-ethylmaleimide (NEM) to irreversibly alkylate all reduced cysteines. Samples were incubated for 30 min at 25°C. The proteins were again precipitated with TCA to remove any unbound

NEM, and pelleted by centrifugation. For differential thiol trapping with AMS, protein pellets were resuspended in DAB buffer supplemented with 10 mM DTT to reduce all *in vivo* oxidized cysteines, and incubated for 1 h at 25°C. Excess DTT was removed by TCA precipitation and centrifugation. All newly accessible cysteines were then modified with 10 mM of the thiol-specific alkylation reagent 4-acetamido-4'-maleimidylstilbene-2,2'-disulfonic acid (AMS), which adds 500 Da mass to every modified cysteine.

As control, we also prepared fully NEM-labeled proteins, which represent the fully reduced species and fully AMS-labeled proteins, which represent the fully oxidized protein species. Cell aliquots were taken, precipitated with TCA and resuspended in DAB buffer supplemented with 10 mM DTT to reduce all *in vivo* thiol modifications. After incubation of the samples for 1 h at 25°C, proteins were precipitated with TCA, centrifuged and resuspended in DAB buffer supplemented with either 100 mM NEM or 10 mM AMS. Proteins were separated on SDS-PAGE and EF-Tu was visualized by western blot analysis using polyclonal antibodies against EF-Tu (provided by Dr. Beckwith).

Thiol trapping with NEM

Bacterial strains were cultivated in LB media at 37°C until OD_{600} of 0.4–0.5 was reached. Then, 3 mM HOCl was added to the medium directly and incubation was continued for 20 min. Before and after the stress treatment, aliquots of 1 ml were taken and acidified with trichloroacetic acid (TCA) to a final concentration of 10%. After 30 min of incubation on ice, precipitated proteins

were pelleted by centrifugation (13,000 rpm, 20 min, 4°C). The protein pellet was resuspendend in DAB buffer (6 M Urea, 200 mM Tris-HCl pH8.5, 10 mM EDTA, and 0.5% w/v SDS) supplemented with 100 mM N-ethylmaleimide (NEM) to irreversibly alkylate all reduced cysteines. Samples were incubated for 30 min at 25°C, split into two aliquots and supplemented with either reducing (5 mM DTT) or non-reducing Laemmli-buffer. To enhance the efficiency of the protein transfer onto the nitrocellulose membrane after separation on SDS-PAGE, gels were incubated with 3% mercaptoethanol for 1 hr prior to the westernblot. EF-Tu was visualized using polyclonal antibodies against *E. coli* EF-Tu (provided by Dr. J. Beckwith).

CHAPTER III

Cellular responses to the oxidizing effects of bleach [2]

ABSTRACT

Hypochlorous acid (HOCl), the active component of household bleach, functions as a powerful antimicrobial. HOCl is naturally produced by cells of the mammalian innate immune system to kill invading pathogens. Despite its widespread use, surprisingly little is known about how bacteria sense and respond to HOCl. Transcriptional, genetic, and biochemical analysis of HOCl-treated *Escherichia coli* identified conserved physiological defenses against bleach treatment. Mediated in part by the HOCl-specific, redox-regulated repressor NemR, cells induce expression of glutathione-dependent and -independent systems to detoxify accumulating methylglyoxal, and re-direct cellular ATP to form inorganic polyphosphate. These results have broad

[2] Data from the following chapter is included as part of manuscript in preparation: Michael J. Gray, Wei-Yun Wholey, Minwook Kim, Erica M. Smith, Claudia M. Cremers, Robert A. Bender, Ursula Jakob. I performed part of the experiments presented here and am the co-first author of the manuscript. I modified the manuscript to emphasize my contributions, which included microarray sample collection, data processing and analysis, intracellular metal analysis, HOCl survival assays, *in vivo* thiol trap experiments, methylglyoxal survival assay, and *in vitro* DNA damage assays.

implications for understanding how cells sense HOCl and prevent cellular damage.

INTRODUCTION

Hypochlorous acid (HOCl), the active component of household bleach, is one of the most commonly used disinfectants in the world. HOCl is naturally generated as an abundant part of the microbiocidal oxidative burst of neutrophils and appears to play a role in controlling bacterial colonization of mucosal epithelia (Klebanoff, 2005). Oxidative damage caused by excessive HOCl production is involved in many human diseases, including chronic inflammation, atherosclerosis, cancer, and Alzheimer's disease (Klebanoff, 2005). Surprisingly, despite its importance and widespread use, only very little is known about how cells respond to, defend against, and potentially survive HOCl stress.

The ability of bacteria to protect themselves against HOCl and to reduce oxidative damage are important strategies to survive within the host and should reveal systems that are capable of dealing with and repairing from HOCl. To our knowledge, no HOCl-specific transcriptional regulator has been identified in any organism to date. This is in contrast to the hydrogen peroxide (OxyR) and superoxide (SoxR) regulons, which have been well characterized (Imlay, 2008). Both these global regulators activate genes needed for removal of oxidants as well as repair enzymes (Imlay, 2008). Cells appear to be protected against bleach-induced oxidative stress by activating the redox-regulated chaperone

Hsp33, which protects proteins against unfolding and irreversible aggregation (Winter *et al.*, 2008).

As shown in chapter II of this thesis, the highly conserved bacterial Hsp33 chaperone prevents specifically the essential elongation factor EF-Tu against oxidative unfolding and degradation in *Vibrio cholerae* (Wholey and Jakob, 2012). A recently conducted genomic expression library screen of bacteria treated with HOCl furthermore identified the regulator YjiE, which appears to mediate some level of bleach-resistance in bacteria (Gebendorfer *et al.*, 2012). The YjiE regulator appears to be activated in HOCl-stressed cell but the protein does not seem to be directly activated by HOCl *in vitro*. It is thus possible that YjiE senses downstream effects mediated by bleach. At this point, it is still unclear whether bacteria utilize any transcriptional regulator that is directly activated by HOCl treatment, which might up-regulate a global protective response(s).

To understand the bacterial response towards bleach treatment in more detail, we conducted microarray studies in the presence and absence of HOCl using Affymetrix *E. coli* GenChips, and validated our findings both through genetic studies and biochemical analyses. We present evidence that we have identified NemR as a highly conserved, bleach-specific transcription factor. Moreover, we discovered that bacterial HOCl survival depends strongly on conserved pathways for methylglyoxal (MGO) detoxification and inorganic polyphosphate (polyP) synthesis. Results of this study help us to shed light into the molecular action of HOCl and to elucidate the bacteria's strategy to counteract HOCl-stress during host defense and bacterial colonization.

RESULTS

Expression analyses of HOCl-treated *E. coli* using Affimetrix GeneChips

To investigate whether HOCl-specific transcription factors and regulons exist in bacteria, I conducted transcriptional microarray analysis in the absence and presence of HOCl. *E. coli* MG1655 was cultivated in MOPS minimum medium supplemented with 0.2% glucose and 0.1 mM thiamine-HCl and treated with 400 μM HOCl during exponential growth (OD_{600}=0.4-0.5). Under these treatment conditions, cells stop growing for about 30 – 60 min upon, after which they recover and resume growth. As the effect of HOCl varied slightly from day to day, growth curve experiments were performed several times prior to the microarray experiments to identify an effective, yet sub-lethal HOCl concentration suitable for our microarray experiments. Cell aliquots were taken before, 5 min and 10 min after HOCl treatment, and the total RNA was isolated. The Microarray Core facility at the University of Michigan, Ann Arbor conducted the sample processing, including cDNA synthesis, array hybridization to the GeneChip, and the image scanning.

I performed the chip background quality assessment and normalizations using Bioconduction implemented in R statistical language (see Experimental procedures for details) (Gentleman *et al.*, 2004). The unprocessed chip images were carefully visualized and examined. No artificial defaults or local artifacts from printing or washing were detected. Boxplots generated by R were then used to examine probe-intensity distributions as shown in Figure 3.1. Boxplots show the difference and variability between arrays as boxes, which are marked with

their maximum and minimum ranges. All boxplots lined up approximately to a horizontal line, indicating that no major discrepancy between probes was found.

To identify HOCl-specific changes in transcriptional regulation and gene expression, I used k-means cluster analysis to organize gene expression into patterns (Bioinformatics course, University of Massachusetts, Amherst). The k-means clustering is a commonly used algorithm for grouping expressions with more than two variables. It creates groups based on the similarities and differences between the given variables.

Compared to other microarray analyses using only two variables, control and treated, the k-means clustering is more suited for our time kinetic measurements. The TM4 MultiExperiment Viewer (MeV) software (Saeed *et al.*, 2003) was used to identify patterns of kinetic gene expression upon HOCl induction and differentially expressed genes. To do so, the expression ratios of all genes after 5 min and 10 min HOCl treatment relative to control conditions were calculated. The 5298 MG1655 probes (4358 genes and 940 intergenic regions) were then separated into 25 clusters as shown in Figure 3.2.

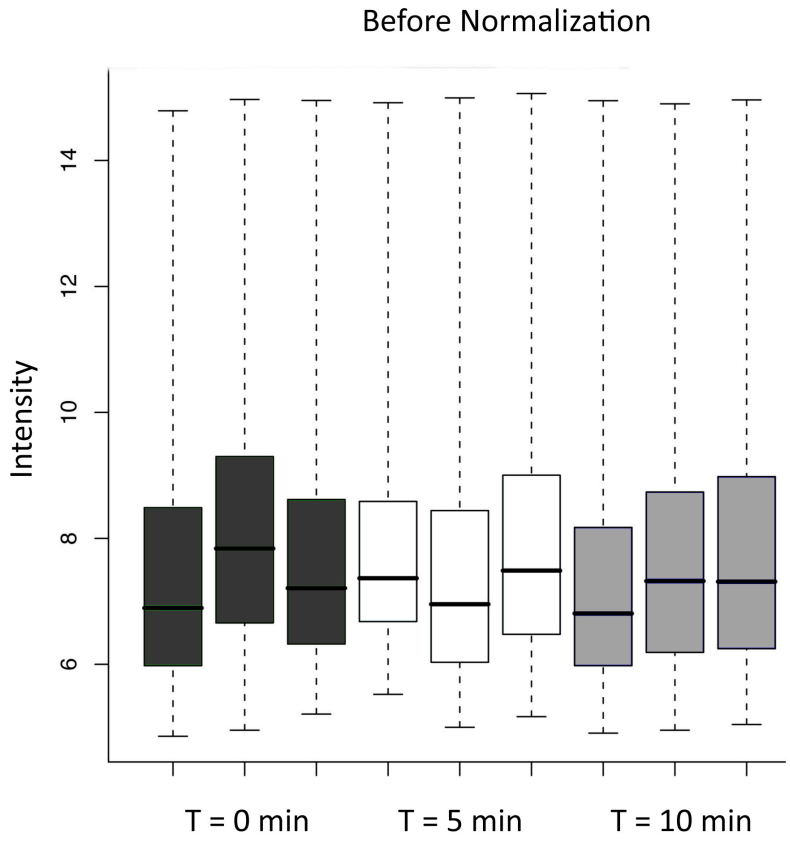

Figure 3.1. Boxplot of microarray probe-intensity distributions. Before (t = 0 min, black) or 5 min (white) or 10 min (gray) after HOCl treatment. Experiments were performed in triplicates.

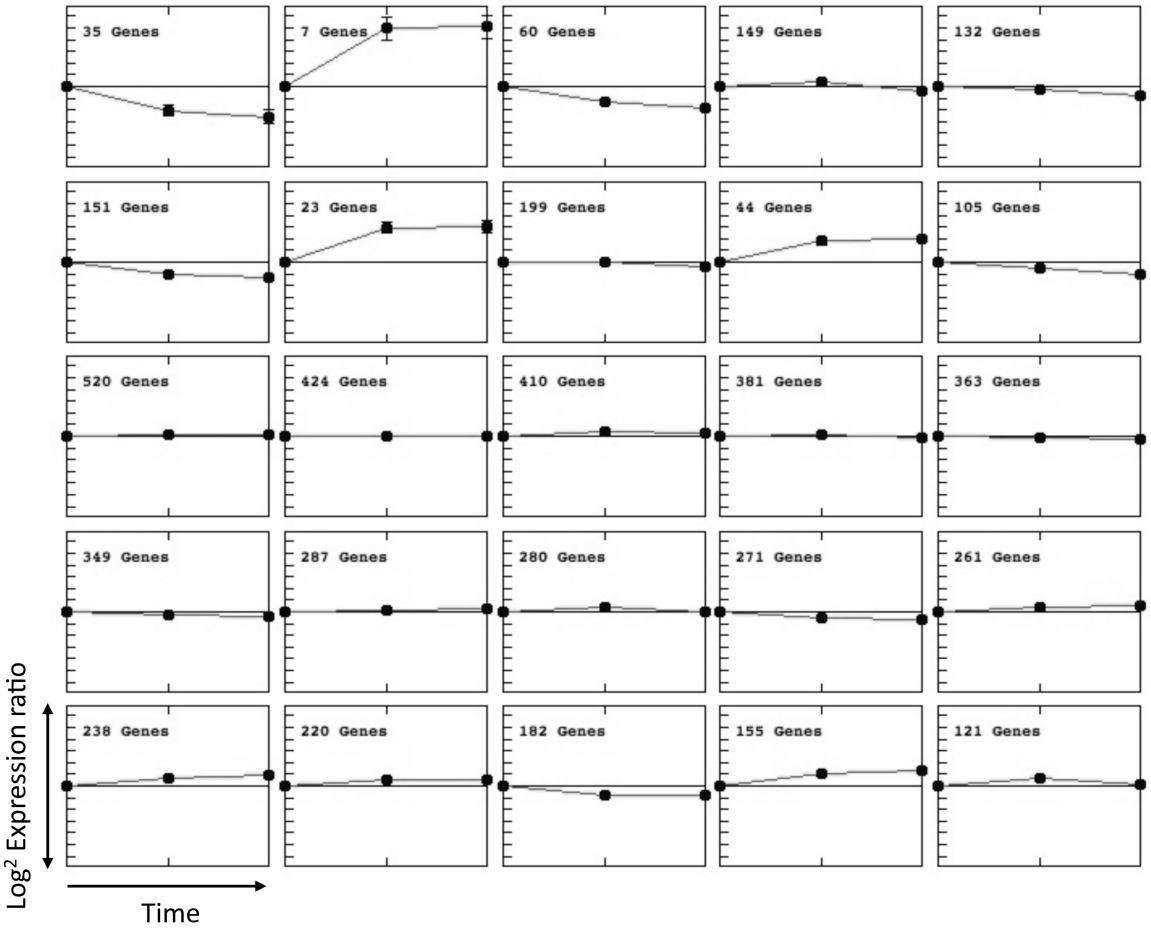

Figure 3.2. Cluster analysis of E. coli expression profiles. The k-mean clustering method was used to separate total of 5298 probe expression patterns into 25 clusters (cluster 1, top left and cluster 25, bottom right) based on log2 transformed ratio at T= 0, 5, and 10 min after HOCl treatment.

Probes in most of the clusters did not reveal any change in the expression level upon HOCl treatment. Only a small set of probes found in cluster 2, 7 and 9 were significantly upregulated in response to bleach while cluster 1 and 3 contained all the down-regulated probes. A total of 225 genes were found to be at least 2-fold up-regulated and 314 genes were found to be at least 2-fold down-regulated upon HOCl stress. The cellular functions and metabolic pathways of these differentially expressed genes are listed in Figure 3.3.

A complete list of all up-regulated and down-regulated gene can be found in Appendix Table 1 and 2.

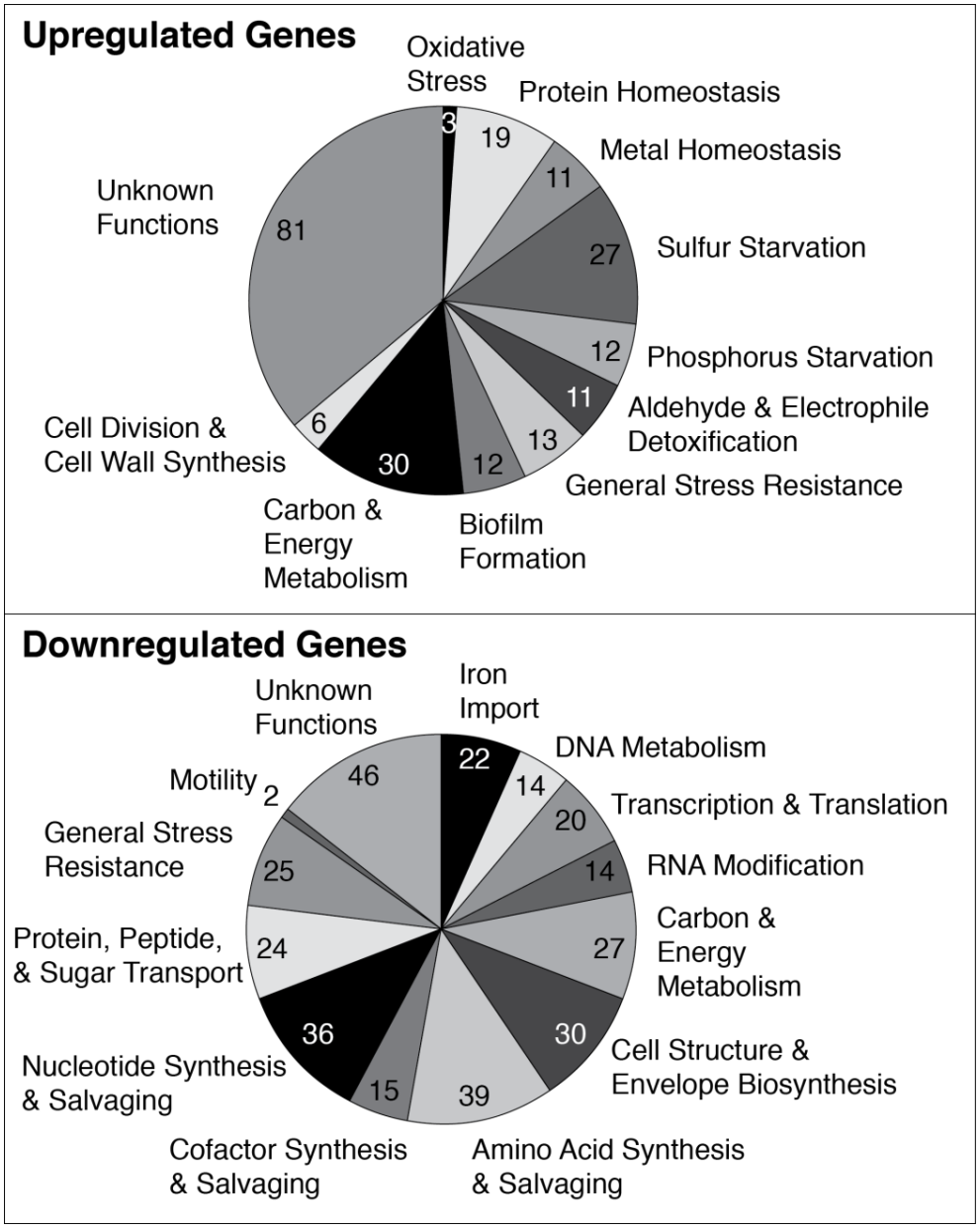

Figure 3.3. Transcriptional response to HOCl. *E. coli* MG1655 was grown to mid-log phase in MOPS minimal glucose and treated with 0.4 mM HOCl. Genes whose expression changed 2-fold or more are indicated in Appendix Tables 1 and 2.

HOCl stress causes protein aggregation and alters metal homeostasis

Of the 4358 genes in *E. coli*, we found that fewer than 5% were significantly up- or downregulated, indicating that HOCl induces a very specific transcriptional response. The pattern of gene expression observed in our microarray was different from the pattern observed during superoxide or hydrogen peroxide oxidative stresses (Imlay, 2008). Very few genes commonly associated with reduction of ROS were up-regulated (i.e., *grxA*, *oxyS*, *sodC*) and those had only very low levels of induction (Imlay, 2008).

Consistent with our previous studies, we found many molecular chaperones (Clp, DnaK, Hsp90, IbpA and IbpB) to be induced upon HOCl stress, confirming that HOCl treatment leads to the accumulation of unfolded and aggregated proteins *in vivo* (EcoGene.org database, (Winter *et al.*, 2008). The entire pathway of purine biosynthesis (a precursor of ATP) was found to be downregulated, validating earlier reports that ATP is depleted during bleach treatment (Winter *et al.*, 2005). In addition, phosphate starvation genes (PstSCAB), which subsequently trigger sigma factor S activation, were induced, suggesting that HOCl decreases intracellular level of free phosphate or re-distribution of intracellular phosphate (Schurdell *et al.*, 2007).

Consistent with HOCl's high reactivity towards thiol groups (Hawkins *et al.*, 2003), we also found 27 upregulated genes associated with sulfur starvation and Cys / Met biosynthesis. For instance, the entire pathway of methionine biosynthesis (MetABCFLN) as well as many components (TauABCD) of the sulfur up-take system were found to be significantly up-regulated (EcoGene.org

database). Together with genes involved in the up-regulation of peptide transporters (IaaA and GcvB) and genes involved in other amino acid biosynthetic pathways (Parry and Clark, 2002, Pulvermacher *et al.*, 2009), our results suggest that new protein synthesis, either *de novo* or from salvage pathways, are needed to replace aggregated or severely damaged proteins upon exposure to HOCl.

We also found a number of genes associated with metal export (copA, cusC, and zntA) to be significantly upregulated upon HOCl-treatment, dedicated to transport copper, cobalt, nickel, and zinc from the cells (EcoGene.org database). Although the zinc uptake transporter (zupT) was two fold up-regulated, it was not considered as significant based on the K-means clustering analysis (Appendix table 1). Conversely, many genes involved in iron import (efeU, entCE, fhuADF, tonB and exBD) were downregulated (EcoGene.org database). These results suggest that excess free metals might accumulate within the cytosol of HOCl-treated cells, which need to be exported through metal exporters. This result is consistent with HOCl's capacity to oxidize metal-coordinating thiol groups, potentially causing metal release (Imlay, 2008).

To examine the intracellular metal contents in HOCl-treated bacteria, I prepared samples for Inductively Coupled Plasma-High Resolution Mass Spectrometry analysis (ICP-analysis). ICP analysis is highly sensitive and capable of determining a wide range of metals at very low concentration (personal communication with the Keck Elemental Geochemistry Laboratory). *E. coli* MG1655 wild type strain was cultivated under the same growth condition as

before and cell aliquots were taken before and after treatment with 0.4 mM HOCl. Cells were washed extensively with metal-free MOPS-EDTA buffer to remove all extracellular metals, corrected for optical density, and submitted for metal content measurements. As shown in Figure 3.4, we found that the intracellular concentration of iron (Fe) and manganese (Mn) dropped by at least 30% in HOCl stressed cells. This result agreed well with our microarray studies, which showed that Fe uptake systems are significantly downregulated and many metal exporters are upregulated. Given that the manganese transporter (*mntH*) transports both Mn and Fe, and its operator region contains a Fur-regulator binding site, in which indicated that manganese up take is also downregulated (Makui *et al.*, 2000, Patzer and Hantke, 2001). An iron-regulated heme synthesis protein (*irr*) appears to be controlled by manganese, in which suggested a crosstalk between some regulations of the metabolism of iron and manganese (Hamza *et al.*, 1998, Puri *et al.*, 2010). Fur regulator senses intracellular Fe level and represses iron uptake systems. The observed decreasing intracellular manganese (Mn) level may possibly due to the Fur facilitated repression of *mntH* transporter. The cellular concentration of calcium (Ca) also decreased while no significant differences were detected in intracellular zinc (Zn), magnesium (Mg) or copper (Cu) content.

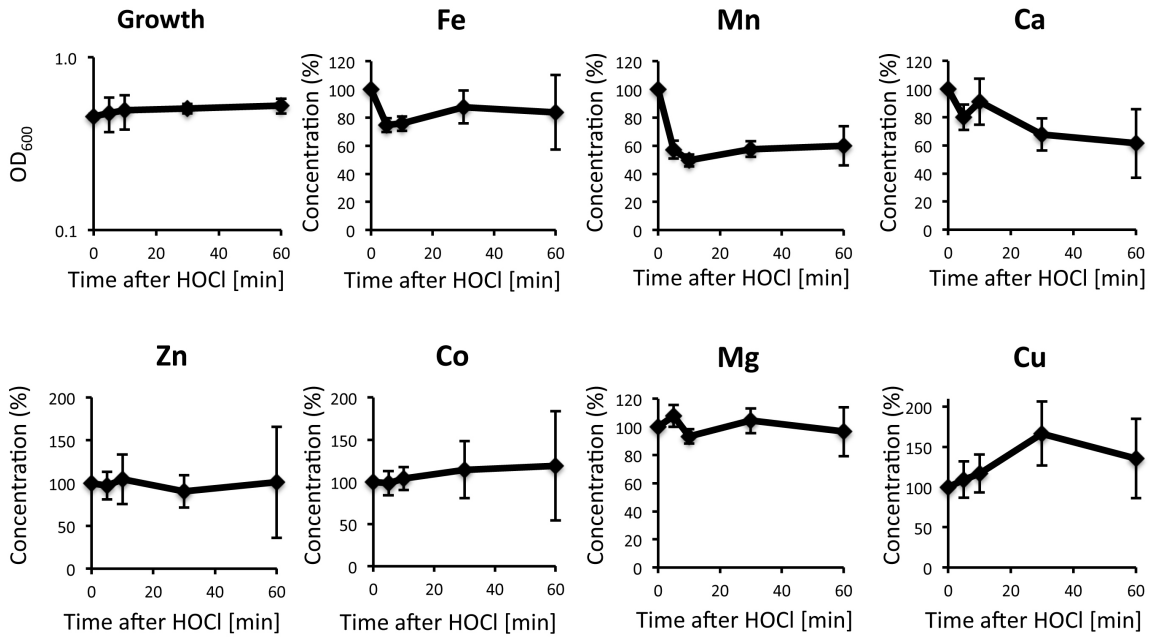

Figure 3.4. Analysis of intracellular metal content after HOCl treatment. *E. coli* MG1655 was cultivated in MOPS minimal glucose medium to mid-log phase and treated with 0.4 mM HOCl. Samples before and after treatment at indicated time points were collected for ICP analysis. Error bars represent standard error from 4 independent replicates.

NemR is a bleach-specific transcriptional repressor

Among the many up-regulated proteins uncovered by microarray analysis, there was a striking induction of genes (dkgA, yqhD, frmRAB, dadA, nemA and gloA) involved in detoxification of reactive aldehydes and electrophiles (Jeudy *et al.*, 2006, Perez *et al.*, 2008, Herring and Blattner, 2004, Wild and Obrepalska, 1982, Umezawa *et al.*, 2008, Gonzalez-Perez *et al.*, 2007, MacLean *et al.*, 1998)

Two of these detoxification genes are under the control of the transcriptional regulator NemR. As homologue of the TetR family of transcriptional repressors, NemR is highly conserved in many different bacteria. NemR was originally identified as *N*-ethylmaleimide (NEM)-specific

transcriptional regulator, controlling the expression of the Nem-reductase NemA (Umezawa *et al.*, 2008). Immediately downstream of *nemA* is the glyoxalase, *gloA*, which is a broadly conserved protein in both prokaryotes and eukaryotes, including humans. GloA catalyzes the detoxification of the strong electrophile methylglyoxal, which is known to be highly toxic to the cell (Munch *et al.*, 2010). In contrast to NEM, which is a non-naturally occurring reagent that alkylates Cys residues irreversibly, HOCl is a physiological oxidant, which rapidly and reversibly modifies Cys thiols (Winter *et al.*, 2008). We decided to pursue the study of NemR, with the possibility that we had identified a bleach-specific transcriptional regulator.

Working with Mike Gray, a postdoc in the lab, we first confirmed our microarray results using quantitative reverse transcription PCR (qRT-PCR). *E. coli* MG1655 and the *ΔnemR* deletion mutant, constructed by Mike, were grown in MOPS minimal glucose medium until mid-log phrase and treated with 0.4 mM HOCl, the same condition used in the microarray studies. Figure 3.5A shows a 70-fold up-regulation of *nemR* and 100-fold and 10-fold up-regulation of the downstream genes *nemA* and *gloA*, respectively within 10 min of HOCl treatment. Both *nemA* and *gloA* expression were NemR-regulated; *nemA* and *gloA* transcripts were constitutively induced and non-responsive to HOCl in a non-polar *nemR* deletion strain (Figure 3.5A). DNA binding studies of purified NemR *in vitro* revealed that NemR is extremely sensitive to oxidation, and binds the *nemR* promoter only in the presence of DTT (Figure 3.5B).

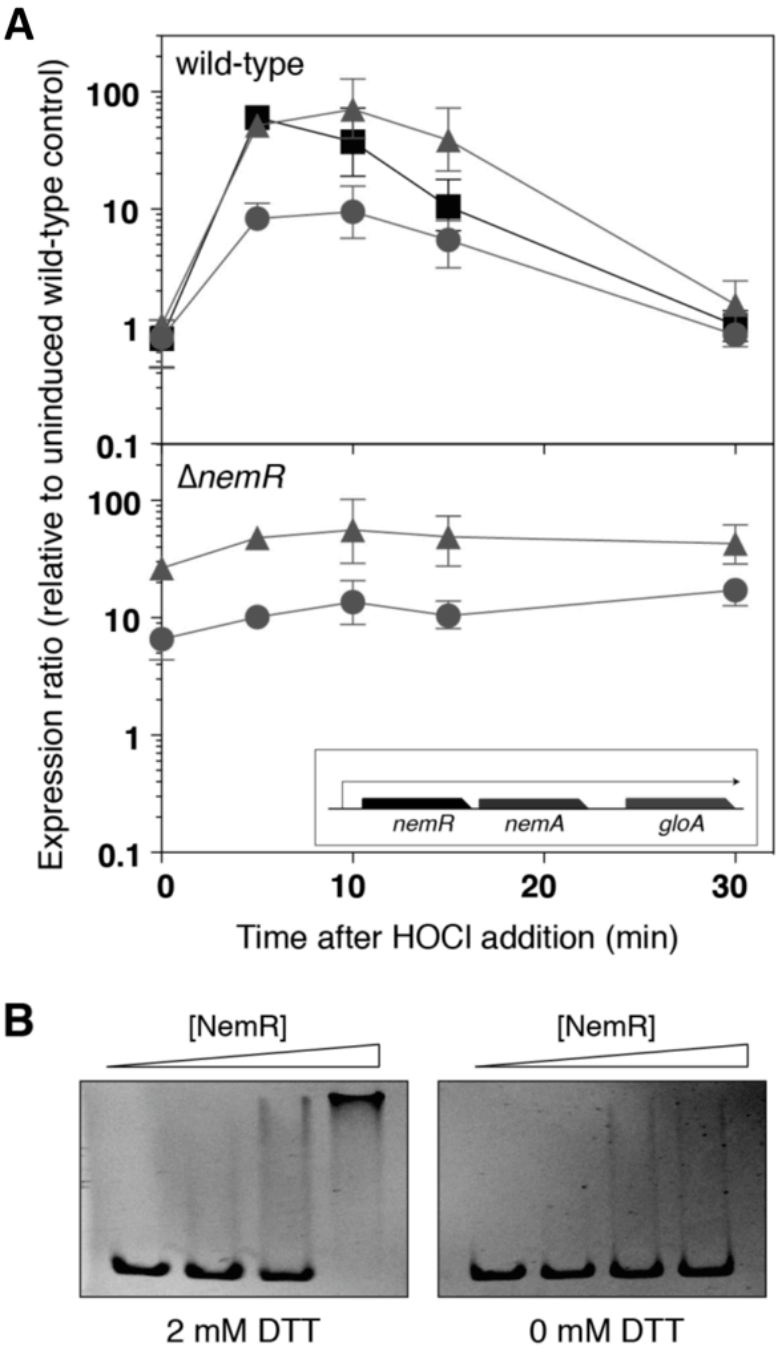

Figure 3.5. NemR is an HOCl-sensing transcriptional repressor. (**A**) *E. coli* MG1655 and the Δ*nemR* mutant were grown to mid-log phase in MOPS minimal glucose and treated with 0.4 mM HOCl. Expression ratios of *nemR* (■), *nemA* (▲), and *gloA* (●) were determined by qRT-PCR. (**B**) 0 - 3 pmol purified NemR was incubated for 30 min with a DNA fragment containing the *nemR* promoter (0.1 pmol), then visualized by PAGE. Experiments were conducted by Mike Gray.

NemR is HOCl-specific and protects cell against HOCl stress

To examine whether the NemR is a HOCl-specific regulator *in vivo*, Mike Gray performed qRT-PCR to monitor the *nemR* transcript levels upon treatment with different oxidants. As shown in Figure 3.6A, NemR showed considerable oxidant specificity. The transcript level of *nemR* was up-regulated in response to HOCl, the related reactive chlorine species *N*-chlorotaurine, and NEM, but not in response to H_2O_2, methyl viologen (paraquat), diethylamine nitric oxide (DEANO), or methylglyoxal (MGO). This result indicates that the transcription of NemR is specifically activated in response to HOCl stress but not in response to any other commonly used oxidative stressors. To elucidate the roles of NemR and its regulated genes, *nemA* and *gloA*, in protecting cells against the toxicity of bleach, we performed HOCl survival assay both in liquid culture and on plates. *E. coli* wild type and the corresponding *ΔnemA* and *ΔgloA* deletion mutants were subjected to 2 mM HOCl challenge in MOPS minimal glucose medium. To examine the number of viable cells survived in bleach stress, aliquots of cells after treatment at indicated time points were taken, serially diluted and spotted on to LB growth plates. As shown in Figure 3.6B, deletion of *nemR* slightly increased HOCl survival while deletion of *nemA* or *gloA* increased HOCl sensitivity. These results indicated that the transcriptional repressor NemR is important for the cellular response to HOCl insults. Removal of the repressor leads to constitutive activation of its regulated genes, *nemA* and *gloA*; hence increased the cell's resistance. Mutants lacking protective genes, *nemA* and *gloA*, however, failed to cope with HOCl stress and died much faster than the

wild type *E. coli* strain. Collectively, our results revealed that we have identified a bleach-specific transcriptional repressor, whose target genes contribute to bacterial HOCl survival.

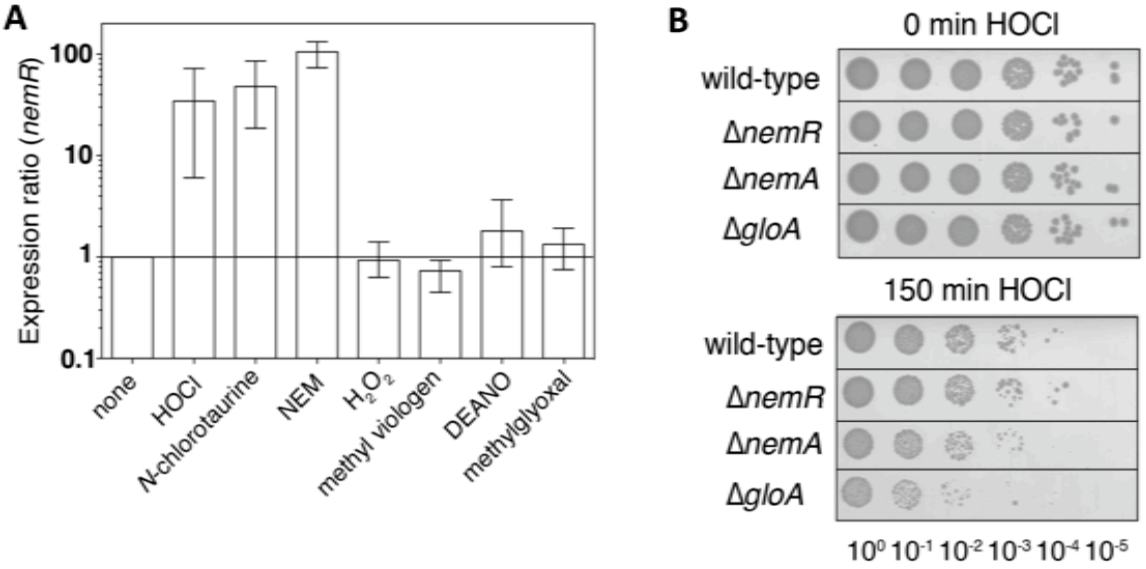

Figure 3.6. NemR is a HOCl-specific and its regulated genes are needed in HOCl stress. (**A**) Expression of *nemR* upon treatment with 0.4 mM HOCl, 0.2 mM *N*-chlorotaurine, 0.1 mM NEM, 2 mM H_2O_2, 0.4 mM methyl viologen, 0.2 mM DEANO or 0.2 mM MGO for 10 min. (**B**) MG1655-derived strains were incubated in MOPS minimal glucose containing 2 mM HOCl, then diluted and spot-titered on LB agar. The qRT-PCR data came from Mike Gray. Survival assays were conducted in collaboration with Mike Gray.

Analysis of thiol status of NemR *in vivo*

Our studies demonstrated that NemR is sensitive to HOCl oxidation and is important for the cellular tolerance towards bleach stress. The fact that the NemR regulator binds to *nemR* promoter DNA only in the presence of the thiol reducing agent DTT (Figure 3.5B) suggested that NemR utilizes some type of oxidative

thiol modification for its activity. Because both NEM and HOCl react very rapidly with Cys residues, we reasoned that HOCl-sensing of NemR might work through thiol modification of critical Cys residue(s). Upon oxidative modification of cysteines, NemR might undergo conformational changes that alter the function of the protein. To explore the possibility that NemR is redox regulated via reversible cysteine modifications, I performed *in vivo* thiol trapping experiments of wild type NemR. An *E. coli* MG1655 *ΔnemR* deletion strain expressing a his-tagged version of NemR from a plasmid was cultivated in MOPS minimal glucose medium until mid-log growth phase and treated with different types of oxidants, including HOCl, the related reactive chlorine species *N*-chlorotaurine (NCT), NEM, methyl viologen (paraquat), and H_2O_2. Cell aliquots were removed before and after treatments, and lysed in the presence of 10% TCA to minimize any further thiol oxidation (Zander *et al.*, 1998). All reduced cysteine thiols were irreversibly alkylated with iodoacetamide (IAM) to prevent non-specific air oxidations, which may be introduced during sample handling.

To determine whether treatment with HOCl leads to inter-molecular disulfide bond formation in the dimeric NemR, I analyzed the migration behavior of NemR upon separation of the proteins on non-reducing SDS gels and visualization of NemR using anti-his-tag antibodies. As shown in Figure 3.7A, HOCl, the related reactive chlorine species *N*-chlorotaurine (NCT), and NEM, but not paraquat or H_2O_2 caused the formation of higher oligomeric bands under non-reducing conditions, indicative of intermolecular disulfide bonds. This result suggested that NemR is indeed a redox-regulated protein, which undergoes

HOCl-mediated disulfide thiol modification *in vivo*. These conformational changes likely cause loss of repressor function and hence induce gene expression.

Redox-regulated proteins typically utilize the oxidation status of conserved cysteines to control their protein function (Giles, 2003). Examination of the amino sequence of NemR revealed that it has six cysteines, one of which (C106) is absolutely conserved among all investigated NemR homologues. To assess which of the cysteines in NemR might be involved in redox regulation, I performed *in vivo* thiol-trapping experiment using *E. coli* BL21 strains, which expressed mutant NemR variants lacking one of the cysteines (i.e., C106S, C98S, C116S, C21S, or C153S). Expression of the histidine-tagged NemR mutant variants was induced with 10 μM IPTG prior to the stress treatment with 1 mM HOCl. As before, all reduced Cys residues were alkylated with IAM and proteins were analyzed on non-reducing SDS gels and subsequently westernblotted. As shown in Figure 3.7B, *E. coli* strains expressing histidine-tagged wild type NemR from a plasmid showed the previously observed accumulation of high molecular weight oligomers. Similar results were found in *E. coli* strains expressing C106S, C21S, and C153S NemR mutant variants. In contrast, however, significantly fewer oligomeric species were observed in NemR variants lacking either C98 or C116, indicating that these two cysteines are involved in undergoing HOCl-mediated disulfide bond formation. These results suggested that oxidation of one or more of NemR's non-conserved Cys might be sufficient to cause oxidation-mediated conformational changes in NemR that lead to derepression. Notably, we observed disulfide crosslinked NemR dimers under

low-expression condition while NemR tetramers were observed under conditions of high NemR expression levels. It remains to be tested which oligomeric structural change will apply to HOCl-treated non-tagged NemR, expressed at physiological concentration. At this point, no correlation between the structural changes upon HOCl treatment and NemR's function under HOCl-stress can be made. Further experiments are needed to test the *in vitro* and *in vivo* function of these two NemR variants. Alternatively, differential thiol trapping experiments can be conducted to elucidate the critical Cys residues involved for NemR's activation.

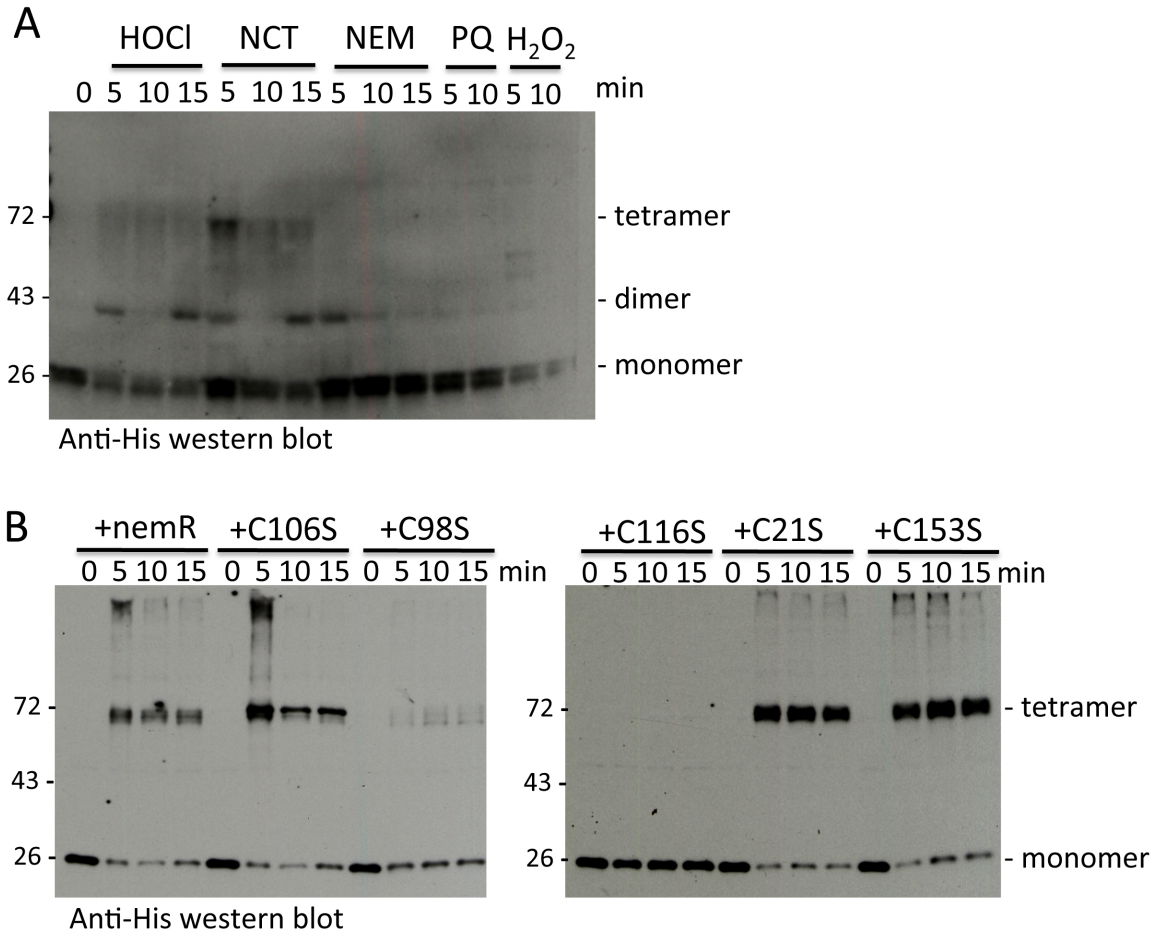

Figure 3.7. Analysis of the thiol status of NemR *in vivo*. (A) *E. coli* MG1655 Δ*nemR* expressing histidine-tagged NemR from a non-induced plasmid was grown in MOPS minimal glucose medium until mid-log growth phase and treated with the indicated oxidants, HOCl (0.4 mM), *N*-chlorotaurine (NCT, 0.2 mM), NEM (0.1 mM), methyl viologen (PQ, 0.4 mM) or H_2O_2 (2 mM). Cell aliquots were removed before and after treatments, lysed in 10% TCA and all reduced cysteine thiols were irreversibly alkylated with iodoacetamide (IAM) while those previously oxidized cysteines remained unaltered. Proteins were analyzed on non-reducing SDS protein gel and NemR was visualized by westernblot using anti-histidine-tag antibodies. (**B**) Similar to **A**, *E. coli* BL21 containing individual histidine-tagged NemR mutant variants was grown in MOPS medium. NemR expression was induced with 10 μM IPTG for 30 min. Cells were treated with 1 mM HOCl duing mid-log growth, and harvested at the indicated time points. As before, samples were alkylated with IAM and visualized by western blot.

Role of HOCl-induced methyglyoxal (MGO) accumulation in bacteria

Our results indicate that bleach-mediated conformational changes in NemR lead to de-repression of gene expression. Release of NemR from the *nemR* promoter induces the expression of *nemA* and *gloA* transcripts. This result raised the question as to how upregulation of *nemA* and *gloA* protects bacteria against HOCl? NemA is a reductase, whose physiological substrate is unknown (Mueller *et al.*, 2010). GloA (glutathione [GSH]-dependent glyoxylase I) is conserved among many prokaryotic and eukaryotic species as the primary methylglyoxal (MGO) detoxifying enzyme (MacLean *et al.*, 1998). MGO is a side product of glycolysis generated by dephosphorylation of dihydroxyacetone phosphate, either spontaneously or by the bacterial enzyme MGO synthase (MgsA) (Booth *et al.*, 2003). MGO causes damages to DNA, lipids and mainly proteins through its ability to crosslink arginine residues (Mironova *et al.*, 2001, Mironova *et al.*, 2005), which results in growth inhibition even at low MGO concentrations (Fraval and McBrien, 1980).

MGO accumulation is highly cytotoxic, and is associated with many oxidative stress-related conditions in humans, including aging, diabetes, atherosclerosis, and neurological disorders (Thornalley, 2008, Rabbani and Thornalley, 2010). The *gloA* encoded glyoxylase I, is the kinetically most important enzyme pathway for MG detoxification (Ferguson *et al.*, 1998). The fact that NemR is a HOCl-specific transcription repressor and the genes it regulates are essential for removal of toxic MGO eletrophile, led to the hypothesis that high level of HOCl stress causes the accumulation of MGO in bacteria.

To investigate the correlation between bleach stress and MGO production, Mike Gray measured the intracellular level of MGO in HOCl treated wild-type *E. coli* cells using HPLC. As illustrated in Figure 3.8A, after 30 min HOCl stress, *E. coli* cells accumulated a significant amount of MGO. The level of MGO in bleach treated cells was about twice more as compared to non-stressed cells. To test the ability of bacteria to combat MGO stress, I performed MGO survival assays. Aliquots of cells before and after treatment with 0.15 mM MGO were taken, serial diluted and spotted on LB growth plate. As shown in Figure 3.8B, deletion of the NemR repressor made *E. coli* cells significantly more resistant to MGO stress. In contrast, deletion mutants lacking the NemR-regulated *gloA* showed hypersensitivity towards MGO stress. These results suggest that the NemR-system is an effective response to detoxify MGO accumulation in HOCl-stressed cells. It is of note that NemR activity is not affected by MGO (Figure 3.6A), suggesting that a separate MGO-specific regulator controls *gloA* expression in the absence of HOCl.

In addition to GloA, we found several other MGO detoxification genes (*frmA, dkgA, yqhD,* and *hchA*) to be upregulated by HOCl (Appendix table 1) (Herring and Blattner, 2004, Jeudy *et al.*, 2006, Perez *et al.*, 2008, Subedi *et al.*, 2011). Both *dkgA* and *yqhD* genes encode NADPH-dependent reductases (Jeudy *et al.*, 2006, Perez *et al.*, 2008, Jarboe, 2011), while *hchA* encodes glyoxalase III (Subedi *et al.*, 2011). These latter three enzymes work independently of glutathione (GSH), and should remain active even after HOCl-mediated oxidation of the cellular GSH pool (Dukan *et al.*, 1999). To assess the

role that these proteins play in detoxifying MGO and protecting against bleach stress, we used *dkgA* or *yqhD* deletion mutants and tested their sensitivity towards HOCl or MGO treatment. As shown in Figure 3.8C, *dkgA* mutant strain had impaired resistance towards MGO treatment and showed significantly reduced viability in HOCl as compared to wild-type *E. coli*. These results illustrate the importance of GSH-dependent and independent MGO detoxification enzymes for HOCl-survival. Our results strongly suggest that HOCl treatment leads to MGO production, which requires rapid detoxification.

Surprisingly, a mutant lacking the MGO-producing enzyme MgsA also had a defect in HOCl stress survival (Figure 3.8C). This result suggested that MGO accumulation is not simply a toxic byproduct of HOCl treatment but that its synthesis in bacteria might serve a beneficial role in tolerating HOCl stress. It is known that MgsA's activity is stimulated by the accumulation of triosephosphates and lack of free phosphate (Booth *et al.*, 2003). It is of note that HOCl-mediated inactivation of glyceraldehyde-3-phosphate dehydrogenase (GAPDH) causes the accumulation of triosephosphates (Leichert *et al.*, 2008). Moreover, HOCl treated cells appear to be phosphate starved as indicated by the HOCl-induced upregulation of the *pho* regulon (Appendix Table 1). These results suggest that MGO production represents a protective response in bacteria, presumably by replenishing cellular phosphate reserves and ridding cells of glycolytic sugar phosphate intermediates, which have long been considered to be toxic (Booth *et al.*, 2003).

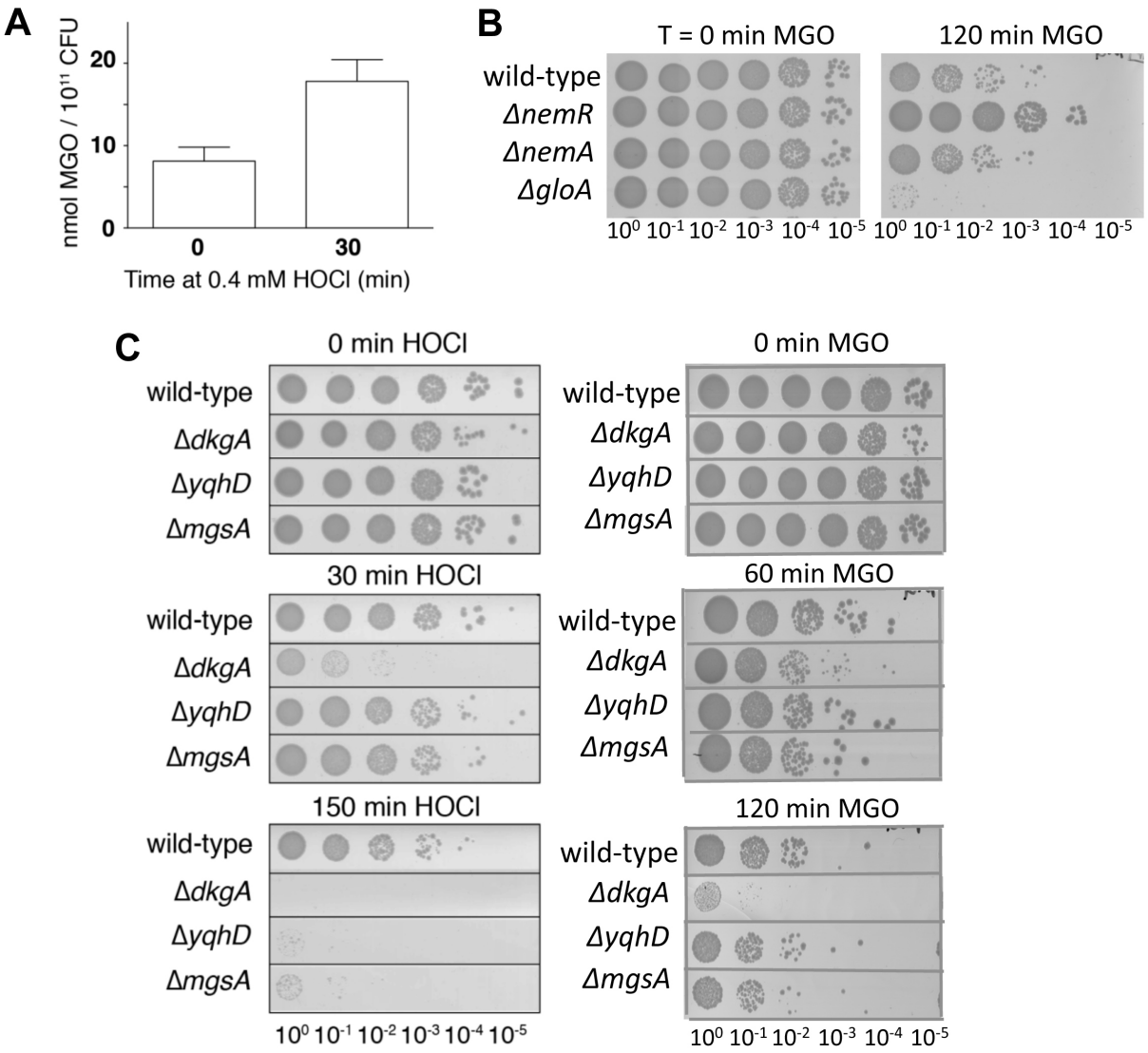

Figure 3.8. Role of MGO accumulation in HOCl stress. (**A**) *E. coli* MG1655 was incubated in MOPS minimal glucose containing 0.4 mM HOCl. Intracellular free MGO was measured by HPLC. (**B** and **C**) MG1655-derived strains were incubated in MOPS minimal glucose containing either 2 mM HOCl or 0.15 mM MGO, samples at indicated time pointes were diluted and spot-titered on LB agar. MGO measurement and HOCl survival assays were conducted by Mike Gray. MGO survival assays were performed by myself.

HOCl induces polyphosphate (polyP) formation

As mentioned previously, twelve genes associated with phosphate starvation response were significantly up-regulated in response to HOCl-treatment. These genes are *iraP, phoRABU, psiEF, pstSAB, yihX and ytfK* (Appendix table 1, EcoGene.org database). The finding that HOCl treatment decreases intracellular levels of free phosphate and leads to phosphate-starvation in bacteria was unexpected. Phosphate does not react with HOCl, and therefore should not be altered by bleach treatment. We thus hypothesized that redistribution of cellular phosphate pools might be responsible for the observed phosphate depletion. One possible fate is the formation of polyphosphate (polyP) crystals, which are synthesized from ATP in cells of all domains of life in response to a variety of stress conditions, (reviewed in (Rao *et al.*, 2009)).

To test our hypothesis, we first analyzed the polyP crystal formation by DAPI staining. *E. coli* wild-type cells were grown in MOPS minimal glucose medium until mid-log phrase and treated with 2 mM HOCl or 2 mM H_2O_2 for 30 min and then stained with DAPI and FM® 4-64. A fluorescence microscope was used to visualize DNA, cell membrane and polyP granules. As shown in Figure 3.9A, polyP crystals started to accumulate in HOCl treatment within 30 min. However, very little polyP was observed in cells treated with H_2O_2. This result suggested that intracellular polyP production is HOCl mediated. PolyP formation is achieved by transferring a phosphate from ATP to a growing polyP chain, and is primarily mediated by the enzyme polyphosphate kinase (*ppk* gene) (Akiyama *et al.*, 1992, Kornberg *et al.*, 1956). Since the depletion of intracellular ATP is

well documented in HOCl stress, we questioned whether the biosynthesis of polyP is cause of the observed ATP decrease or the inactivation of ATP-generating proteins, as previously assumed (Winter *et al.*, 2005). To test this idea, we performed *in vivo* ATP measurements in both wild type and *Δppk* deletion mutants, which are defective in polyP formation, and monitored cellular levels of ATP before and after HOCl treatment. As shown in Figure 3.9B, we observed an over 60% decline of ATP in *E. coli* wild-type cells within 30 min of HOCl treatment. In contrast, the cellular ATP pool of the *Δppk* deletion mutant decreased by less than 20%. These results revealed that polyphosphate kinase actively synthesizes polyP upon exposure to bleach, and that wild type *E. coli* cells re-directs over 40% of their cellular ATP pool to polyP production.

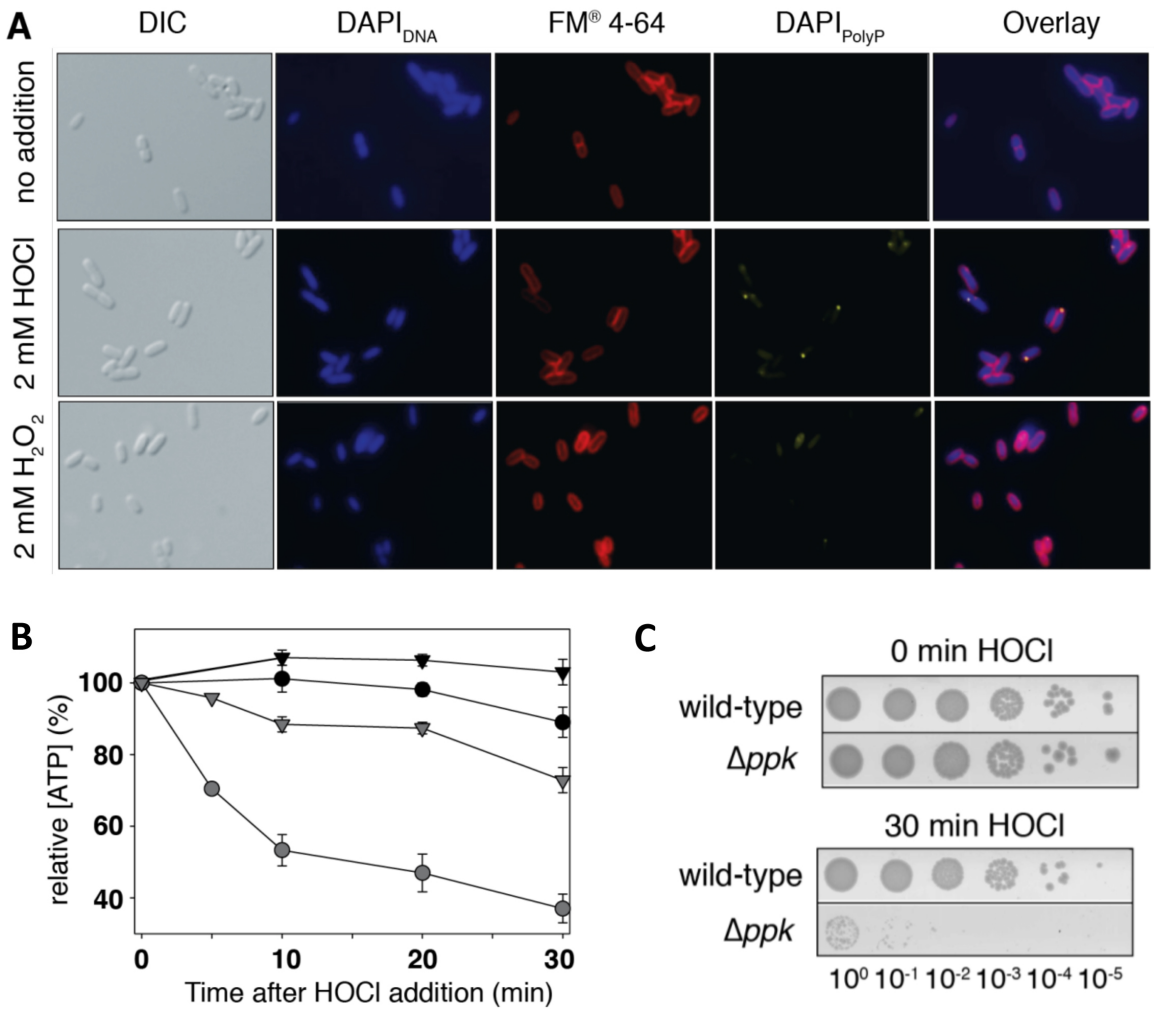

Figure 3.9. PolyP accumulation protects DNA against HOCl damage. (**A**) *E. coli* MG1655 was incubated 30 min in MOPS minimal glucose medium containing oxidants, stained with DAPI and FM® 4-64, and visualized by differential interference contrast (DIC) microscopy. DNA, cell membranes, and polyP granules were visualized by fluorescence microscopy. (**B**) Cellular ATP levels in MG1655 (circles) and the Δ*ppk* mutant (triangles) with 0 (black) or 1 mM (grey) HOCl. Concentration is expressed as a percentage of the initial value for each sample. (**C**) MG1655-derived strains were incubated in MOPS minimal glucose containing 2 mM HOCl, then diluted and spot-titered on LB agar.

Polyphosphate protects against oxidative DNA damage *in vitro*

To examine the role of polyP formation in bacterial bleach survival, we performed HOCl survival assay using the *E. coli* wild type and the *Δppk* deletion strain. As shown in Figure 3.9C, deletion of polyphosphate kinase made cells extremely sensitive to HOCl stress. This result demonstrated that the formation of PolyP crystals serves a highly protective role in bacterial bleach response. No single role has been established for the protective function of polyP (Achbergerova and Nahalka, 2011). Our microarray studies showed that HOCl treatment causes metal transport genes to be upregulated (Appendix Table 1). Excess of free metals, particularly iron, in combination with oxidants causes severe oxidative damages to many molecules, including DNA. As polyP are highly negatively charged, we hypothesized that polyP might be beneficial by chelating metal ions and preventing iron-mediated DNA damage. Highly reactive hydroxal radicals (OH•) are continuously generated by hydrogen peroxide (H_2O_2) in the presence of ferrous ions as catalyst (Fenton, 1894). HOCl also reacts with ferrous ions and generates free radicals in a Fenton-like reaction but in a much faster manner (Folkes *et al.*, 1995).

To investigate the protective role of polyP in iron-mediated oxidative DNA damage, I performed a DNA damage assay *in vitro*. Purified and linearized pBAD30 plasmid DNA was incubated with ferrous sulfate ($FeSO_4$) and H_2O_2, (*i.e.* Fenton reaction) in the presence or absence of various concentrations of polyP. After 45 min of incubation at 25°C, DNA samples were analyzed on 1% agarose gels. As shown in Figure 3.10A, DNA was completely degraded in the presence

of $FeSO_4$ and H_2O_2. In contrast, in the presence of polyP, DNA was completely protected against degradation. Notably, the equal molar ratio of monophosphates only slightly protected DNA against iron-mediated damage as shown in Figure 3.10B. These results demonstrate that polyP formation protects DNA against oxidative damage *in vitro*. A recent study has shown that tripolyphosphate and ATP stabilize iron and decrease of hydroxyl radical in Fenton reaction (Rachmilovich-Calis *et al.*, 2011). It is possible that ATP might prevent DNA degradation in a way similar to polyP. It remains now to be tested whether the same effects contribute to the protective effect of polyP formation *in vivo*.

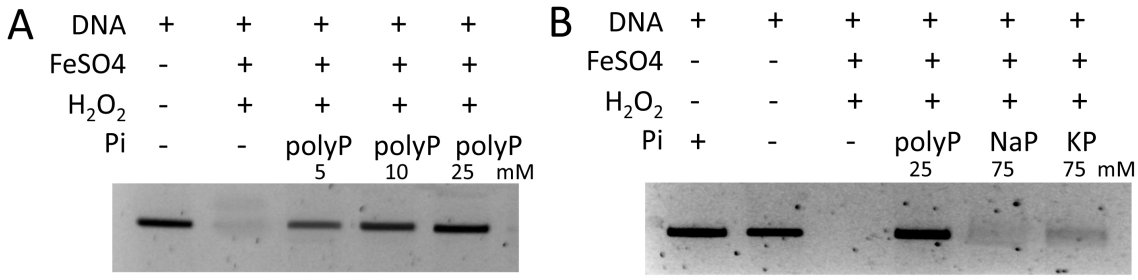

Figure 3.10. Polyphosphate protects DNA from Fenton mediated damage. (**A** and **B**) Linearized plasmid DNA (0.5 µM) was incubated 30 min at room temperature with $FeSO_4$ (50 µM), H_2O_2 (5 mM), and sodium polyP (25 mM, “polyP”), sodium phosphate (75 mM, "NaP"), or potassium phosphate (75 mM, "KP"), as indicated.

DISCUSSION

The potent oxidant HOCl is naturally produced by cells of the innate immune response as antimicrobial agent to kill invading pathogens, and is also the active component in household bleach. Previous studies have showed that HOCl induces widespread oxidative protein unfolding both *in vitro* and *in vivo* (Winter *et al.*, 2008). Moreover, upon exposure to HOCl, the cellular level of ATP decreases quickly, inhibiting ATP-dependent chaperones and enzymes (Winter *et al.*, 2005). Thus, HOCl impairs essential metabolic pathways by depleting ATP. Consistent with these results, we found that HOCl-treated bacteria induce the expression of numerous chaperones while down-regulating most ATP synthesis related genes.

Our metal content analysis nicely confirmed our microarray analysis, which suggested that metals released from aggregated proteins were pumped to the extracellular space during bleach stress. This result, however, differs from a separate study published by Gebendorfer *et al*. While their microarray results also indicated that many iron acquisition genes are down-regulated in the presence of HOCl, analysis of intracellular iron levels using electron paramagnetic resonance (EPR) measurements revealed unchanged iron levels in HOCl stressed cells (Gebendorfer *et al.*, 2012). One possible explanation for this discrepancy may be due to the differences in growth media. Gebendorfer *et al.* used LB rich medium as compared to the MOPS minimal glucose medium, which was used in this study. It is possible that cells grown in rich media have stronger and tighter cell membrane structures, which prevents iron from leaking

through permeases. Two main ingredients of LB media, yeast extract and tryptone, are complex mixtures of small peptides and other cellular components. Upon exposure to HOCl, peptide transporters are activated to assist newly protein synthesis (result of both studies). By doing so, it is possible that iron-containing peptides found in LB medium are transported into cytosol and hence increased intracellular iron level.

One main aspect of this microarray analysis was to identify HOCl-specific transcriptional regulators, which are necessary for bacteria to mount an effective HOCl response. Through the use of global expression profiling microarray studies, we identified two candidate genes. The first one is the transcriptional repressor NemR, which we have now shown to be a highly HOCl-specific, redox-regulated transcriptional repressor. The second regulator is a predicted transcriptional activator, YkgD, (Appendix table 1), whose downstream targets have not been functionally characterized. Deletion of YkgD makes cells highly HOCl-sensitive, suggesting that the downstream targets of YkgD, which ranked among the top five up-regulated genes in HOCl-treated cells, are essential for HOCl survival. The protective role of YkgD in response to HOCl stress remains to be identified in subsequence studies.

Two detoxification genes, whose expression is controlled by NemR, are encoded by *nemA* and *gloA*. Both of these genes encode proteins which are involved in aldehyde detoxification systems dedicated to reduce toxic aldehydes and electrophile methylglyoxal (MGO). Phenotypic studies revealed that *E. coli* strains lacking the *gloA* gene are highly sensitive towards bleach treatment

(Figure 3.5D). Together with the finding of MGO accumulation in HOCl treated wild type cells (Figure 3.7A), we can conclude that HOCl induces the MGO production. MGO is naturally occurring and enzymatically generated to release a phosphate from dihydroxyacetone phosphate (DHAP) in glycolytic pathway (Booth *et al.*, 2003). MGO synthesis requires a condition that is low in phosphate and high in DHAP (Hopper and Cooper, 1972), and the primary role of its production is to replenish free phosphate within the cell (Booth *et al.*, 2003). These results correlate well with our observation as HOCl causes phosphate starvation and inactivates GapDH, hence accumulating the substrates of methylglyoxal synthase.

Pathways in bacteria that facilitate MGO detoxification involve aldo-keto reductases (AKR), glyoxylase I (gloA gene), and glyoxalase II (gloB gene). A large group of NADPH-dependent oxidoreductases, including YqhD (also up-regulated in our microarray studies), belong to the AKR family. The Glucose-6-phosphate dehydrogenase (G6PD), an important enzyme that regenerates NADPH pool, is upregulated upon oxidative stresses, suggesting a disrupted intracellular NADPH pool and the cell's need to renew NADPH (Sandoval *et al.*, 2011, Pomposiello *et al.*, 2001, Blanchard *et al.*, 2007). These results suggested that the role of AKRs mediated MGO removal might be very limited in oxidative stress. It has long been known that the glyoxalase I and II work together to convert MGO to D-lactate in the presence of glutathione (GSH) (Cooper, 1984) and the system is the kinetically most important enzyme pathway for MG detoxification (Ferguson *et al.*, 1998). However, we did not observe the up-

regulation of glyoxalase II in our microarray studies (Appendix table 1). One recent report showed that the *gloB* deletion mutant had an impaired MGO detoxification but survived in a similar behavior as wild-type cells upon MGO stress, indicating that glyoxalase II may have only limited role in response to MGO (Ozyamak *et al.*, 2010). Given that NemR's transcription does not respond to MGO (Figure 3.6A), NemR-mediated MGO detoxification through GloA might be a HOCl-specific response, and not simply a consequence of sugar metabolism imbalance. Notably, the MGO synthase (*mgsA* gene) was slightly up-regulated in response to bleach treatment in our study, providing futher evidence that MGO production may has a beneficial role in bleach stress.

At this point, it is still unclear how NemR becomes activated in response to HOCl. Consistent with HOCl's high reactivity towards thiol groups, we found that NemR undergoes HOCl-specific oligomerization *in vivo*, indicating disulfide bond formation between two or more Cys residues on neighboring monomers (Figure 3.7A). Disulfide bond formation may possibly cause loss of repressor function, hence inducing gene expression. Homology searches revealed that NemR has six cysteines, of which one, cysteine 106 (C106), is absolutely conserved. Mike Gray, a postdoc in the lab, showed that C106 is critical for NemR's DNA binding activity. A NemR mutant variant containing only C106 acted very similar towards HOCl treatment as wild type NemR, suggesting that C106 is sufficient for HOCl sensing. In contrast, a NemR mutant variant lacking all six cysteines was constitutively de-repressed. A mutant that contained all but C106 was still reactive to HOCl but showed a much faster return to pre-stress repression,

suggesting that one or more of the non-conserved were needed. These results agree with my thiol trapping analysis, which suggested that C98 and C116 play a role in HOCl-mediated conformational change, which likely leads to de-repression (Figure 3.7B). Further experiments are necessary to elucidate the correlation between HOCl-mediated structural changes and functions.

The discovery that polyphosphates (polyP) accumulate in bacterial cells upon exposure to bleach was unexpected (Figure 3.9). PolyP is a chain of many hundreds or thousands of phosphates linked together by the same high-energy phosphoanhydride bonds found in ATP. Relatively little is known about polyP metabolism. Polyphosphate is a stable molecule that resists wide ranges of harsh conditions and is a rich energy source (reviewed in (Rao *et al.*, 2009)). The fact that *E. coli Δppk* mutant strains lacking the ability to generate polyP are severely impaired in HOCl survival (Figure 3.9C) clearly revealed the protective role of polyP in bleach stress. We have now demonstrated that polyP protects against iron-mediated DNA damage *in vitro* (Figure 3.10). These results suggest that polyP formation might be a programmed response, required to avoid the dangerous consequence of bleach insults. In a recent *Salmonella* intracellular infection study, macrophage-engulfed bacteria also showed increased glyoxalase I (*gloA*) expression, indicative of phosphate limitation (Eriksson *et al.*, 2003). These results implicate that GloA-induction and polyP formation is essential also during pathogenesis.

In conclusion, *E. coli*'s survival of HOCl treatment depends on fundamental changes in carbon and phosphate metabolism. MGO detoxification

plays a major role in HOCl survival, as does production of polyP, which protects DNA against metal-catalyzed oxidative damage. Both responses are universally conserved, suggesting that these pathways may be important for combating HOCl stress in both pro- and eukaryotic cells.

EXPERIMENTAL PROCEDURES

Bacterial strains and growth conditions

All *Escherichia coli* strains used in this study are listed in Table S3. *E. coli* was grown at 37°C in lysogenic broth (LB; Fisher) or MOPS minimal medium (Teknova) containing 0.2% glucose, 1.32 mM K_2HPO_4, and 10 μM thiamine. For experiments in which bacterial cultures were exposed to HOCl, all glassware was acid-washed. Where indicated, ampicillin was at 100 μg ml^{-1}, kanamycin was at 50 μg ml^{-1}, and chloramphenicol was at 12.5 or 34 μg ml^{-1}. Unless otherwise indicated, chemicals were purchased from Fisher or Sigma-Aldrich. Methylglyoxal (MGO) and *N*-chlorotaurine were synthesized as previously described and prepared fresh before each use (Kellum *et al.*, 1978, Peskin and Winterbourn, 2001).

Microarray expression and data processing

E. coli MG1655 was grown in MOPS minimal glucose medium at 37°C with aeration to an OD_{600} of 0.4 - 0.5, and HOCl was added to a final concentration of 400 μM. 0.5 ml samples were collected in liquid nitrogen immediately before, 5 min after, and 10 min after HOCl addition, and total RNA

was prepared using the RNeasy® Midi kit (Qiagen). cDNA synthesis, array hybridization to Affymetrix GeneChip *E. coli* genome 2.0 Arrays, and imaging were performed according to Affymetrix guidelines at the Affymetrix and Microarray Core facility at the University of Michigan, Ann Arbor. The raw images .DAT file and the raw averaged probe intensities .CEL files were received from the Core and the qualities of these raw data were analyzed using the "*affy"* package of Bioconductor implemented in R statistical language (Gentleman *et al.*, 2004). I wrote these scripts as part of a Bioinformatics course project (University of Massachusetts, Amherst), which was used to analyze quality controls of microarray data. The finalized results later went in the publication (Blanchard *et al.*, 2007). The scripts used in R command window were slightly modified and listed in table 3.1.

The first step of data processing is to convert the probe intensities into a readable format. In Affymetrix microarray, a probe set is a collection of 20 probes, located thought out the chip, designed to interrogate a given gene sequence. Bioconductor packages were first installed by typing the scripts (1-2) in an R command window. The R working directory, a folder contained all .DAT and .CEL files of microarrays to be analyzed, was set by typing script (3). Bioconductor would analyze only files stored in the working directory folder. Scripts (4) and (5) loaded affymetrix analysis library and read the .CEL files. The raw averaged probe intensities of each probe from each chip were then converted into a single value and stored in a temporary HOClarray.data file. To

ensure the data was loaded correctly, script (6) was used to display details of HOClarray.data file.

It is necessary to perform quality-checks on the unprocessed data before extensively data analysis is involved. An examination of the raw images for manufacturing defaults or artificially introduced errors, such as hair or dust, was the first step in the analysis. To examine probe intensities images for the chips in the dataset, the image function scripts (7-10) are used to generate a .pdf file contained all chip images. This step was memory and space intensive and took a while to finish. Boxplots was then used to examine probe-intensity distributions by using scripts (11-15) to generate a .pdf file. Once the quality of raw data was assured, to compare multiple microarrays, a normalization of all data was needed. Normalization reduces any possible systematic errors might occurred during process and brings probe intensities distribution of all chips to an equal, comparable range. Robust Multichip Average (RMA) normalization approach is a common and frequent used method to analyze multiple microarray expression profiles. The "*exprsso"* function implemented in Bioconductor was used to perform RMA background correction, normalization using the quantiles method, probe specific PM / MM correction using the pmonly method, and summary expression values using the medianpolish method. Scripts (16-19) were used to convert the HOClarray.data intensity data file into a normalized expression file, named HOClarray_exprsso.txt. Note that the expression values are log2-transformed data. These data can be converted to the natural scale by exponentiating (e.g., convert by using 2^x , where x is the expression value). The

up-to-date *E. coli* gene annotation file was then downloaded from the Affymetrix website and used to annotate the probes in the expression text file. All expression values of non-MG1655 probes (including pathogenic E. coli CFT073, EDL933, SAKAI and internal controls) were removed. Affymetrix chip was designed as a universal fit to evaluate more than one *E. coli* strains. Signals came from non-MG1655 probes were most likely due to non specific binding.

Table 3.1: Scripts used in R command window

Number	Script
1	source("http://www.bioconductor.org/getBioC.R")
2	getBioC()
3	setwd("/Users/weiyun/Microarray/FOLDER ")
4	library(affy)
5	HOClarray.data <- ReadAffy()
6	HOClarray.data
7	pdf("HOCldata_images.pdf")
8	par(mfrow=c(2,3))
9	image(HOClarray.data)
10	graphics.off()
11	pdf("BoxPlot-preNormal.pdf")
12	boxplot(HOClarray.data, col=c(1,1,1,0,0,0,8,8,8),
13	ylab=("Intensity", xlab="T=0min, T=5min, T=10min")
14	title("Before Normalization")
15	graphics.off()
16	HOCl.expresso <- expresso(HOClarray.data,
17	bgcorrect.method="rma",normalize.method="quantiles"
18	,pmcorrect.method="pmonly", summary.method="medianpolish")
19	write.exprs(HOCl.expresso, file="HOClarray_expresso.txt")

Gene expression clustering analysis

The TM4 MultiExperiment Viewer (MeV) software (Saeed *et al.*, 2003) was used to identify patterns of gene expression and differentially expressed genes. K-means clustering using Euclidean distance metrics implemented in MeV was used to classify the gene expression changes and patterns recognition. A total of

5298 MG1655 probes (4358 genes and 940 intergenic regions) were separated into 25 clusters with 100 iterations. The pattern of each cluster was evaluated based on three variables, untreated control and two log2 transformed ratios: untreated / 5 min after HOCl and untreated / 10 min after HOCl. Probes in each cluster have similar expression patterns to each other and dissimilar to those in other clusters.

Metal analysis

E. coli MG1655 was grown in MOPS minimal medium containing 0.2% glucose, 1.32 mM K_2HPO_4, and 10 μM thiamine until mid-log phase (OD_{600}=0.4-0.5) and treated with 400 μM HOCl. Cell aliquots before, and defines time points after treatment were collected in duplicate, then quenched with 1.5 mM sodium thiosulfate. Cells were washed three times with metal-free 10 mM MOPS buffer containing 1 mM EDTA, and once with sterile metal-free water to remove all extracellular metals. Then, cells were completely dehydrated using a 98°C heating block and resuspended (adjusted to $2x10^9$ cell/ml) in metal-free 30% nitric acid at 65°C. Intracellular metal contents were analyzed using the Inductively Coupled Plasma-High Resolution Mass Spectrometry (ICP-HRMS) at Keck Elemental Geochemistry Laboratory in the department of Geological Sciences, University of Michigan.

In vivo thiol trapping with IAM

Bacterial strains were cultivated in MOPS minimal glucose media containing 0.2% glucose, 1.32 mM K_2HPO_4, and 10 μM thiamine at 37°C until OD_{600} of 0.4–0.5 and treated with the indicated oxidants. Before and after the stress treatment, aliquots of 1 ml cells were taken and acidified with trichloroacetic acid (TCA) to a final concentration of 10%. After 30 min of incubation on ice, precipitated proteins were pelleted by centrifugation (13, 000 rpm, 20 min, 4°C). The protein pellet was resuspendend in DAB buffer (6 M Urea, 200 mM Tris-HCl pH 8.5, 10 mM EDTA, and 0.5% w/v SDS) supplemented with 0.8 M iodoacetamide (IAM) to irreversibly alkylate all reduced cysteines. Samples were incubated for 30 min at 25°C, then supplemented with non-reducing Laemmli-buffer. Protein samples were analyzed with 12%-Tris TGX gels (Bio-Rad) and visualized with anti-his westernblot.

In vitro DNA damage assay

Assay conditions were modified from (Zhao *et al.*, 2002). Plasmid pBAD30 (4.9kb)(Guzman *et al.*, 1995) was linearized with *Eco*RI (FastDigest, Fermentas). A typical 20 μl reaction contained 0.5 μM DNA in 20 mM Tris buffer (pH 7.5), 50 μM ferrous sulfate ($FeSO_4$-$7H_2O$), and 5 mM hydrogen peroxide (H_2O_2, Fisher Scientific) in the absence or presence of the indicated concentrations of sodium polyphosphate (Acros), sodium phosphate (Fisher Scientific) or potassium phosphate (Fisher Scientific). The concentration of polyP was calculated using the molecular mass of a tri-phosphate (367.9 g/mol) as reference. A large batch

of DNA in Tris buffer was made and split into 5 reactions: one left untreated as loading control, one with $FeSO_4$ and H_2O_2 as damage control, and three with different phosphate additions to examine DNA protective effects. Following incubation at room temperature for 30 min, 3 µl 6x loading dye was added to stop reactions and DNA samples were immediately analyzed using 0.8% agarose gel electrophoresis.

Hypochlorous acid survival assays

E. coli strains were grown at 37°C with aeration in 10 ml MOPS minimal medium containing 0.2% glucose, 1.32 mM K_2HPO_4, and 10 µM thiamine to an OD_{600} of 0.4 - 0.6, then harvested by centrifugation. Cells were then resuspended to an OD_{600} of 0.35 in 10 ml fresh medium containing 2 - 3 mM HOCl in acid-washed 125 ml baffled flasks and incubated at 37°C with shaking at 200 rpm. Aliquots of cells (0.5 ml) were harvested immediately before and at time points 30 min to 5 hours after addition of HOCl by centrifugation (2 min @ 16,000 x g), rinsed with MOPS minimal medium containing 10 mM sodium thiosulfate, but no glucose, K_2HPO_4, or thiamine, then stored at 4°C until the completion of the time course. 10-fold dilution series of each sample in 0.9% NaCl were performed using a Precision XS Microplate Sample Processor (Bio-Tek), which also spotted 5 µL aliquots of each dilution on LB agar plates, which were incubated overnight at 37°C. HOCl stress tolerance of each strain was tested at least 6 times. Absolute survival after 0.5 to 5 hours in 2 - 3 mM HOCl varied from day to day,

but relative survival between mutants and wild-type was consistent, and representative results from an experiment performed on a single day are shown.

Reverse transcriptase PCR analysis

E. coli strains were grown at 37°C with shaking (200 rpm) to an OD_{600} of 0.45 in MOPS minimal medium containing 0.2% glucose, 1.32 mM K_2HPO_4, and 10 μM thiamine, then oxidants were added as described in the text. Samples (0.5 ml) were collected at the indicated times and immediately frozen in liquid nitrogen. RNA was prepared from the cells using the RNeasy® Mini kit (Qiagen) and contaminating DNA was removed using the DNA-free™ kit (Ambion). SuperScript® III reverse transcriptase (Invitrogen) was used to generate cDNA and reverse transcriptase PCR reactions were set up using SYBR® GreenER™ qRT-PCR mix (Invitrogen). RT-PCR reactions were run on a Mastercycler® ep realplex^2 real-time PCR system (Eppendorf).

Expression ratios for the tested genes after addition of oxidants were calculated in comparison to expression of each gene in uninduced MG1655 cultures by the $\Delta\Delta C_t$ method (Pfaffl, 2001). Expression of the tested genes was normalized to expression of *rrsD*, encoding 16S rRNA, the expression of which did not change under the conditions tested here (not shown).

Gel mobility shift assays

Gel mobility shift assays were performed using a 222 bp fragment of *E. coli* MG1655 genomic DNA containing the *nemR* promoter region (P_{nemR}). P_{nemR}

was PCR amplifed using primers [33] and [34], then purified using the Qiagen PCR purification kit. Different amounts of purified NemR protein (as indicated) were incubated in an anaerobic chamber (Coy Laboratory Products, Inc.) with 0.1 pmol of P_{nemR} for 30 min at 37°C in the presence of 10 mM Tris-HCl (pH 7.8 @ 4°C), 150 mM NaCl, 3 mM magnesium acetate, and 10% glycerol with or without the addition of 2 mM DTT, then immediately separated by electrophoresis (100 V for 1.5 h) on 10% TBE-PAGE gels (Bio-Rad). DNA fragments were stained with ethidium bromide and visualized by UV fluorescence.

Microscopy to visualize polyphosphate granules

E. coli cultures were prepared as described above for HOCl survival assays, stained (10 min @ 25°C) with 50 μg ml^{-1} 4'-6-diamidino-2-phenylindole (DAPI) and 1 μg ml^{-1} N-(3-triethylammoniumpropyl)-4-(6-(4-(diethylamino)phenyl)hexatrienyl)pyridinium dibromide (FM® 4-64) (Molecular Probes), then fixed to glass slides using poly-L-lysine and Citifluor mountant media (Ted Pella, Inc.). Cells were visualized by differential interference contrast (DIC) microscopy, and DNA, polyP granules (Aschar-Sobbi *et al.*, 2008), and cell membranes were visualized by fluorescence microscopy using the 100X oil immersion objective of an Olympus BX61 upright microscope (Olympus America, Inc.) controlled by the Metamorph Basic software package (v. 7.7.2.0)(Molecular Devices, Inc.). DNA was visualized by DNA-DAPI fluorescence (387 ± 11 nm excitation, 440 ± 40 nm emission), polyphosphate granules were visualized by polyphosphate-DAPI fluorescence (420 ± 40 nm ex., 535 ± 30 nm em.)(Aschar-

Sobbi *et al.*, 2008), and cell membranes were visualized by FM® 4-64 fluorescence (560 ± 25 nm ex., 607 ± 34 nm em.).

Quantification of intracellular free methylglyoxal

Intracellular free MGO in *E. coli* cultures was measured using a modification of a previously described HPLC method (Subedi *et al.*, 2011). *E. coli* strains were grown at 37°C with aeration to an OD_{600} of 0.45 in filter-sterilized (0.2 µm) MOPS minimal medium containing 0.2% glucose, 1.32 mM K_2HPO_4, and 10 µM thiamine, then HOCl was added to a final concentration of 400 µM. Aliquots of cells (10 ml) were harvested immediately before and 30 min after addition of HOCl by centrifugation (10 min @ 3,000 x g @ 4°C), rinsed with cold phosphate-buffered saline containing 10 mM sodium thiosulfate (PBS-st), then resuspended in 4.5 ml cold PBS-st. Cells were lysed by sonication (2 min at 5 sec on, 5 sec off on ice), 0.5 ml of 5 M perchloric acid was added, samples were incubated 10 min on ice, then centrifuged 10 min @ 15,000 rpm @ 4°C. Supernatants were derivatized at 20 °C for 4 h with 500 nmol of *o*-phenylenediamine (*o*-PD) and 2.5 nmol of 5-methylquinoxaline (as an internal standard), then desalted with 1 ml C18 Sep-Pak cartridges (Waters), dried overnight under vacuum, and resuspended in 200 µL of 82% (v/v) 10 mM KH_2PO_4, 18% (v/v) acetonitrile.

2-Methylquinoxaline (2-MQ), the quinoxaline derivative of MGO, and the 5-MQ internal standard were detected by reverse phase HPLC separation of 100 µL samples, using a Waters™ 2690 Separation Module equipped with an 4.6 x

250 mm C18 column (GRACE/Vydac®) and a Waters™ 996 Photodiode Array Detector. The mobile phase was 82% (v/v) 10 mM KH_2PO_4, 18% (v/v) acetonitrile. Quinoxalines were detected by their absorbance at 315 nm and quantified using standard curves of 2-MQ and 5-MQ, as appropriate. 2-MQ and 5-MQ eluted at 9.8 and 16.1 min, respectively.

In vivo ATP measurements

In vivo ATP measurements were carried out as described by Yang *et al*. (Yang *et al.*, 2002). Briefly, MG1655 wild-type or Δ*ppk* deletion cells were grown in MOPS minimal medium containing 0.2% glucose, 1.32 mM K_2HPO_4, and 10 µM thiamine at 37°C to an OD_{600} of approximately 0.5, at which point cells were treated with 1 mM HOCl. At the indicated time points 100 µl bacterial culture was added to 900 µl boiling 40 mM HEPES (pH 7.8), 4 mM $MgSO_4$ and rapidly shaken for 4 min at 99°C. After boiling, the samples were transferred on ice, and the total ATP content was determined using a luciferase activity assay. For this 50 µl sample were transferred in triplicate in a 96 well plate format. 150 µl assay buffer (140 µM luciferin, 0.1 µM luciferase, 0.1 mg ml^{-1} BSA in 100 mM KH_2PO_4 pH 7.8, 25 mM glycylglycine, 0.2 mM EDTA) was added and bioluminescence was recorded for 2 min.

CHAPTER IV

Conclusions and future directions

Failure of organisms to protect themselves against molecular damage mediated by hypochlorous acid (HOCl) stress can be lethal. The severe damage caused by the highly reactive oxidant HOCl leads to protein unfolding and aggregation, DNA fragmentation, lipid peroxidation and eventually cause cellular death. In human innate immune cells, myeloperoxidase-mediated HOCl generation in response to the phagocytosis of invading pathogens is utilized to kill the pathogens (Klebanoff, 2005, Winterbourn *et al.*, 2006). However, a plethora of uncontrolled HOCl production causes injuries to the surrounding tissue and can lead to human chronological inflammatory diseases (Pattison *et al.*, 2012, Prokopowicz *et al.*, 2012).

At this point it is not fully understood how invading pathogens can protect themselves against the oxidative insults and survive exposure to HOCl stress. Elucidating the ability of bacteria to respond to HOCl treatment has the potential to develop novel antimicrobial strategies and perhaps to identify conserved repair pathways associated with chronic inflammatory diseases. In my thesis, I report about response systems that bacteria have developed to enhance their survival

upon exposure to HOCl. Major questions, however, remain to be answered as outlined below.

V. cholerae Hsp33 null mutant is temperature sensitive

The heat shock protein Hsp33 is a redox-regulated chaperone, which is highly conserved in bacteria as well as in a few pathogenic eukaryotes (Winter *et al.*, 2005, Jakob *et al.*, 1999). Hsp33 has been shown to protect bacteria against many different oxidative stress conditions, including HOCl stress (Winter *et al.*, 2008, Winter *et al.*, 2005). Activation of Hsp33 requires both oxidative and protein-unfolding conditions, which is either achieved upon incubation with fast acting HOCl or by combining the slow oxidant H_2O_2 with unfolding conditions such as heat shock temperatures (Ilbert *et al.*, 2007, Winter *et al.*, 2008). The temperature sensitive phenotype of a *V. cholerae ΔhslO* mutant was hence unexpected, as heat or H_2O_2 alone cannot activate Hsp33 *in vitro*, and because that corresponding *E. coli ΔhslO* mutants do not exert a growth defect at elevated temperature. My finding that the temperature sensitive growth phenotype of the *V. cholerae ΔhslO* mutant is strictly oxygen dependent raised the question whether *V. cholerae* might be already more oxidatively stressed than *E. coli* cells under normal aerobic growth conditions.

To examine the potential difference(s) in the *in vivo* oxidant levels of wild type *E. coli* and *V. cholerae* strains, I first utilized the hydrogen peroxide sensor protein HyPer, which is a ratiometric fluorescent probe, comprised of an OxyR-YFP fusion protein. HyPer changes its fluorescence excitation maxima upon

peroxide-mediated oxidation and can be used to determine endogenous peroxide levels (Belousov *et al.*, 2006). Unfortunately, the high expression of plasmid-encoded HyPer led to rapid aggregation in *E. coli*, making this analysis impossible. I thus performed the quantitative *in vivo* thiol trapping technique OxICAT (Leichert *et al.*, 2008) to compare the oxidation status of cysteine thiols in *E. coli* and *V. cholerae* wild type strains as read-out for intrinsic oxidative stress levels. Both bacterial strains showed high levels of protein thiol oxidation under aerobic growth conditions in LB medium at 37°C, which was not significantly different in these strains. This leaves the question open as to whether higher levels of oxidants exist in *V. cholerae* that are responsible for triggering the activation of Hsp33 at elevated temperature. To further test this question, one could overexpress the peroxide-detoxifying catalase in the *V. cholera ΔhslO* mutant strain and analyze the temperature sensitivity of this strain. As the heat alone cannot activate Hsp33, one would expect to observe no growth defect in *V. cholera ΔhslO* mutants, which are equipped with a higher capacity to detoxify oxidants. To directly examine the intracellular levels of oxidant, one possibility is to make use of another plasmid-encoded ratiometric redox-sensitive probe, such as the HOCl-probe-1 or roGFP and compare their oxidation ratios in *E. coli* and *V. cholerae* wild type stains under normal aerobic growth condition (Yuan *et al.*, 2012, Hanson *et al.*, 2004). The caveat of this approach is the solubility levels of these probes when expressed in different bacteria.

EF-Tu is a major client protein of Hsp33 in *V. cholerae*

By using a genetic library screen, I found that both temperature and HOCl sensitive phenotypes of *V. cholerae* Hsp33 deletion mutant were fully abrogated when the mutant bacteria expressed the *E. coli* elongation factor EF-Tu. This result suggested that presence of *E. coli* EF-Tu is important for survival and that *V. cholerae* EF-Tu is likely an essential target of protection guarded by Hsp33 under HOCl stress. By protecting a single crucial HOCl-stress sensitive protein against stress-mediated unfolding and degradation, Hsp33 apparently provides enhanced HOCl-stress tolerance to bacteria, such as *Vibrio*. It would be now interesting to know, which protein is the essential client protein of Hsp33 in *E. coli*. To address this question, one could treat *E. coli* cells expressing a tagged version of Hsp33 with HOCl and crosslink the total cellular proteins at different time points after the treatment. Client proteins bound to tagged-Hsp33 can be subsequently purified and identified with mass spectrometry (MS). To examine whether these newly identified client proteins are essential, one could compare them to the lists of *E. coli* essential proteins that have been previously established (Baba et al. 2006)(Butland *et al.*, 2005). If *E. coli* has a single survival factor protein, activated Hsp33 would preferentially protect it at an earlier time point.

Does *E. coli* EF-Tu act as chaperone *in vivo*?

The finding that expression of *E. coli* EF-Tu rescues the growth phenotype of the *V. cholerae ΔhslO* mutant strain suggested that the complementing *E. coli*

EF-Tu might function as a chaperone, analogous to Hsp33. Previous *in vitro* studies showed that purified elongation factor EF-Tu protects commonly used chaperone substrates against aggregation and assists protein refolding, suggesting that EF-Tu might be a potential chaperone (Caldas *et al.*, 1998, Kudlicki *et al.*, 1997). However, I was unable to find any increased stabilization or decreased aggregation in response to heat or HOCl stress for any other *Vibrio* protein in *hslO* deletion mutants expressing *E. coli* EF-Tu using solubility and aggregation assays. It is possible that these assay are not sensitive enough to show differences in protein levels in Coomassie blue-stained SDS PAGE as it is difficult to detect small variations in protein levels by naked eye, especially when protein bands are comprised of several proteins. A more advanced method to detect changes in solubility would be to use two-dimensional SDS gel electrophoresis, which allows much better separation and quantification of each protein. Levels of HOCl-mediated protein aggregates in the *V. cholerae hslO* deletion mutant and the corresponding strain complemented with *E. coli* EF-Tu would be compared and assessed.

One possible scenario is that *E.coli* EF-Tu is more HOCl-resistant and "simply" functions by replacing *V. cholerae* EF-Tu as a translation factor. To address this possibility, we generated a translational-inactive variant of *E. coli* EF-Tu (i.e., EF-Tu^{Q97P}), which has been previously shown to be unable to form ternary complexes with aminoacyl-tRNA (Navratil and Spremulli, 2003). This mutagenesis was very challenging to perform as the mutation (as well as mutations for other translational inactive mutants) resided in a highly GC-rich

region of the EF-Tu gene. Once we transformed this mutated *E. coli* EF-Tu variant into *V. cholerae ΔhslO* mutant and tested growth phenotypes, we did not observe any effect of the mutant EF-Tu on our *ΔhslO* phenotype. As shown in figure 4.1, however, analysis of the protein expression level using western blot showed that the EF-Tu^{Q97P} expression levels were much lower in the *hslO* deletion strain as compared to wild type *V. cholerae.* This mutant *E. coli* EF-Tu variant appears to be highly sensitive to oxidative degradation in *V. cholerae* and requires the presence of Hsp33 for stabilization. Thus, I was unable to directly evaluate the role that enhanced translation rates exerted by *E. coli* EF-Tu in the *V. cholerae hslO* deletion mutant might play. Yet, we did not find any major discrepancy in the rate of protein translation in the *V. cholerae ΔhslO* mutant strain, which expresses much lower levels of EF-Tu as compared to the wild type strain using pulse chase experiment. In addition, we also found that presence of *E. coli* EF-Tu protects already synthesized *V. cholerae* EF-Tu against protein degradation under HOCl stress, where new protein synthesis is stalled. Thus, it is very unlikely that *E. coli* EF-Tu works simply by increasing the rate of *V. cholerae* EF-Tu translation.

However, to ultimately address this question, one could perform pulse chase experiments to uncouple the rate of translation and protein degradation. *V. cholerae ΔhslO* mutant and its derivative strain overexpressing plasmid-encoded *E. coli* EF-Tu will be cultivated either at elevated temperature or in the presence of HOCl. If *E. coli* EF-Tu rescues the growth defect of *V. cholerae ΔhslO* mutant by replacing *V. cholerae* EF-Tu as a translation factor, plasmid-encoded

expression of *E. coli* EF-Tu would increase the level of protein translation in *V. cholerae ΔhslO* mutant strains. In contrast, if *E. coli* EF-Tu acted as a chaperone *in vivo*, one would expect to see that addition of *E. coli* EF-Tu reduced protein degradation in Hsp33 depleted *V. cholerae* stain at either heat shock or HOCl stress. If *E. coli* EF-Tu exploits both protein translation and chaperone activity in *V. cholerae ΔhslO* mutant, protein synthesis inhibitor, for instance tetracycline or chloramphenicol, can be used to dissect that which functions may play more important role under HOCl stress. By adding chloramphenicol to HOCl treated *V. cholerae ΔhslO* mutant expressing plasmid-encoded *E. coli* EF-Tu, if the chaperone activity is essential to protect *V. cholerae* against protein aggregation, the growth phenotype of this mutant should not be altered by protein translation inhibitor. However, if the protein translation activity of *E. coli* EF-Tu is necessary to restore cells' recover, the inhibited-*E. coli* EF-Tu would fail to rescue the stress-sensitive phenotype of *V. cholerae ΔhslO* mutant.

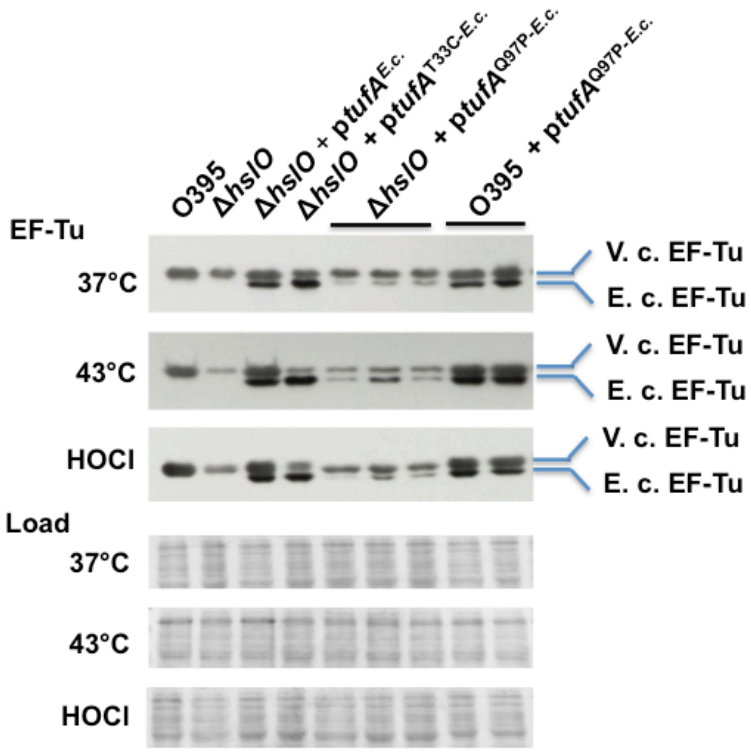

Figure 4.1. Analysis of *E. coli* EF-Tu variants protein level in *V. cholerae*. Wild type *V. cholerae* O395 or the *hslO* deletion strain containing plasmids encoding either wild type *E. coli* EF-Tu, EF-Tu^{T33C} or different clones of the translationally inactive EF-Tu^{Q97P} were cultivated at 37°C or 43°C until mid-log phase was reached. To evaluate the effects of HOCl on cellular EF-Tu levels, the 37°C cultures were split and either left untreated or incubated with 3 mM HOCl for 20 min. To analyze the steady state levels of EF-Tu in these strains, cell aliquots were taken and the proteins were separated by SDS-PAGE. EF-Tu was visualized by Western blot using antibodies against *E. coli* EF-Tu. As shown in this figure, levels of *E. coli EF*-Tu^{Q97P} in O395 are very high while the same clones transformed into the *hslO* deletion strain harbor very little soluble protein. This result suggests that the translationally inactive *EF*-Tu^{Q97P} variant is unstable in *hslO* deletion strains of *V. cholerae*.

Analysis of the *in vivo* thiol status of EF-Tu

We found that *V. cholerae* EF-Tu is exquisitely more sensitive to HOCl than *E. coli* EF-Tu and forms disulfide-linked high molecular weight complexes upon oxidative stress treatment. Moreover, I showed that expression of *E. coli* EF-Tu stabilizes *V. cholerae* EF-Tu levels *in vivo* under stress conditions, which

is likely the reason for its ability to confer enhanced HOCl tolerance in *V. cholerae*. Introduction of Cys33 (the only additional cysteine residue in *V. cholerae* EF-Tu) into the *E. coli* EF-Tu protein increased the oxidative stress sensitivity of *E. coli* EF-Tu and abrogated its protective function when expressed in the *V. cholerae ΔhslO* mutant strain. This result suggested that presence of Cys33 confers oxidative stress sensitivity to EF-Tu.

To examine the conservation of this cysteine, I performed a Position-Specific Iterative BLAST (PSI-BLAST) search, which is a method that is more sensitive in selecting distant evolutionary relationships than a standard protein-protein BLAST search (http://www.ncbi.nlm.nih.gov/blast). I used the *E. coli* EF-Tu protein sequence as query running with 5 iterations with 500 maximal sequences. I did not identify a single sequence that contains a cysteine at the corresponding position. This suggests that this cysteine residue is not evolutionary conserved. I also performed a normal protein-protein BLAST and found that only within the six different orders under *proteobacteria gamma subdivision* class, sequences from the *Vibrionaceae* order have a cysteine residue at the corresponding position, while all other sequences have a threonine residue. I then performed a protein-protein BLAST using *V. cholerae* EF-Tu as query. Again, only 32 sequences belonging to the *Vibrionaceae* order were found to have the cysteine at that position. None of the other sequences have a cysteine at this or nearby positions. These results suggest that this cysteine acquisition of *V. cholerae* might be a recent event in evolution.

It is possible that wild type *E. coli* EF-Tu forms complexes with *V. cholerae* EF-Tu, which in turn stabilizes *Vibrio* EF-Tu and prevents its premature degradation in the *hslO* deletion mutant. To directly test this model, co-immunoprecipitation could be performed. A tagged *E. coli* EF-Tu or EF-Tu^{T33C} variant would be expressed in the *V. cholerae ΔhslO* mutant strain. Cells will be treated with HOCl. If wild type *E. coli* EF-Tu formed complexes with *V. cholerae* EF-Tu, two EF-Tu bands (*V. cholerae* and *E. coli* EF-Tu are distinguishable on 12% SDS-PAGE) will be observed on western blot. Since expression of *E. coli* EF-Tu^{T33C} variant does not exert a cytoprotective function during HOCl stress, one would not expect to observe *V. cholerae* EF-Tu to co-immunoprecipitate under HOCl stress.

NemR repressor is a HOCl-specific transcription regulator

Transcriptional expression profiling using microarrays in *E. coli* in combination with qRT-PCR analysis and biochemical studies revealed the protein NemR as a highly conserved, HOCl-specific regulator in bacteria. Downstream targets of NemR include the glyoxylase GloA, which appears to protect cells against HOCl by detoxifying methylglyoxal that accumulates in response to HOCl treatment. NemR belongs to the TetR family of transcriptional repressors and is highly conserved in many different bacteria. By working with Mike Gray, a postdoc in the lab, we confirmed that HOCl is the main activator of NemR as exposure to other physiologically relevant oxidants did not affect the transcription level of *nemR* or NemR's target genes. An *E. coli* mutant strain

lacking the NemR repressor showed slightly increased HOCl resistance while mutants lacking the downstream target genes, *nemA* or *gloA* showed significantly reduced tolerance towards HOCl stress.

These results suggested that NemR mediated methylglyoxal (MGO) elimination is one of the cellular strategies to dampen HOCl-mediated toxicity. Notably, the MG-detoxifying enzyme glyoxylase is universally conserved and might play a role in mammalian HOCl-detoxification as well (Munch *et al.*, 2010). These results suggest that we have identified the first HOCl-specific transcriptional regulator in bacteria. Overexpression of the regulator YjiE has been recently suggested to enhance HOCl survival in *E. coli* (Gebendorfer *et al.*, 2012). However, given that HOCl cannot directly activate YjiE protein *in vitro*, it remains questionable whether this regulator is indeed a HOCl-specific transcriptional regulator. Potentially, YjiE could sense secondary effects mediated by HOCl and thus be activated in cells upon exposure of HOCl.

What is the activation mechanism NemR regulator?

Our studies demonstrated that NemR is exquisitely sensitive to HOCl-mediated oxidation and is important for increasing the cellular tolerance towards bleach stress. Given that HOCl reacts very rapidly with cysteine residues in proteins, it is likely that NemR utilizes some type of oxidative thiol modification to regulate its DNA binding activity. Examination of its amino sequence revealed that NemR contains six cysteines. I performed *in vivo* thiol trapping experiment to examine the possibility that NemR undergoes HOCl-mediated disulfide bond

formation *in vivo*. Indeed, in the presence of HOCl and low expression levels of NemR, disulfide-crosslinked NemR dimers were detected. NemR tetramers were detected under high NemR expression levels, suggesting that high concentrations of NemR, the proteins associate into higher oligomerization states. The accompanying conformational changes in NemR might cause loss of NemR's DNA binding activity and therefore induce gene expression. At this point, however, no correlation between the observed structural changes upon HOCl treatment and NemR's function can be made. It remains to be tested, which oligomer configuration will apply to NemR at its physiological concentration upon exposure of HOCl treatment. A purified anti-NemR antibody is now available that can be used to monitor the *in vivo* thiol status of endogenous NemR before and after bleach treatment.

The mechanism promoting the HOCl-mediated activation of NemR remains unclear. The absolutely conserved cysteine 106 in NemR appears to be critical for its DNA binding activity as well as for HOCl-sensing. My *in vivo* thiol trapping experiment showed that oligomer formation of NemR upon HOCl treatment was abrogated in NemR mutant variants lacking C98 or C116. These results suggest that several cysteines are oxidized by HOCl and might be involved in inactivating the NemR repressor. Further experiments aimed to elucidate the role of individual cysteines in NemR's regulation are clearly needed. One could conduct differential thiol trapping experiments using single and double cysteine variants of NemR to address this question.

Although cysteines are most likely to be involved in the redox regulation of NemR, it is also possible that methionine oxidation plays a role. An *in vitro* activity assay showed that *E. coli* GroEL is inactivated through methionine oxidation, indicating that oxidative modification of methionine also leads to functional activity changes of proteins (Khor *et al.*, 2004). It would be interesting to explore whether methionine oxidation is involved in the redox regulation of NemR. One could cultivate bacteria in methionine-free medium containing norleucine, the carbon-containing analog, and determine whether methionine-free NemR is still responsive to HOCl treatment (Luo and Levine, 2009). MS/MS analysis is another good way to examine potential oxidative modifications on methionine residues in HOCl-treated NemR. Understanding what oxidative modifications are present in NemR upon exposure to HOCl would provide the necessary clues as to the mechanism by which HOCl regulates NemR's activity.

Analysis of the protective role of polyphosphates

My genome-wide transcriptional microarray analysis reveled that HOCl-treated cells are phosphate starved while polyphosphate crystals accumulate. Mike Gray discovered that deletion of polyphosphate kinase (*ppk* gene), which catalyzes polyphosphate formation, makes bacteria extremely sensitive to HOCl stress, indicating that polyphosphate plays a an oxidative stress-protective role in bacteria. By conducting *in vitro* DNA damage assay, I showed that polyphosphates protect DNA against oxidative damage mediated by the Fenton reaction. The *in vivo* significance of this finding remains now to be tested.

The integrity of genomic DNA can be assessed by whole cell DNA damage assays, which use an agarose gel-based technique to visualize damaged DNA (Jeong *et al.*, 2008). Fragmentation of DNA *in vivo* can be examined by using the Apo-Direct Kit, which uses terminal transferases to add specific fluorescein dyes on each 3′-hydroxyl ends of DNA (Erental *et al.*, 2012). The degree of DNA fragmentations is then measured by the intensity of fluorescence. Alternatively, fragmentation of DNA can be visualized with DAPI staining (Kumar *et al.*, 2011). The broken DNA pieces appear as many small "crumbles" within the cell as compared to an evenly distributed smooth area in untreated control bacteria. Other common DNA damages are lesions and crosslinks, which can be quantified with long range PCR (Macomber *et al.*, 2007). The primers are designed to amplify a 10-kilobase region from any genomic DNA template. Any damages to the template would stall PCR polymerase and reduce the product yield. To elucidate whether polyphosphates play a role in protecting DNA *in vivo*, these assays should be performed in wt and *ppk* deletion mutant strains in the absence and presence of HOCl stress.

Relatively little is known about polyphosphate metabolism and its function. It is possible that polyphosphate exerts its protective power on other cellular macromolecules in addition to DNA. As *ppk* deletion mutants treated with HOCl accumulate higher levels of chaperones (M. Gray, personal information), it is conceivable that polyphosphate protects proteins against HOCl- or MGO-induced protein unfolding. Standard *in vitro* chaperone activity assay can be performed as pilot studies to examine whether polyphosphate has the ability to prevent protein

aggregation *in vitro*. If this proves to be the case, one could conduct *in vivo* solubility and aggregation assay to examine levels of HOCl-mediated protein aggregation. Comparison of wild type bacteria and *ppk* deletion strains will reveal whether polyphosphate accumulation plays a role in protecting proteins against oxidative unfolding mediated by HOCl.

Other unknown cellular responses against HOCl stress

Only 5% of *E. coli* genes were significantly upregulated in response to HOCl from the total gene pool of *E. coli*, indicating that bacterial cells have a very specific transcriptional profile upon exposure to HOCl. What we investigated here in more detail is only the tip of the iceberg, as 81 of the discovered genes (36%) are categorized to have no known function. The main goal of this microarray study was to identify HOCl-specific transcriptional regulator(s), which are essential for bacteria to protect against HOCl stress. In addition to the transcriptional repressor NemR, I found several other potential regulators that are heavily induced upon HOCl stress. One of these regulators is the predicted transcriptional activator YkgD, whose downstream targets have not been functionally characterized. Genes regulated by YkgD are ranked among the top five up-regulated genes in HOCl-treated cells. Moreover, preliminary studies showed that deletion of *ykgD* makes cells highly HOCl-sensitive, suggesting that YkgD is an important activator that increases cellular HOCl resistance. The next step towards understanding the bacterial strategies that ameliorate survival upon exposure to HOCl treatment would be to characterize the protective role that YkgD plays under HOCl stress. In addition, it would be interesting to explore the

function of the other unknown genes that are massively upregulated by HOCl, as the anti-HOCl stress response appears to be a synergistic effort of regulating several independent pathways in the cell.

Conclusion

This thesis revealed that bacteria undergo fundamental changes in carbon and phosphate metabolism in response to HOCl stress and demonstrated that a single essential protein can determine the stress sensitivity of a whole organism. Bacteria have evolved clever strategies to protect themselves against the toxic effects of the potent oxidant HOCl. Methylglyoxal detoxification and polyphosphate generation appear to play essential roles in assisting pathogens to endure HOCl stress, whether mediated by host defense or secreted at mucosal barrier. Both responses are universally conserved, suggesting that these pathways might be important for repair mechanisms associated with chronic inflammatory diseases as well.

APPENDIX

Table A.1. Genes upregulated 2-fold or more after 0.4 mM HOCl treatment. Fold change is expressed as the expression ratio between 0 min (before HOCl addition) and expression at either 5 or 10 min after HOCl addition. Ratios of 2 or greater are indicated in bold text. Genes whose expression pattern clustered significantly differently from unregulated genes (by K-means clustering analysis) are indicated with grey shading.

Name	Locus Tag	Function	Expression			Fold Change	
			0 min	5 min	10 min	5 min	10 min
Oxidative Stress Response							
grxA	b0849	glutaredoxin 1, redox coenzyme for ribonucleotide reductase (RNR1a)	556.1	1561.0	1385.4	**2.8**	**2.5**
oxyS	b4458	OxyS sRNA activates genes that detoxify oxidative damage	319.8	747.3	665.2	**2.3**	**2.1**
sodC	b1646	superoxide dismutase, Cu, Zn	1628.3	2459.5	3493.6	1.5	**2.1**
Protein Homeostasis							
clpA	b0882	ATPase and specificity subunit of ClpA-ClpP ATP-dependent serine protease, chaperone activity	3108.2	5471.4	6287.5	1.8	**2.0**
clpB	b2592	protein disaggregation chaperone	1987.1	7682.4	10514.6	**3.9**	**5.3**
cpxP	b3914	periplasmic protein combats stress	1006.2	1905.5	2354.7	1.9	**2.3**
cpxP	b3913	periplasmic protein combats stress	971.0	1933.6	2187.0	2.0	**2.3**
dnaJ	b0015	chaperone Hsp40, co-chaperone with DnaK	1900.3	4359.5	5794.0	**2.3**	**3.0**
dnaK	b0014	chaperone Hsp70, co-chaperone with DnaJ	4231.0	11579.0	13501.2	**2.7**	**3.2**
eco	b2209	ecotin, a serine protease inhibitor	367.4	635.6	852.9	1.7	**2.3**
groL	b4143	chaperonin GroEL, large subunit of GroESL	6796.6	13510.8	15931.	2.0	**2.3**
groS	b4142	chaperonin GroES, small subunit of GroESL	6470.8	14304.9	16003.4	**2.2**	**2.5**

grpE	b2614	heat shock protein	3389.1	6910.2	7783.1	**2.0**	**2.3**
hslO	b3401	heat shock protein Hsp33	845.9	1432.3	2094.7	1.7	**2.5**
hslR	b3400	ribosome-associated heat shock protein Hsp15	2155.2	4014.4	5475.3	1.9	**2.5**
hslU	b3931	molecular chaperone and ATPase component of HslUV protease	2776.6	5137.0	5872.7	1.9	**2.1**
hslV	b3932	peptidase component of the HslUV protease	1658.3	4144.4	4496.1	**2.5**	**2.7**
htpG	b0473	molecular chaperone HSP90 family	2145.9	7072.4	8602.6	**3.3**	**4.0**
ibpA	b3687	heat shock chaperone	664.6	11142.3	11848.5	**16.8**	**17.8**
ibpB	b3686	heat shock chaperone	308.6	8085.1	9080.7	**26.2**	**29.4**
lon	b0439	DNA binding ATP-dependent protease	3423.0	7232.2	9323.7	**2.1**	**2.7**
pepT	b1127	peptidase T	888.7	1647.8	2090.0	1.9	**2.4**
ybbN	b0492	DnaK co-chaperone, thioredoxin-like protein	2693.8	4985.2	5493.7	1.9	**2.0**
Metal Homeostasis							
chaB	b1217	cation transport regulator	809.5	1163.5	1642.1	1.4	**2.0**
comR	b1111	copper-responsive DNA-binding transcriptional regulator	700.5	2650.4	2827.7	**3.8**	**4.0**
copA	b0484	copper/silver efflux transporter	525.5	2268.9	2309.5	**4.3**	**4.4**
cueO	b0123	multicopper oxidase (laccase)	1076.3	2853.7	3224.2	**2.7**	**3.0**
cusC	b0572	copper/silver efflux system, outer membrane component	604.5	1798.6	1620.7	**3.0**	**2.7**
ftnA	b1905	cytoplasmic ferritin iron storage protein	2491.0	7159.3	6006.4	**2.9**	**2.4**
iscR	b2531	DNA-binding transcriptional repressor (senses Fe-S stress)	3923.3	9825.4	10491.0	**2.5**	**2.7**
rcnR	b2105	DNA-binding transcriptional repressor of *rcnA*	764.4	2012.1	2068.9	**2.6**	**2.7**
zntA	b3469	zinc, cobalt and lead efflux system	213.3	3278.8	1514.0	**15.4**	**7.1**
zntR	b3292	DNA-binding transcriptional activator in response to Zn(II)	299.7	552.4	628.3	1.8	**2.1**
zupT	b3040	zinc transporter	1124.1	2315.5	2480.9	**2.1**	**2.2**
Sulfur Starvation							
cbl	b1987	DNA-binding transcriptional activator of cysteine biosynthesis	927.5	6877.5	7190.1	**7.4**	**7.8**
cysA	b2422	sulfate/thiosulfate transporter subunit	4239.8	10033.7	11009.2	**2.4**	**2.6**
cysC	b2750	adenosine 5'-phosphosulfate kinase	2192.8	5367.9	5178.4	**2.4**	**2.4**
cysD	b2752	sulfate adenylyltransferase subunit 2	6331.9	14966.7	15234.7	**2.4**	**2.4**
cysN	b2751	sulfate adenylyltransferase, subunit 1	5980.1	13119.0	12951.3	**2.2**	**2.2**
cysP	b2425	thiosulfate-binding protein	5491.2	15094.0	14837.4	**2.7**	**2.7**
cysQ	b4214	PAPS (adenosine 3'-phosphate 5'-phosphosulfate) 3'(2'),5'-bisphosphate nucleotidase	905.9	1572.8	1868.7	1.7	**2.1**
cysU	b2424	sulfate/thiosulfate transporter subunit	2044.7	5845.9	5257.1	**2.9**	**2.6**
cysW	b2423	sulfate/thiosulfate transporter subunit	171.5	477.9	456.9	**2.8**	**2.7**
fliY	b1920	cystine-binding periplasmic protein	5791.6	11541.1	12065.0	2.0	**2.1**

		precursor					
metA	b4013	homoserine O-succinyltransferase	1698.8	9623.4	7740.9	**5.7**	**4.6**
metB	b3939	cystathionine gamma-synthase	1826.6	13604.9	10042.0	**7.4**	**5.5**
metC	b3008	cystathionine beta-lyase	1397.4	4983.4	4862.2	**3.6**	**3.5**
metF	b3941	5,10-methylenetetrahydrofolate reductase	4036.4	18269.6	14969.1	**4.5**	**3.7**
metI	b0198	D-methionine transport system permease protein	2671.1	7824.4	6598.4	**2.9**	**2.5**
metJ	b3938	DNA-binding transcriptional repressor, S-adenosylmethionine-binding	2665.2	7925.9	6420.1	**3.0**	**2.4**
metL	b3940	fused aspartokinase II/homoserine dehydrogenase II	1098.6	7174.2	5339.1	**6.5**	**4.9**
metN	b0199	D-methionine transport ATP-binding protein	2182.3	8257.9	6625.7	**3.8**	**3.0**
mmuM	b0261	CP4-6 prophage; S-methylmethionine:homocysteine methyltransferase	803.3	5014.3	3343.4	**6.2**	**4.2**
mmuP	b0260	CP4-6 prophage; predicted S-methylmethionine transporter	315.6	3203.7	1863.8	**10.2**	**5.9**
sbp	b3917	sulfate transporter subunit	1883.3	14407.4	16290.1	**7.7**	**8.6**
ssuA	b0936	alkanesulfonate transporter subunit	153.9	390.6	504.0	**2.5**	**3.3**
ssuE	b0937	NAD(P)H-dependent FMN reductase	123.3	259.2	354.9	**2.1**	**2.9**
tauA	b0365	taurine-binding periplasmic protein	186.7	1240.5	2031.8	**6.6**	**10.9**
tauB	b0366	taurine transport ATP-binding protein	169.5	670.7	1153.3	**4.0**	**6.8**
tauC	b0367	taurine transport system permease protein	215.3	619.3	1167.1	**2.9**	**5.4**
ybdL	b0600	methionine aminotransferase, PLP-dependent	285.9	4023.7	2363.4	**14.1**	**8.3**
Phosphorus Starvation							
iraP	b0382	anti-RssB factor, RpoS stabilzer during Pi starvation; anti-adapter protein	1117.9	3141.0	4290.8	**2.8**	**3.8**
phoA	b0383	alkaline phosphatase	795.4	2891.5	3734.7	**3.6**	**4.7**
phoB	b0399	DNA-binding response regulator in two-component regulatory system with PhoR (or CreC)	208.3	1510.3	1243.8	**7.2**	**6.0**
phoR	b0400	sensory histidine kinase in two-component regulatory system with PhoB	118.5	505.0	441.2	**4.3**	**3.7**
phoU	b3724	negative regulator of PhoR/PhoB two-component regulator	1272.8	3191.6	4928.4	**2.5**	**3.9**
psiE	b4030	phosphate-starvation-inducible protein	305.5	635.5	734.8	**2.1**	**2.4**
psiF	b0384	phosphate starvation-inducible protein	948.8	2019.4	2923.4	**2.1**	**3.1**
pstA	b3726	phosphate transport system permease protein	793.8	2962.6	3126.3	**3.7**	**3.9**
pstB	b3725	phosphate transport ATP-binding protein	2553.8	6608.2	8320.7	**2.6**	**3.3**
pstS	b3728	phosphate-binding periplasmic protein precursor	2431.1	14601.3	13472.7	**6.0**	**5.5**
yihX	b3885	alpha-D-Glucose-1-P phosphatase,	973.8	1726.3	2205.8	1.8	**2.3**

		anomer-specific					
ytfK	b4217	hypothetical protein, PhoB regulon	425.0	877.2	1051.8	**2.1**	**2.5**
Detoxification of Aldehydes and Electrophiles							
dkgA	b3012	2,5-diketo-D-gluconate reductase	1592.9	4443.4	6369.3	**2.8**	**4.0**
frmA	b0356	alcohol dehydrogenase class III / glutathione-dependent formaldehyde dehydrogenase	932.1	6225.8	12198.9	**6.7**	**13.1**
frmB	b0355	S-formylglutathione hydrolase	347.0	1923.3	5543.9	**5.5**	**16.0**
frmR	b0357	transcriptional repressor of *frmRAB* operon	1321.2	9580.4	16182.8	**7.3**	**12.2**
gloA	b1651	glyoxalase I, Ni-dependent	2704.1	9036.3	9883.5	**3.3**	**3.7**
hchA	b1967	Hsp31 molecular chaperone, glyoxalase III	1438.1	2081.2	3037.8	1.4	**2.1**
nemA	b1650	N-ethylmaleimide reductase	899.5	11042.4	11771.8	**12.3**	**13.1**
nemR	b1649	transcriptional repressor of *nemA*	1172.7	7210.8	7686.2	**6.1**	**6.6**
paoA	b0286	PaoABC aldehyde oxidoreductase, 2Fe-2S subunit	351.1	445.2	724.6	1.3	**2.1**
yqhC	b3010	transcriptional activator	431.6	2584.3	3044.4	**6.0**	**7.1**
yqhD	b3011	alcohol dehydrogenase, NAD(P)-dependent	773.8	11850.5	15758.6	**15.3**	**20.4**
General Stress Resistance							
aidB	b4187	isovaleryl CoA dehydrogenase, transcriptional repressor invovled in response to alkylating agents	470.2	736.3	1041.1	1.6	**2.2**
alaE	b2670	inducible L-alanine exporter	100.2	141.1	215.0	1.4	**2.1**
iraD	b4326	RpoS stabilizer after DNA damage, anti-RssB factor	152.2	571.4	951.1	**3.8**	**6.2**
marA	b1531	DNA-binding transcriptional dual activator of multiple antibiotic resistance	755.5	2642.5	2504.1	**3.5**	**3.3**
marR	b1530	DNA-binding transcriptional repressor of multiple antibiotic resistance	584.8	1421.8	1377.7	**2.4**	**2.4**
mdtK	b1663	multidrug efflux system transporter	471.4	915.8	958.9	1.9	**2.0**
raiA	b2597	cold shock protein associated with 30S ribosomal subunit	4086.1	9842.6	10913.2	**2.4**	**2.7**
sbmC	b2009	DNA gyrase inhibitor	873.0	1780.0	2290.6	**2.0**	**2.6**
sulA	b0958	SOS cell division inhibitor	790.9	1408.8	1675.9	1.8	**2.1**
uspB	b3494	universal stress protein	571.0	1446.3	1858.4	**2.5**	**3.3**
uspD	b3923	stress-induced protein	1018.3	2064.7	2808.1	**2.0**	**2.8**
uspG	b0607	universal stress protein	668.2	1416.7	1648.8	**2.1**	**2.5**
yodD	b1953	stress-induced protein	747.6	1403.1	2032.5	1.9	**2.7**
Biofilm Formation							
ariR	b1166	connector protein for RcsB regulation of biofilm and acid-resistance	111.0	220.9	348.0	2.0	**3.1**
bdcA	b4249	c-di-GMP binding protein involved in biofilm dispersal	228.5	407.9	514.6	1.8	**2.3**
bdcR	b4250	predicted transcriptional repressor of *bdcA*	373.6	783.3	1028.8	**2.1**	**2.8**
bdcR	b4251	predicted transcriptional repressor of *bdcA*	465.3	968.3	1189.4	**2.1**	**2.6**

bhsA	b1112	biofilm, cell surface and signaling protein	865.8	16640.2	17387.0	**19.2**	**20.1**
bssR	b0836	repressor of biofilm formation by indole transport regulation	216.0	319.5	474.2	1.5	**2.2**
bssS	b1060	biofilm regulator	1093.6	2726.3	3786.3	**2.5**	**3.5**
mqsA	b3021	antitoxin for MqsR toxin; predicted transcriptional regulator	304.7	633.6	664.8	**2.1**	**2.2**
mqsR	b3022	GCU-specific mRNA interferase toxin of the MqsR-MqsA toxin-antitoxin system and biofilm/motility regulator	695.0	1711.0	1680.6	**2.5**	**2.4**
tabA	b4252	biofilm modulator regulated by toxins	635.8	1152.9	1726.7	1.8	**2.7**
ycgZ	b1164	connector protein for RcsB regulation of biofilm and acid-resistance	195.5	316.6	393.3	1.6	**2.0**
ymgA	b1165	connector protein for RcsB regulation of biofilm	273.0	434.1	641.2	1.6	**2.3**
ymgC	b1167	protein involved in biofilm formation	53.0	106.3	155.8	**2.0**	**2.9**
Carbon and Energy Metabolism							
add	b1623	adenosine deaminase	442.9	555.8	888.3	1.3	**2.0**
astC	b1748	succinylornithine transaminase, PLP-dependent	446.8	794.8	1063.0	1.8	**2.4**
cdh	b3918	CDP-diacylglycerol phosphotidylhydrolase	521.1	1126.4	1326.0	**2.2**	**2.5**
dadA	b1189	D-amino acid dehydrogenase small subunit	621.7	1830.2	2157.4	**2.9**	**3.5**
dadX	b1190	alanine racemase	441.9	961.5	1242.3	**2.2**	**2.8**
fucU	b2804	L-fucose mutarotase	529.3	1094.4	1365.4	**2.1**	**2.6**
gadE	b3512	DNA-binding transcriptional activator	395.6	652.4	839.9	1.6	**2.1**
gcvB	b4443	GcvB sRNA gene divergent from *gcvA*;	301.6	1633.6	2245.4	**5.4**	**7.4**
glgS	b3049	glycogen synthesis protein	1965.3	4420.1	5852.2	**2.2**	**3.0**
glpD	b3426	sn-glycerol-3-phosphate dehydrogenase, aerobic, FAD/NAD(P)-binding	312.4	551.2	646.9	1.8	**2.1**
gltP	b4077	glutamate/aspartate:proton symporter	473.5	861.4	1205.6	1.8	**2.5**
iaaA	b0828	isoaspartyl peptidase	2574.7	8129.9	7895.2	**3.2**	**3.1**
kdgK	b3526	2-dehydro-3-deoxygluconokinase	447.4	867.2	1296.0	1.9	**2.9**
kduD	b2842	2-deoxy-D-gluconate 3-dehydrogenase	296.7	438.1	664.7	1.5	**2.2**
kduI	b2843	5-keto-4-deoxyuronate isomerase	215.8	366.2	676.9	1.7	**3.1**
ldhA	b1380	fermentative D-lactate dehydrogenase, NAD-dependent	869.5	1963.6	2517.6	**2.3**	**2.9**
moaB	b0782	molybdopterin biosynthesis protein B	2019.8	3559.3	4235.0	1.8	**2.1**
nanM	b4310	N-acetylneuraminic acid mutarotase	533.6	824.1	1179.7	1.5	**2.2**
narU	b1469	nitrate/nitrite transporter	193.5	368.6	535.4	1.9	**2.8**
qorA	b4051	quinone oxidoreductase, NADPH-dependent	727.9	1299.8	1627.8	1.8	**2.2**
qorB	b4211	NAD(P)H:quinone oxidoreductase	597.8	3131.5	4082.4	**5.2**	**6.8**
qorR	b4212	redox-responsive transcriptional repressor	343.5	1243.4	1256.5	**3.6**	**3.7**
rhtB	b3824	homoserine, homoserine lactone and S-	478.5	988.3	996.5	**2.1**	**2.1**

		methyl-methionine efflux pump					
sdaA	b1814	L-serine deaminase I	505.5	820.3	1176.1	1.6	**2.3**
tam	b1519	trans-aconitate methyltransferase	679.3	1064.8	1514.0	1.6	**2.2**
tdh	b3616	threonine 3-dehydrogenase, NAD(P)-binding	901.9	1423.2	1998.3	1.6	**2.2**
treF	b3519	cytoplasmic trehalase	634.9	1010.9	1365.8	1.6	**2.2**
xylB	b3564	xylulokinase	284.4	460.4	573.7	1.6	**2.0**
yecC	b1917	hypothetical amino-acid ABC transporter ATP-binding protein	1788.9	3617.9	4439.6	**2.0**	**2.5**
yecS	b1877	hypothetical amino-acid ABC transporter permease protein	1337.5	2965.3	3290.0	**2.2**	**2.5**
Cell Division and Cell Wall Biosynthesis							
blc	b4149	outer membrane lipoprotein (lipocalin)	1275.0	1971.7	2559.9	1.5	**2.0**
bolA	b0435	regulator of penicillin binding proteins and beta lactamase transcription (morphogene)	2054.1	3849.9	5127.3	1.9	**2.5**
dacC	b0839	D-alanyl-D-alanine carboxypeptidase (penicillin-binding protein 6a)	1027.1	1849.7	2265.2	1.8	**2.2**
erfK	b1990	L,D-transpeptidase linking Lpp to murein	437.0	702.3	876.7	1.6	**2.0**
fic	b3361	cell filamentation protein	892.2	1771.7	2594.8	2.0	**2.9**
ynhG	b1678	murein L,D-transpeptidase	1087.1	1577.5	2228.6	1.5	**2.0**
Unknown Functions							
csiD	b2659	carbon starvation induced gene	470.8	780.5	1229.9	1.7	**2.6**
flxA	b1566	Qin prophage; predicted protein	215.2	281.5	513.7	1.3	**2.4**
fxsA	b4140	suppressor of F exclusion of phage T7	451.2	1477.1	1489.8	**3.3**	**3.3**
hiuH	b1970	hydroxyisourate hydrolase	351.0	589.8	1066.8	1.7	**3.0**
nlpA	b3661	cytoplasmic membrane lipoprotein-28	2462.6	10966.4	11870.3	**4.5**	**4.8**
phnB	b4107	hypothetical protein	647.5	1107.1	1587.0	1.7	**2.5**
rygC	b4446	sRNA, function unknown; paralogous to the other QUAD sRNA genes	228.6	355.7	548.5	1.6	**2.4**
ryjA	b4459	Novel sRNA, function unknown	296.2	670.4	720.0	**2.3**	**2.4**
yaeH	b0163	hypothetical protein	955.5	1633.5	2022.8	1.7	**2.1**
yaeP	b4406	hypothetical protein	843.4	1725.1	2012.6	**2.0**	**2.4**
ybaA	b0456	hypothetical protein	231.5	349.7	509.2	1.5	**2.2**
ybdH	b0599	predicted oxidoreductase	582.2	3034.3	2102.9	**5.2**	**3.6**
ybeD	b0631	hypothetical protein	1046.3	2064.0	2431.8	2.0	**2.3**
ybeL	b0643	hypothetical protein	2098.1	4090.2	5303.7	1.9	**2.5**
ybeM	b0626	putative amidase (pseudogene)	342.9	642.2	832.6	1.9	**2.4**
ybgS	b0753	hypothetical protein	365.5	594.7	949.2	1.6	**2.6**
ybiB	b0800	predicted transferase/phosphorylase	1110.5	1898.9	2302.3	1.7	**2.1**
ybjQ	b0866	hypothetical protein	1400.2	2433.4	3167.7	1.7	**2.3**
yccX	b0968	weak acylphosphatase	997.5	1829.8	2332.3	1.8	**2.3**
yceH	b1067	hypothetical protein	1596.2	3005.7	3325.1	1.9	**2.1**
yceK	b1050	predicted lipoprotein	531.2	795.7	1144.7	1.5	**2.2**

ycgB	b1188	hypothetical protein	833.0	1521.9	1930.5	1.8	**2.3**
ychH	b1205	predicted inner membrane protein	637.2	1221.1	1655.7	1.9	**2.6**
yciW	b1287	predicted oxidoreductase	2090.4	7512.9	7531.6	**3.6**	**3.6**
ycjF	b1322	conserved inner membrane protein	188.9	558.2	754.6	**3.0**	**4.0**
ycjX	b1321	conserved protein with nucleoside triphosphate hydrolase domain	415.2	1362.5	1678.3	**3.3**	**4.0**
ydhZ	b1675	hypothetical protein	398.7	617.2	827.9	1.5	**2.1**
yeaG	b1783	protein kinase, function unknown; autokinase	4858.5	7337.4	10145.1	1.5	**2.1**
yedP	b1955	predicted mannosyl-3-phosphoglycerate phosphatase	345.7	569.5	822.6	1.6	**2.4**
yedY	b1971	predicted reductase	476.4	795.5	1081.8	1.7	**2.3**
yeeD	b2012	hypothetical protein	1288.4	3136.7	2911.3	**2.4**	**2.3**
yeeE	b2013	predicted inner membrane protein	1821.9	4297.0	3986.8	**2.4**	**2.2**
yegP	b2080	hypothetical protein	1909.3	2930.3	4373.3	1.5	**2.3**
yfcZ	b2343	hypothetical protein	377.9	702.9	819.9	1.9	**2.2**
yfdY	b2377	predicted inner membrane protein	776.6	1858.4	2156.5	**2.4**	**2.8**
yffB	b2471	predicted reductase, function unknown, ArsC family; low abundance protein	1124.7	2078.2	2336.8	1.8	**2.1**
yffO	b2446	CPZ-55 prophage; predicted protein	407.5	665.1	828.2	1.6	**2.0**
yffP	b2447	CPZ-55 prophage; predicted protein	326.9	601.1	775.8	1.8	**2.4**
yffR	b2449	CPZ-55 prophage; predicted protein	930.7	1743.9	2011.1	1.9	**2.2**
yfhH	b2561	predicted DNA-binding transcriptional regulator	376.8	562.0	781.3	1.5	**2.1**
ygaM	b2672	hypothetical protein	2473.3	3660.1	5408.8	1.5	**2.2**
ygaP	b2668	inner membrane associated rhodanese / sulfur transferase	356.9	1277.2	1776.7	**3.6**	**5.0**
ygaU	b2665	hypothetical protein	2075.0	3161.6	4496.8	1.5	**2.2**
ygaV	b2667	tributylin chloride-responsive transcriptional repressor of *ygaVP*	293.9	880.7	1226.7	**3.0**	**4.2**
ygbE	b2749	conserved inner membrane protein	1571.5	3285.0	3484.9	**2.1**	**2.2**
ygdR	b2833	hypothetical lipoprotein	650.4	1094.6	1473.8	1.7	**2.3**
yghA	b3003	predicted glutathionylspermidine synthase, with NAD(P)-binding Rossmann-fold domain	493.5	896.2	1299.1	1.8	**2.6**
yhaH	b3103	predicted inner membrane protein	708.9	1340.3	1586.8	1.9	**2.2**
yhaL	b3107	hypothetical protein	1356.2	2315.2	2819.5	1.7	**2.1**
yhcN	b3238	hypothetical protein	742.2	1253.1	1984.4	1.7	**2.7**
yhcO	b3239	predicted barnase inhibitor	560.9	900.1	1202.3	1.6	**2.1**
yhdN	b3293	hypothetical protein	1143.8	2172.3	2487.5	1.9	**2.2**
yhfG	b3362	hypothetical protein	610.1	1178.8	1742.0	1.9	**2.9**
yhhA	b3448	hypothetical protein	414.2	1140.4	1805.3	**2.8**	**4.4**
yhjD	b3522	putative alternate lipid exporter, suppressor of *msbA* and KDO essentiality, inner membrane protein	711.1	1139.2	1423.1	1.6	**2.0**
yhjG	b3524	predicted outer membrane biogenesis protein, AsmA family	335.1	561.9	789.8	1.7	**2.4**

yhjY	b3548	hypothetical protein	654.1	1379.4	1702.1	**2.1**	**2.6**
yiaG	b3555	predicted transcriptional regulator, HTH_CROC1 family	1641.1	2578.5	3828.1	1.6	**2.3**
yiiS	b3922	hypothetical protein	894.9	1868.1	2417.7	**2.1**	**2.7**
yjbJ	b4045	predicted stress response protein	517.5	870.2	1619.5	1.7	**3.1**
yjdI	b4126	hypothetical protein	755.0	1244.7	1749.5	1.6	**2.3**
yjdJ	b4127	predicted acyltransferase with acyl-CoA N-acyltransferase domain	1748.6	2878.2	4131.0	1.6	**2.4**
yjfY	b4199	hypothetical protein	149.0	284.3	414.9	1.9	**2.8**
yjgB	b4269	predicted alcohol dehydrogenase, Zn-dependent and NAD(P)-binding	379.9	529.4	768.1	1.4	**2.0**
yjgH	b4248	predicted mRNA endoribonuclease	712.1	1137.7	1683.5	1.6	**2.4**
yjiP	b4339	hypothetical protein (pseudogene)	503.1	938.2	1060.0	1.9	**2.1**
yjiR	b4340	fused predicted DNA-binding transcriptional regulator/predicted aminotransferase	337.0	715.3	710.8	**2.1**	**2.1**
ykgB	b0301	conserved inner membrane protein	178.7	10345.7	11528.0	**57.9**	**64.5**
ykgC	b0304	pyridine nucleotide-disulfide oxidoreductase	429.6	15566.7	15736.2	**36.2**	**36.6**
ykgD	b0305	predicted DNA-binding transcriptional regulator	153.7	1813.4	1517.9	**11.8**	**9.9**
ykgE	b0306	predicted oxidoreductase	343.4	1403.2	1108.4	**4.1**	**3.2**
ykgF	b0307	predicted amino acid dehydrogenase with NAD(P)-binding domain and ferridoxin-like domain	330.9	1082.0	869.1	**3.3**	**2.6**
ykgI	b0303	predicted periplasmic protein	79.4	7763.1	9147.8	**97.7**	**115.2**
ymgE	b1195	transglycosylase associated protein	541.3	812.0	1373.8	1.5	**2.5**
yoaC	b1810	hypothetical protein	844.2	1623.1	2596.5	1.9	**3.1**
yodB	b1974	cytochrome b561 homolog	256.1	448.6	517.1	1.8	**2.0**
yodC	b1957	hypothetical protein	2089.2	3537.1	5153.7	1.7	**2.5**
yohC	b2135	inner membrane protein, Yip1 family	364.2	652.5	1060.7	1.8	**2.9**
yphA	b2543	predicted inner membrane protein	521.5	864.2	1166.6	1.7	**2.2**
yqfA	b2899	inner membrane protein, hemolysin III family HylIII	351.3	1406.4	1343.6	**4.0**	**3.8**
yqjG	b3102	predicted S-transferase	559.5	915.1	1436.4	1.6	**2.6**

Table A.2. Genes downregulated 2-fold or more after 0.4 mM HOCl treatment. Fold change is expressed as the ratio between expression at either 5 or 10 min after HOCl addition and expression at 0 min (before HOCl addition). Ratios of -2 or less are indicated in bold text. Genes whose expression pattern clustered significantly differently from unregulated genes (by K-means clustering analysis) are indicated with grey shading.

Name	Locus Tag	Function	Expression			Fold Change	
			0 min	5 min	10 min	5 min	10 min
Metal Homeostasis							
afuB	b0263	non-functioning membrane component of an ABC superfamily ferric cation transporter	1833.8	336.6	405.7	**-5.4**	**-4.5**
bfd	b3337	Bacterioferritin-associated ferredoxin	1160.5	432.1	474.9	**-2.7**	**-2.4**
cirA	b2155	ferric iron-catecholate outer membrane transporter	530.6	176.1	173.2	**-3.0**	**-3.1**
efeO	b1018	periplasmic protein component of the EfeUOB ferrous iron transporter	1828.7	367.3	344.2	**-5.0**	**-5.3**
efeU	b1017	ferrous iron permease component of the EfeUOB ferrous iron transporter	867.2	213.9	224.1	**-4.1**	**-3.9**
exbB	b3006	membrane spanning protein in TonB-ExbB-ExbD complex	1683.8	351.9	407.2	**-4.8**	**-4.1**
exbD	b3005	membrane spanning protein in TonB-ExbB-ExbD complex	2743.3	532.2	590.3	**-5.2**	**-4.6**
fecI	b4293	KpLE2 phage-like element; RNA polymerase, sigma 19 factor	984.2	327.3	283.4	**-3.0**	**-3.5**
fecR	b4292	KpLE2 phage-like element; transmembrane signal transducer for ferric citrate transport	615.1	302.6	303.1	**-2.0**	**-2.0**
fepA	b0584	ferrienterobactin receptor precursor	957.6	493.2	371.6	-1.9	**-2.6**
fepB	b0592	ferrienterobactin-binding periplasmic protein precursor	318.3	150.4	114.4	**-2.1**	**-2.8**
fepC	b0588	ferric enterobactin transport ATP-binding protein	384.2	188.0	161.2	**-2.0**	**-2.4**
fepD	b0590	ferric enterobactin transport system permease protein	389.1	226.5	184.9	-1.7	**-2.1**
fes	b0585	enterobactin/ferric enterobactin esterase	376.4	197.3	166.1	-1.9	**-2.3**
fhuA	b0150	ferrichrome outer membrane transporter	1617.6	244.0	298.4	**-6.6**	**-5.4**
fhuC	b0151	ferrichrome transport ATP-binding protein	1022.9	430.6	392.5	**-2.4**	**-2.6**
fhuD	b0152	ferrichrome-binding periplasmic protein precursor	234.8	99.4	75.0	**-2.4**	**-3.1**
fhuF	b4367	ferric iron reductase involved in ferric	1391.9	171.8	190.5	**-8.1**	**-7.3**

		hydroximate transport					
fiu	b0805	predicted iron outer membrane transporter	450.4	129.2	97.0	**-3.5**	**-4.6**
tonB	b1252	membrane spanning protein in TonB-ExbB-ExbD complex	1177.6	355.8	362.5	**-3.3**	**-3.2**
yedV	b1968	predicted sensory kinase in two-component regulatory system with YedW	216.1	104.9	75.3	**-2.1**	**-2.9**
yqjH	b3070	predicted siderophore interacting protein	1170.1	574.4	515.3	**-2.0**	**-2.3**
DNA Metabolism							
dinI	b1061	DNA-damage-inducible protein I	2821.7	1587.5	1302.9	-1.8	**-2.2**
dnaE	b0184	DNA polymerase III alpha subunit	1190.3	566.8	543.5	**-2.1**	**-2.2**
hda	b2496	ATPase regulatory factor involved in DnaA inactivation	1546.0	586.6	457.5	**-2.6**	**-3.4**
holD	b4372	DNA polymerase III subunit ps	1941.2	935.7	961.8	**-2.1**	**-2.0**
hsdS	b4348	specificity determinant for *hsdM* and *hsdR*	1249.6	568.8	360.4	**-2.2**	**-3.5**
mcrB	b4346	5-methylcytosine-specific restriction enzyme McrBC, subunit McrB	348.4	196.5	162.8	-1.8	**-2.1**
mcrC	b4345	5-methylcytosine-specific restriction enzyme McrBC, subunit McrC	243.0	143.4	98.1	-1.7	**-2.5**
mutL	b4170	methyl-directed mismatch repair protein	206.0	131.2	101.8	-1.6	**-2.0**
nth	b1633	DNA glycosylase and apyrimidinic (AP) lyase (endonuclease III)	451.7	226.2	189.6	**-2.0**	**-2.4**
recB	b2820	exonuclease V (RecBCD complex), beta subunit	652.8	400.2	313.4	-1.6	**-2.1**
recQ	b0799	ATP-dependent DNA helicase	1122.0	640.6	489.3	-1.8	**-2.3**
stpA	b2669	DNA binding protein, nucleoid-associated	2482.1	1422.8	1233.7	-1.7	**-2.0**
xerC	b3811	site-specific tyrosine recombinase	2297.9	1382.7	1021.8	-1.7	**-2.2**
xseA	b2509	exonuclease VII, large subunit	2287.2	1137.9	1119.1	**-2.0**	**-2.0**
Transcription and Translation							
infA	b0884	translation initiation factor IF-1	6126.7	2710.6	2708.5	**-2.3**	**-2.3**
nusB	b0416	transcription antitermination protein	3368.8	1459.8	1248.5	**-2.3**	**-2.7**
prfC	b4375	peptide chain release factor 3	3931.5	2100.9	1925.6	-1.9	**-2.0**
rho	b3783	transcription termination factor	7231.4	3177.8	2952.4	**-2.3**	**-2.4**
rimM	b2608	16S rRNA-processing protein	13972.6	8392.0	6055.3	-1.7	**-2.3**
rimN	b3282	predicted ribosome maturation factor	1940.7	906.5	1004.5	**-2.1**	-1.9
rimO	b0835	methyltransferase responsible for methylthiolation of the β carbon of the D88 residue of 30S ribosomal subunit protein S12	1489.5	506.7	544.1	**-2.9**	**-2.7**
rplB	b3317	50S ribosomal protein L2	17185.8	12741.7	7861.3	-1.3	**-2.2**
rplD	b3319	50S ribosomal protein L4	14893.6	10811.0	6417.5	-1.4	**-2.3**
rplS	b2606	50S ribosomal protein L19	9261.3	4632.0	2935.8	**-2.0**	**-3.2**
rplW	b3318	50S ribosomal protein L23	15935.6	12406.7	7918.0	-1.3	**-2.0**
rpmF	b1089	50S ribosomal subunit protein L32	4459.4	2775.1	2161.4	-1.6	**-2.1**
rpmG	b3636	50S ribosomal protein L33	10779.4	5839.4	4831.3	-1.8	**-2.2**
rpmH	b3703	50S ribosomal protein L34	9827.1	3417.9	3296.6	**-2.9**	**-3.0**
rpsA	b0911	30S ribosomal protein S1	17966.0	8390.4	7528.0	**-2.1**	**-2.4**

rpsI	b3230	30S ribosomal protein S9	11359.2	6456.5	4583.7	-1.8	**-2.5**
rpsJ	b3321	30S ribosomal protein S10	19758.5	14320.5	9295.4	-1.4	**-2.1**
rpsP	b2609	30S ribosomal protein S16	13617.7	7923.5	5854.3	-1.7	**-2.3**
rpsT	b0023	30S ribosomal protein S20	7298.6	3637.9	3032.5	**-2.0**	**-2.4**
rpsU	b3065	30S ribosomal protein S21	6651.8	3093.6	2832.5	**-2.2**	**-2.3**
RNA Modification							
dusB	b3260	tRNA-dihydrouridine synthase B	11117.7	4621.6	4519.4	**-2.4**	**-2.5**
gidB	b3740	AMP-dependent methyltransferase, glucose-inhibited cell-division protein	781.8	411.9	383.4	-1.9	**-2.0**
mnmA	b1133	tRNA (5-methylaminomethyl-2-thiouridylate)-methyltransferase	2140.5	977.7	983.8	**-2.2**	**-2.2**
pcnB	b0143	poly(A) polymerase I	2559.2	1102.7	1032.6	**-2.3**	**-2.5**
queA	b0405	S-adenosylmethionine:tRNA ribosyltransferase-isomerase	1416.8	688.4	623.5	**-2.1**	**-2.3**
rhlE	b0797	putative ATP-dependent RNA helicase	1190.7	420.2	474.9	**-2.8**	**-2.5**
rluC	b1086	23S rRNA pseudouridylate synthase	1618.3	770.3	693.7	**-2.1**	**-2.3**
rnb	b1286	exoribonuclease II	5175.5	2798.6	2202.9	-1.8	**-2.3**
rnhB	b0183	ribonuclease HII, degrades RNA of DNA-RNA hybrids	973.7	393.8	438.5	**-2.5**	**-2.2**
rnpA	b3704	protein C5 component of RNase P	8261.6	1566.4	1391.9	**-5.3**	**-5.9**
rsmB	b3289	16S rRNA m5C967 methyltransferase, S-adenosyl-L-methionine-dependent	890.1	439.1	428.3	**-2.0**	**-2.1**
rsmF	b1835	predicted methyltransferase	689.8	363.4	334.6	-1.9	**-2.1**
trmD	b2607	tRNA (guanine-N(1)-)-methyltransferase	15756.4	10522.7	7171.3	-1.5	**-2.2**
yibK	b3606	predicted rRNA methylase	656.4	360.5	312.0	-1.8	**-2.1**
Carbon and Energy Metabolism							
aceK	b4016	isocitrate dehydrogenase kinase/phosphatase	1361.4	577.8	522.9	**-2.4**	**-2.6**
ansA	b1767	cytoplasmic L-asparaginase I	2696.8	1360.8	1340.7	**-2.0**	**-2.0**
atpH	b3735	F1 sector of membrane-bound ATP synthase, delta subunit	8778.3	6749.0	4113.5	-1.3	**-2.1**
atpI	b3739	F1 sector of membrane-bound ATP synthase, membrane-bound accesory subunit	3845.9	2400.7	1736.7	-1.6	**-2.2**
caiF	b0034	DNA-binding transcriptional activator	870.9	701.6	415.8	-1.2	**-2.1**
cyoA	b0432	cytochrome o ubiquinol oxidase subunit II	12777.3	7879.6	4768.1	-1.6	**-2.7**
cyoB	b0431	cytochrome o ubiquinol oxidase subunit I	11314.5	8414.5	4794.6	-1.3	**-2.4**
fdoG	b3894	formate dehydrogenase-O, large subunit	649.9	408.6	307.6	-1.6	**-2.1**
gatA	b2094	galactitol-specific enzyme IIA component of PTS	13857.5	9618.3	4195.8	-1.4	**-3.3**
gatB	b2093	galactitol-specific enzyme IIB component of PTS	8996.1	7226.7	3849.8	-1.2	**-2.3**
gatD	b2091	galactitol-1-phosphate dehydrogenase, Zn-dependent and NAD(P)-binding	1896.6	1687.6	915.7	-1.1	**-2.1**
gatZ	b2095	D-tagatose 1,6-bisphosphate aldolase 2, subunit	14881.1	11073.8	7165.8	-1.3	**-2.1**
gpsA	b3608	glycerol-3-phosphate dehydrogenase (NAD+)	4550.9	2339.3	1956.6	-1.9	**-2.3**

mqo	b2210	malate:quinone oxidoreductase	917.7	430.0	357.7	**-2.1**	**-2.6**
nuoE	b2285	NADH:ubiquinone oxidoreductase, chain E	5905.7	3920.6	2814.0	-1.5	**-2.1**
nuoF	b2284	NADH:ubiquinone oxidoreductase, chain F	3623.5	2340.9	1582.5	-1.5	**-2.3**
nuoG	b2283	NADH:ubiquinone oxidoreductase, chain G	1182.5	736.9	458.1	-1.6	**-2.6**
nuoH	b2282	NADH:ubiquinone oxidoreductase, membrane subunit H	3345.5	2606.8	1485.6	-1.3	**-2.3**
nuoM	b2277	NADH:ubiquinone oxidoreductase, membrane subunit M	1008.0	747.9	494.4	-1.3	**-2.0**
pdhR	b0113	transcriptional regulator of pyruvate dehydrogenase complex	1124.0	579.9	534.1	-1.9	**-2.1**
puuD	b1298	gamma-Glu-GABA hydrolase	2267.1	1200.1	1115.0	-1.9	**-2.0**
puuP	b1296	putrescine importer	509.1	294.1	255.2	-1.7	**-2.0**
sdhB	b0724	succinate dehydrogenase catalytic subunit	7586.3	6425.3	3777.6	-1.2	**-2.0**
sdhC	b0721	succinate dehydrogenase cytochrome b556 large membrane subunit	8376.3	5245.5	3325.6	-1.6	**-2.5**
sdhD	b0722	succinate dehydrogenase cytochrome b556 small membrane subunit	6318.8	4355.9	2729.5	-1.5	**-2.3**
sucA	b0726	2-oxoglutarate dehydrogenase E1 component	7518.5	5725.8	3268.7	-1.3	**-2.3**
yfiD	b2579	pyruvate formate lyase subunit	1269.3	597.8	502.4	**-2.1**	**-2.5**
Cell Structure and Envelope Biosynthesis							
accC	b3256	acetyl-CoA carboxylase, biotin carboxylase subunit	5200.5	3093.4	2532.8	-1.7	**-2.1**
ampG	b0433	muropeptide transporter	684.8	274.3	234.2	**-2.5**	**-2.9**
arnA	b2255	fused UDP-L-Ara4N formyltransferase/UDP-GlcA C-4'-decarboxylase	1244.3	675.2	605.6	-1.8	**-2.1**
cld	b0587	regulator of length of O-antigen component of lipopolysaccharide chains	1008.2	461.0	463.7	**-2.2**	**-2.2**
dacA	b0632	D-alanyl-D-alanine carboxypeptidase (penicillin-binding protein 5)	1979.3	1167.2	946.6	-1.7	**-2.1**
kdtA	b3633	3-deoxy-D-manno-octulosonic-acid transferase (KDO transferase)	425.3	225.7	197.6	-1.9	**-2.2**
lolC	b1116	outer membrane-specific lipoprotein transporter subunit	1288.9	553.5	553.8	**-2.3**	**-2.3**
lpxB	b0182	lipid-A-disaccharide synthase	1178.3	584.1	613.8	**-2.0**	-1.9
lpxH	b0524	UDP-2,3-diacylglucosamine hydrolase	857.9	400.7	355.3	**-2.1**	**-2.4**
lpxP	b2378	palmitoleoyl-acyl carrier protein (ACP)-dependent acyltransferase	535.7	247.8	244.7	**-2.2**	**-2.2**
lpxT	b2174	undecaprenyl pyrophosphate phosphatase	490.3	264.9	233.0	-1.9	**-2.1**
mepA	b2328	penicillin-insensitive murein endopeptidase	1182.7	481.3	408.8	**-2.5**	**-2.9**
mrcA	b3396	penicillin-binding protein 1a: murein transglycosylase/murein transpeptidase	879.9	508.0	408.8	-1.7	**-2.2**
mrdA	b0635	transpeptidase involved in peptidoglycan synthesis (penicillin-binding protein 2)	551.0	248.0	244.6	**-2.2**	**-2.3**

mrdB	b0634	cell wall shape-determining protein	687.9	370.3	311.5	-1.9	**-2.2**
mreC	b3250	rod shape-determining protein	1720.7	577.3	449.4	**-3.0**	**-3.8**
mreD	b3249	rod shape-determining protein	1250.6	523.8	507.2	**-2.4**	**-2.5**
prc	b1830	carboxy-terminal protease for penicillin-binding protein 3	2902.0	1202.6	1031.0	**-2.4**	**-2.8**
rfaC	b3621	ADP-heptose:LPS heptosyl transferase I	1245.0	470.3	442.4	**-2.6**	**-2.8**
rfaF	b3620	ADP-heptose:LPS heptosyltransferase II	2793.8	1127.5	1063.6	**-2.5**	**-2.6**
rfaL	b3622	O-antigen ligase	1472.6	404.6	339.4	**-3.6**	**-4.3**
rfbD	b2040	dTDP-4-dehydrorhamnose reductase subunit, NAD(P)-binding, of dTDP-L-rhamnose synthase	3210.0	1609.9	1538.0	**-2.0**	**-2.1**
rfbX	b2037	predicted polisoprenol-linked O-antigen transporter	1123.2	567.6	502.2	**-2.0**	**-2.2**
rffG	b3788	dTDP-glucose 4,6-dehydratase	1609.6	949.5	793.8	-1.7	**-2.0**
tolQ	b0737	membrane spanning protein in TolA-TolQ-TolR complex	1407.6	647.6	669.8	**-2.2**	**-2.1**
tolR	b0738	membrane spanning protein in TolA-TolQ-TolR complex	1323.1	611.7	612.7	**-2.2**	**-2.2**
wbbI	b2331	conserved protein	1555.9	1135.1	675.0	-1.4	**-2.3**
wecB	b3786	UDP-N-acetyl glucosamine-2-epimerase	1029.8	552.7	486.3	-1.9	**-2.1**
wecC	b3787	UDP-N-acetyl-D-mannosaminuronic acid dehydrogenase	2435.2	1215.1	923.4	**-2.0**	**-2.6**
yhbJ	b3205	regulates the expression of GlmS by controlling the processing and stability of the small RNA regulator GlmZ	3470.9	2069.1	1623.6	-1.7	**-2.1**
Amino Acid Synthesis and Salvage							
alaA	b2290	glutamate-pyruvate aminotransferase	1972.6	1233.7	964.3	-1.6	**-2.0**
argA	b2818	fused acetylglutamate kinase homolog (inactive)/amino acid N-acetyltransferase	3517.2	871.6	852.8	**-4.0**	**-4.1**
argB	b3959	acetylglutamate kinase	6576.6	2388.7	1874.9	**-2.8**	**-3.5**
argC	b3958	N-acetyl-gamma-glutamyl-phosphate reductase	4942.8	1228.6	1097.3	**-4.0**	**-4.5**
argD	b3359	bifunctional acetylornithine aminotransferase/ succinyldiaminopimelate aminotransferase	3744.6	837.9	772.4	**-4.5**	**-4.8**
argF	b0273	CP4-6 prophage; ornithine carbamoyltransferase 2, chain F	6137.3	2523.6	1449.5	**-2.4**	**-4.2**
argH	b3960	argininosuccinate lyase	2495.6	1221.9	1110.8	**-2.0**	**-2.2**
argI	b4254	ornithine carbamoyltransferase 1	2233.9	1732.8	923.4	-1.3	**-2.4**
aroA	b0908	5-enolpyruvylshikimate-3-phosphate synthetase	1884.5	798.5	489.5	**-2.4**	**-3.8**
aroF	b2601	3-deoxy-D-arabino-heptulosonate-7-phosphate synthase, tyrosine-repressible	5830.9	3317.9	1970.7	-1.8	**-3.0**
aroH	b1704	3-deoxy-D-arabino-heptulosonate-7-phosphate synthase, tryptophan repressible	1735.7	852.3	713.5	**-2.0**	**-2.4**

aroL	b0388	shikimate kinase II	2541.4	1017.6	819.8	**-2.5**	**-3.1**
artJ	b0860	Arginine-binding periplasmic protein 2 precursor	4178.1	1903.1	875.0	**-2.2**	**-4.8**
artM	b0861	arginine transport system permease protein	951.8	456.4	417.2	**-2.1**	**-2.3**
carA	b0032	carbamoyl phosphate synthetase small subunit, glutamine amidotransferase	11159.5	2373.5	716.9	**-4.7**	**-15.6**
carB	b0033	carbamoyl-phosphate synthase large subunit	9062.3	5108.2	1675.2	-1.8	**-5.4**
glnL	b3869	sensory histidine kinase in two-component regulatory system with GlnG	674.8	378.7	184.2	-1.8	**-3.7**
glnQ	b0809	glutamine ABC transporter ATP-binding component	2218.5	1659.7	1030.2	-1.3	**-2.2**
gltF	b3214	periplasmic protein involved in induction of nitrogen metabolism genes	1214.2	863.1	577.0	-1.4	**-2.1**
hisI	b2026	fused phosphoribosyl-AMP cyclohydrolase/phosphoribosyl-ATP pyrophosphatase	3375.6	2326.5	1681.1	-1.5	**-2.0**
hisM	b2307	histidine/lysine/arginine/ornithine transporter subunit	1692.7	762.6	689.1	**-2.2**	**-2.5**
ilvC	b3774	ketol-acid reductoisomerase, NAD(P)-binding	13451.8	8152.8	5370.6	-1.6	**-2.5**
ilvH	b0078	acetolactate synthase III, thiamin-dependent, small subunit	2933.9	2250.2	1327.7	-1.3	**-2.2**
ilvI	b0077	acetolactate synthase III, large subunit	5692.4	4276.8	2775.0	-1.3	**-2.1**
livF	b3454	high-affinity branched-chain amino acid transport ATP-binding protein	2029.6	1040.8	512.0	-1.9	**-4.0**
livG	b3455	high-affinity branched-chain amino acid transport ATP-binding protein	3008.8	1710.4	883.3	-1.8	**-3.4**
livH	b3457	high-affinity branched-chain amino acid transport system permease protein	4950.3	3479.5	2228.0	-1.4	**-2.2**
livM	b3456	high-affinity branched-chain amino acid transport system permease protein	4263.6	2691.5	1582.4	-1.6	**-2.7**
lysC	b4024	aspartate kinase III	3571.8	2384.9	1676.1	-1.5	**-2.1**
lysP	b2156	Lysine-specific permease	3806.5	862.6	952.5	**-4.4**	**-4.0**
putP	b1015	proline:sodium symporter	1488.7	748.5	708.1	**-2.0**	**-2.1**
serC	b0907	3-phosphoserine / phosphohydroxythreonine aminotransferase	6965.9	4665.1	2696.9	-1.5	**-2.6**
thrA	b0002	fused aspartokinase I and homoserine dehydrogenase I	12171.0	7483.3	5244.2	-1.6	**-2.3**
thrB	b0003	homoserine kinase	8398.0	4721.8	3125.7	-1.8	**-2.7**
thrC	b0004	threonine synthase	8486.2	4682.5	2754.5	-1.8	**-3.1**
trpD	b1263	fused glutamine amidotransferase (component II) of anthranilate synthase/anthranilate phosphoribosyl transferase	3598.5	2445.7	1190.8	-1.5	**-3.0**
trpE	b1264	component I of anthranilate synthase	2547.1	1308.6	840.3	-1.9	**-3.0**
tyrA	b2600	fused chorismate mutase T/prephenate dehydrogenase	2504.2	1776.0	968.6	-1.4	**-2.6**
yeeF	b2014	predicted amino-acid transporter	3329.6	1276.5	967.0	**-2.6**	**-3.4**
Cofactor Synthesis and Salvage							

btuB	b3966	vitamin B_{12} outer membrane transporter	1538.7	838.7	604.5	-1.8	**-2.5**
btuF	b0158	vitamin B_{12} transporter subunit: periplasmic-binding component of ABC superfamily	919.8	438.5	355.1	**-2.1**	**-2.6**
dxs	b0420	1-deoxyxylulose-5-phosphate synthase, thiamine-requiring, FAD-requiring	2021.9	1181.8	892.1	-1.7	**-2.3**
entA	b0596	2,3-dihydroxybenzoate-2,3-dehydrogenase	702.5	362.6	323.5	-1.9	**-2.2**
entB	b0595	isochorismatase	1120.4	634.4	536.3	-1.8	**-2.1**
entC	b0593	isochorismate synthase	763.4	163.4	134.0	**-4.7**	**-5.7**
entE	b0594	2,3-dihydroxybenzoate-AMP ligase component of enterobactin synthase multienzyme complex	386.6	66.4	55.6	**-5.8**	**-7.0**
folC	b2315	bifunctional folylpolyglutamate synthase/ dihydrofolate synthase	2123.5	1036.5	888.2	**-2.0**	**-2.4**
folD	b0529	bifunctional 5,10-methylene-tetrahydrofolate dehydrogenase/ 5,10-methylene-tetrahydrofolate cyclohydrolase	3389.8	1974.5	1477.5	-1.7	**-2.3**
nudJ	b1134	bifunctional thiamin pyrimidine pyrophosphate hydrolase/ thiamin pyrophosphate hydrolase	593.4	261.3	274.3	**-2.3**	**-2.2**
pdxA	b0052	4-hydroxy-L-threonine phosphate dehydrogenase, NAD-dependent	3015.6	955.4	730.6	**-3.2**	**-4.1**
pdxH	b1638	pyridoxamine 5'-phosphate oxidase	1699.7	1013.0	758.6	-1.7	**-2.2**
pdxY	b1636	pyridoxine kinase	1155.1	606.1	475.3	-1.9	**-2.4**
ribE	b0415	riboflavin synthase subunit beta	5138.7	2715.6	2402.2	-1.9	**-2.1**
thiI	b0423	sulfurtransferase required for thiamine and 4-thiouridine biosynthesis	2086.6	802.2	742.9	**-2.6**	**-2.8**
Nucleotide Synthesis and Salvage							
apt	b0469	adenine phosphoribosyltransferase	3286.3	1061.1	1123.8	**-3.1**	**-2.9**
codA	b0337	cytosine deaminase	5944.0	3049.0	1284.4	-1.9	**-4.6**
codB	b0336	cytosine transporter	6138.6	2460.9	760.8	**-2.5**	**-8.1**
cytR	b3934	DNA-binding transcriptional dual regulator	1386.3	847.2	641.9	-1.6	**-2.2**
gpt	b0238	guanine-hypoxanthine phosphoribosyltransferase	2020.7	755.3	767.0	**-2.7**	**-2.6**
gsk	b0477	Inosine-guanosine kinase	995.3	439.2	441.9	**-2.3**	**-2.3**
guaB	b2508	IMP dehydrogenase	8133.0	4995.1	2314.3	-1.6	**-3.5**
ndk	b2518	multifunctional nucleoside diphosphate kinase and apyrimidinic endonuclease and 3'-phosphodiesterase	4490.9	1296.1	988.1	**-3.5**	**-4.5**
nupC	b2393	nucleoside (except guanosine) transporter	305.1	154.4	117.7	**-2.0**	**-2.6**
prsA	b1207	phosphoribosylpyrophosphate synthase	6148.8	1336.0	839.4	**-4.6**	**-7.3**
purB	b1131	adenylosuccinate lyase	7208.2	2754.5	1462.1	**-2.6**	**-4.9**
purC	b2476	phosphoribosylaminoimidazole-succinocarboxamide synthase	6457.3	4061.8	1389.9	-1.6	**-4.6**
purD	b4005	phosphoribosylglycinamide synthetase phosphoribosylamine-glycine ligase	5364.8	2981.8	955.9	-1.8	**-5.6**
purE	b0523	N5-carboxyaminoimidazole ribonucleotide mutase	4627.9	933.8	521.7	**-5.0**	**-8.9**

purF	b2312	amidophosphoribosyltransferase	6033.2	1818.8	1065.8	**-3.3**	**-5.7**
purH	b4006	fused IMP cyclohydrolase/phosphoribosylaminoimidazolecarboxamide formyltransferase	7788.7	4088.8	1214.8	-1.9	**-6.4**
purK	b0522	N5-carboxyaminoimidazole ribonucleotide synthase	2454.1	505.6	221.0	**-4.9**	**-11.1**
purL	b2557	phosphoribosylformyl-glycineamide synthetase	5998.3	3030.3	987.0	**-2.0**	**-6.1**
purM	b2499	phosphoribosylaminoimidazole synthetase	5872.5	2001.7	528.6	**-2.9**	**-11.1**
purN	b2500	phosphoribosylglycinamide formyltransferase	4916.3	1576.4	948.7	**-3.1**	**-5.2**
purR	b1658	DNA-binding transcriptional repressor, hypoxanthine-binding	1541.4	1314.2	703.2	-1.2	**-2.2**
purT	b1849	phosphoribosylglycinamide formyltransferase 2	4062.0	2451.1	841.4	-1.7	**-4.8**
purU	b1232	formyltetrahydrofolate deformylase	3800.7	1649.2	1386.4	**-2.3**	**-2.7**
pyrC	b1062	dihydroorotase	6593.6	3895.2	1465.5	-1.7	**-4.5**
pyrD	b0945	dihydroorotate dehydrogenase	2039.0	224.3	98.8	**-9.1**	**-20.6**
pyrF	b1281	orotidine 5'-phosphate decarboxylase	1897.5	578.0	487.0	**-3.3**	**-3.9**
pyrG	b2780	CTP synthetase	4746.5	2726.5	2169.2	-1.7	**-2.2**
pyrH	b0171	uridylate kinase	6208.9	3882.4	2787.1	-1.6	**-2.2**
pyrI	b4244	aspartate carbamoyltransferase regulatory subunit	12847.9	10642.9	5443.2	-1.2	**-2.4**
pyrL	b4246	*pyrBI* operon leader peptide	3320.4	1391.2	1003.5	**-2.4**	**-3.3**
rihA	b0651	ribonucleoside hydrolase 1	510.2	265.1	204.2	-1.9	**-2.5**
tsx	b0411	nucleoside channel, receptor of phage T6 and colicin K	2804.7	1389.3	1019.5	**-2.0**	**-2.8**
upp	b2498	uracil phosphoribosyltransferase	8945.5	5375.6	2778.8	-1.7	**-3.2**
uraA	b2497	uracil transporter	3454.7	1367.9	392.9	**-2.5**	**-8.8**
yicE	b3654	putative purine permease	2086.3	874.5	439.5	**-2.4**	**-4.7**
yieG	b2493	predicted inner membrane protein	799.1	236.6	117.4	**-3.4**	**-6.8**
Transport of Peptides, Proteins, and Sugars							
dppB	b3543	dipeptide transporter	1521.2	905.7	574.8	-1.7	**-2.6**
dppC	b3542	dipeptide transport system permease protein	3104.8	1756.3	1243.9	-1.8	**-2.5**
dppD	b3541	dipeptide transport ATP-binding protein	1840.3	972.6	714.9	-1.9	**-2.6**
dppF	b3540	dipeptide transport ATP-binding protein	1326.9	827.6	593.3	-1.6	**-2.2**
lamB	b4036	maltose outer membrane porin (maltoporin)	2116.1	1328.1	979.4	-1.6	**-2.2**
malE	b4034	maltose transporter subunit	3217.5	1912.9	1153.1	-1.7	**-2.8**
malK	b4035	fused maltose transport subunit, ATP-binding component of ABC superfamily/regulatory protein	1252.7	510.6	374.9	**-2.5**	**-3.3**
malM	b4037	maltose regulon periplasmic protein	1242.9	761.9	582.3	-1.6	**-2.1**
mglA	b2149	fused methyl-galactoside transporter subunits of ABC superfamily: ATP-binding components	502.4	298.0	227.9	-1.7	**-2.2**
mglC	b2148	methyl-galactoside transporter subunit	279.6	195.2	133.1	-1.4	**-2.1**
oppB	b1244	oligopeptide permease ABC transporter membrane component	2033.5	939.4	544.2	**-2.2**	**-3.7**
oppC	b1245	oligopeptide transport system permease	2754.9	1458.3	940.4	-1.9	**-2.9**

		protein					
potA	b1126	putrescine/spermidine ABC transporter ATPase	3080.8	1463.0	1615.6	**-2.1**	-1.9
potB	b1125	spermidine/putrescine ABC transporter membrane component	1702.3	718.2	764.1	**-2.4**	**-2.2**
potC	b1124	spermidine/putrescine ABC transporter membrane component	3511.3	1508.1	1593.0	**-2.3**	**-2.2**
proV	b2677	glycine betaine transporter subunit	1241.2	715.0	490.0	-1.7	**-2.5**
rbsA	b3749	fused D-ribose transporter subunits of ABC superfamily: ATP-binding components	721.3	426.5	301.3	-1.7	**-2.4**
rbsD	b3748	high affinity ribose transport protein	2333.6	1527.7	871.0	-1.5	**-2.7**
secD	b0408	SecYEG protein translocase auxillary subunit	3515.9	1807.9	1641.8	-1.9	**-2.1**
secF	b0409	SecYEG protein translocase auxillary subunit	2888.8	1541.1	1272.9	-1.9	**-2.3**
sppA	b1766	protease IV (signal peptide peptidase)	1245.4	666.9	531.1	-1.9	**-2.3**
tat	b3839	Sec-independent protein translocase protein	1129.1	591.6	531.6	-1.9	**-2.1**
yidC	b3705	cytoplasmic insertase into membrane protein, Sec system	3304.8	1392.2	1426.7	**-2.4**	**-2.3**
yojI	b2211	fused predicted multidrug transport subunits of ABC superfamily: membrane component/ATP-binding component	758.9	193.5	191.8	**-3.9**	**-4.0**
General Stress Response							
cspB	b1557	prophage; cold shock protein	292.3	129.9	179.9	**-2.3**	-1.6
cspF	b1558	prophage; cold shock protein	209.8	101.2	108.1	**-2.1**	-1.9
cvpA	b2313	membrane protein required for colicin V production	7617.1	2103.6	1326.2	**-3.6**	**-5.7**
cvrA	b1191	predicted cation/proton antiporter	319.1	181.7	151.3	-1.8	**-2.1**
evgS	b2370	hybrid sensory histidine kinase in two-component regulatory system with EvgA	228.3	99.4	64.4	**-2.3**	**-3.5**
fis	b3261	DNA-binding transcriptional dual regulator	5036.6	2126.8	1915.8	**-2.4**	**-2.6**
gppA	b3779	Guanosine-5'-triphosphate,3'-diphosphate pyrophosphatase	1641.8	728.7	680.4	**-2.3**	**-2.4**
mdoC	b1047	membrane protein required for modification of periplasmic glucan	366.6	162.6	163.2	**-2.3**	**-2.2**
mdoG	b1048	glucan biosynthesis protein, periplasmic	3300.8	1757.6	1151.4	-1.9	**-2.9**
mdoH	b1049	glucan biosynthesis: glycosyl transferase	1832.1	867.7	502.0	**-2.1**	**-3.6**
rcsD	b2216	phosphotransfer intermediate protein in two-component regulatory system with RcsBC	857.1	567.4	416.3	-1.5	**-2.1**
rsxB	b1628	electron transport complex protein RnfB	1192.8	594.6	652.7	**-2.0**	-1.8
rsxC	b1629	electron transport complex protein RnfC	1202.1	476.7	425.1	**-2.5**	**-2.8**
rsxD	b1630	electron transport complex protein RnfD	541.5	216.5	205.5	**-2.5**	**-2.6**
rsxE	b1632	predicted inner membrane NADH-quinone reductase	736.5	394.7	322.5	-1.9	**-2.3**
rsxG	b1631	electron transport complex protein RnfG	630.3	260.0	247.8	**-2.4**	**-2.5**
rttR	b4425	rtT sRNA, processed from tyrT	1739.5	589.1	634.7	**-3.0**	**-2.7**

		transcript may modulate the stringent response; putative Tpr protein					
speD	b0120	S-adenosylmethionine decarboxylase	4036.4	2343.2	1709.5	-1.7	**-2.4**
spoT	b3650	bifunctional (p)ppGpp synthetase II/ guanosine-3',5'-bis pyrophosphate 3'-pyrophosphohydrolase	2087.6	1026.0	922.0	**-2.0**	**-2.3**
spr	b2175	predicted peptidase, outer membrane lipoprotein	4461.8	2902.9	2230.7	-1.5	**-2.0**
suhB	b2533	inositol-1-monophosphatase	1508.5	317.8	358.9	**-4.7**	**-4.2**
typA	b3871	GTP-binding protein	6613.6	3348.8	3205.2	**-2.0**	**-2.1**
yehT	b2125	predicted response regulator in two-component system with YehU	399.8	232.0	198.9	-1.7	**-2.0**
yjgF	b4243	enamime/imine deaminase	14383.1	11512.4	6344.1	-1.2	**-2.3**
yqgB	b2939	hypothetical protein	2664.3	1217.1	876.9	**-2.2**	**-3.0**
Motility							
flgB	b1073	flagellar component of cell-proximal portion of basal-body rod	395.4	280.8	173.5	-1.4	**-2.3**
flgE	b1076	flagellar hook protein	691.7	406.5	246.4	-1.7	**-2.8**
Unknown							
bcsG	b3538	predicted inner membrane protein	793.1	456.2	345.9	-1.7	**-2.3**
fruL	b0079	very hypothetical *fruR/shI* operon leader peptide	1775.9	1196.3	788.4	-1.5	**-2.3**
hflD	b1132	predicted lysogenization regulator	3007.0	1292.0	1118.9	**-2.3**	**-2.7**
nmpC	b0499	pseudogene	9526.0	5315.3	2370.6	-1.8	**-4.0**
wbbJ	b2033	predicted acyl transferase	2216.6	1699.9	1087.7	-1.3	**-2.0**
yagI	b0254	CP4-6 prophage; predicted DNA-binding transcriptional regulator	1354.8	783.7	667.3	-1.7	**-2.0**
ybaN	b0468	conserved inner membrane protein	1214.9	473.0	485.9	**-2.6**	**-2.5**
ybdB	b0597	hypothetical protein	556.7	324.2	270.6	-1.7	**-2.1**
ybeA	b1706	hypothetical protein	2518.1	1050.5	1003.5	**-2.4**	**-2.5**
ybeB	b0637	hypothetical protein	2365.0	1070.8	1050.3	**-2.2**	**-2.3**
ybgF	b0742	hypothetical protein	7843.5	4387.2	3438.4	-1.8	**-2.3**
ybhC	b0772	predicted pectinesterase	1855.3	1019.6	870.4	-1.8	**-2.1**
ybjE	b0874	predicted transporter	1003.7	362.4	314.5	**-2.8**	**-3.2**
ycaO	b1754	conserved protein	850.3	263.8	234.4	**-3.2**	**-3.6**
yccW	b0967	predicted methyltransferase	2069.9	1109.6	1024.8	-1.9	**-2.0**
ycdB	b1509	conserved protein	817.8	220.4	233.1	**-3.7**	**-3.5**
yceA	b1045	hypothetical protein	2249.1	914.2	823.7	**-2.5**	**-2.7**
ycgF	b1163	blue light-responsive regulator of YcgE	667.4	230.7	244.4	**-2.9**	**-2.7**
ydcX	b1445	hypothetical protein	773.1	274.2	333.7	**-2.8**	**-2.3**
ydiI	b1686	hypothetical protein	1795.0	1508.0	846.3	-1.2	**-2.1**
ydiJ	b1687	predicted FAD-linked oxidoreductase	2630.9	2190.5	820.3	-1.2	**-3.2**
ydiY	b1722	hypothetical protein	1013.3	231.0	238.3	**-4.4**	**-4.3**
yeaD	b1780	hypothetical protein	2634.4	2179.8	1214.2	-1.2	**-2.2**
yeaZ	b1807	predicted peptidase	805.3	391.6	386.2	**-2.1**	**-2.1**
yejL	b2187	hypothetical protein	2303.9	1056.6	1048.9	**-2.2**	**-2.2**
yejM	b2188	predicted hydrolase, inner membrane	834.4	412.1	372.6	**-2.0**	**-2.2**
yfcA	b2327	conserved inner membrane protein	812.0	279.1	241.0	**-2.9**	**-3.4**
yfcL	b2325	hypothetical protein	1638.8	576.8	478.7	**-2.8**	**-3.4**
yfcM	b2326	hypothetical protein	1150.0	460.5	356.7	**-2.5**	**-3.2**

yfdH	b2351	CPS-53 (KpLE1) prophage; bactoprenol glucosyl transferase	3637.4	1236.7	1102.5	**-2.9**	**-3.3**
yfdI	b2352	CPS-53 (KpLE1) prophage; predicted inner membrane protein	1736.3	793.6	237.1	**-2.2**	**-7.3**
yfiP	b2583	hypothetical protein	387.1	196.9	190.7	**-2.0**	**-2.0**
yfjW	b2642	CP4-57 prophage; predicted inner membrane protein	332.7	181.3	117.1	-1.8	**-2.8**
ygaH	b2683	predicted inner membrane protein	1411.2	843.3	490.1	-1.7	**-2.9**
ygaZ	b2682	predicted transporter	1125.4	671.2	419.6	-1.7	**-2.7**
ygiQ	b0866	hypothetical protein	1851.5	605.5	540.0	**-3.1**	**-3.4**
ygiQ	b0964	hypothetical protein	1611.5	540.9	517.6	**-3.0**	**-3.1**
yhbY	b3180	predicted RNA-binding protein	4665.8	2328.6	2205.4	**-2.0**	**-2.1**
yhgF	b3407	predicted transcriptional accessory protein	1942.5	1272.6	962.0	-1.5	**-2.0**
yhiD	b3508	predicted Mg(2+) transport ATPase inner membrane protein	463.1	249.2	213.0	-1.9	**-2.2**
yibQ	b3614	predicted polysaccharide deacetylase	471.2	248.3	199.1	-1.9	**-2.4**
yigB	b3812	predicted hydrolase	1138.4	617.2	450.9	-1.8	**-2.5**
yijP	b1168	conserved inner membrane protein	3262.5	1355.0	1379.8	**-2.4**	**-2.4**
ykfG	b0235	pseudogene	1811.6	1001.4	766.8	-1.8	**-2.4**
yliE	b0833	conserved inner membrane protein	360.3	251.1	171.0	-1.4	**-2.1**
ymfA	b1122	predicted inner membrane protein	266.1	152.9	108.5	-1.7	**-2.5**
yncE	b1452	hypothetical protein	2407.4	1279.7	886.0	-1.9	**-2.7**
yneE	b1520	conserved inner membrane protein	378.9	207.5	189.9	-1.8	**-2.0**

REFERENCE

Achbergerova, L. and J. Nahalka (2011) Polyphosphate--an ancient energy source and active metabolic regulator. *Microb Cell Fact* **10**: 63.

Adams, S., P. Green, R. Claxton, S. Simcox, M.V. Williams, K. Walsh and C. Leeuwenburgh (2001) Reactive carbonyl formation by oxidative and non-oxidative pathways. *Front Biosci* **6**: A17-24.

Akiyama, M., E. Crooke and A. Kornberg (1992) The polyphosphate kinase gene of Escherichia coli. Isolation and sequence of the ppk gene and membrane location of the protein. *J Biol Chem* **267**: 22556-22561.

Albert, C.J., J.R. Crowley, F.F. Hsu, A.K. Thukkani and D.A. Ford (2001) Reactive chlorinating species produced by myeloperoxidase target the vinyl ether bond of plasmalogens: identification of 2-chlorohexadecanal. *The Journal of biological chemistry* **276**: 23733-23741.

Alderman, C.J., P.R. Bunyard, B.M. Chain, J.C. Foreman, D.S. Leake and D.R. Katz (2002a) Effects of oxidised low density lipoprotein on dendritic cells: a possible immunoregulatory component of the atherogenic micro-environment? *Cardiovasc Res* **55**: 806-819.

Alderman, C.J., S. Shah, J.C. Foreman, B.M. Chain and D.R. Katz (2002) The role of advanced oxidation protein products in regulation of dendritic cell function. *Free Radic Biol Med* **32**: 377-385.

Armesto, X., Canle, ML., Santaballa, JA (1993) α-amino acids chlorination in aqueous media. *Tetrahedron* **49**: 275-285.

Arnhold, J., E. Monzani, P. Furtmuller, M. Zederbauer, L. Casella and C. Obinger (2006) Kinetics and thermodynamics of halide and nitrite oxidation by mammalian heme peroxidases. *Eur. J. Inorg. Chem*: 3801-3811.

Arnhold, J., A.N. Osipov, H. Spalteholz, O.M. Panasenko and J. Schiller (2002) Formation of lysophospholipids from unsaturated phosphatidylcholines under the influence of hypochlorous acid. *Biochim Biophys Acta* **1572**: 91-100.

Aschar-Sobbi, R., A.Y. Abramov, C. Diao, M.E. Kargacin, G.J. Kargacin, R.J. French and E. Pavlov (2008) High sensitivity, quantitative measurements of polyphosphate using a new DAPI-based approach. *J Fluoresc* **18**: 859-866.

Ashby, M.T., A.C. Carlson and M.J. Scott (2004) Redox buffering of hypochlorous acid by thiocyanate in physiologic fluids. *J Am Chem Soc* **126**: 15976-15977.

Bae, Y.S., M.K. Choi and W.J. Lee (2010) Dual oxidase in mucosal immunity and host-microbe homeostasis. *Trends Immunol* **31**: 278-287.

Beal, J.L., S.B. Foster and M.T. Ashby (2009) Hypochlorous acid reacts with the N-terminal methionines of proteins to give dehydromethionine, a potential biomarker for neutrophil-induced oxidative stress. *Biochemistry* **48**: 11142-11148.

Beck, B.D. (1979) Polymerization of the bacterial elongation factor for protein synthesis, EF-Tu. *Eur J Biochem* **97**: 495-502.

Belousov, V.V., A.F. Fradkov, K.A. Lukyanov, D.B. Staroverov, K.S. Shakhbazov, A.V. Terskikh and S. Lukyanov (2006) Genetically encoded fluorescent indicator for intracellular hydrogen peroxide. *Nat Methods* **3**: 281-286.

Blanchard, J.L., W.Y. Wholey, E.M. Conlon and P.J. Pomposiello (2007) Rapid changes in gene expression dynamics in response to superoxide reveal SoxRS-dependent and independent transcriptional networks. *PLoS One* **2**: e1186.

Booth, I.R., G.P. Ferguson, S. Miller, C. Li, B. Gunasekera and S. Kinghorn (2003) Bacterial production of methylglyoxal: a survival strategy or death by misadventure? *Biochemical Society transactions* **31**: 1406-1408.

Butland, G., J.M. Peregrin-Alvarez, J. Li, W. Yang, X. Yang, V. Canadien *et al.* (2005) Interaction network containing conserved and essential protein complexes in Escherichia coli. *Nature* **433**: 531-537.

Caldas, T.D., A. El Yaagoubi and G. Richarme (1998) Chaperone properties of bacterial elongation factor EF-Tu. *J Biol Chem* **273**: 11478-11482.

Carr, A.C., J.J. van den Berg and C.C. Winterbourn (1996) Chlorination of cholesterol in cell membranes by hypochlorous acid. *Archives of biochemistry and biophysics* **332**: 63-69.

Carr, A.C., M.C. Vissers, N.M. Domigan and C.C. Winterbourn (1997) Modification of red cell membrane lipids by hypochlorous acid and haemolysis by preformed lipid chlorohydrins. *Redox Rep* **3**: 263-271.

Chang, M.W., F. Toghrol and W.E. Bentley (2007) Toxicogenomic response to chlorination includes induction of major virulence genes in Staphylococcus aureus. *Environ Sci Technol* **41**: 7570-7575.

Chapman, A.L., C.C. Winterbourn, S.O. Brennan, T.W. Jordan and A.J. Kettle (2003) Characterization of non-covalent oligomers of proteins treated with hypochlorous acid. *Biochem J* **375**: 33-40.

Chen, S., J. Lu, C. Sun and H. Ma (2010) A highly specific ferrocene-based fluorescent probe for hypochlorous acid and its application to cell imaging. *Analyst* **135**: 577-582.

Chen, X., K.A. Lee, E.M. Ha, K.M. Lee, Y.Y. Seo, H.K. Choi *et al.* (2011) A specific and sensitive method for detection of hypochlorous acid for the imaging of microbe-induced HOCl production. *Chem Commun (Camb)* **47**: 4373-4375.

Cooper, R.A. (1984) Metabolism of methylglyoxal in microorganisms. *Annu Rev Microbiol* **38**: 49-68.

Davies, M.J., C.L. Hawkins, D.I. Pattison and M.D. Rees (2008) Mammalian heme peroxidases: from molecular mechanisms to health implications. *Antioxid Redox Signal* **10**: 1199-1234.

De Spiegeleer, P., K. Vanoirbeek, A. Lietaert, J. Sermon, A. Aertsen and C.W. Michiels (2005) Investigation into the resistance of lactoperoxidase tolerant Escherichia coli mutants to different forms of oxidative stress. *FEMS Microbiol Lett* **252**: 315-319.

Defeu Soufo, H.J., C. Reimold, U. Linne, T. Knust, J. Gescher and P.L. Graumann (2010) Bacterial translation elongation factor EF-Tu interacts and colocalizes with actin-like MreB protein. *Proc Natl Acad Sci U S A* **107**: 3163-3168.

Dever, G., L.J. Stewart, A.R. Pitt and C.M. Spickett (2003) Phospholipid chlorohydrins cause ATP depletion and toxicity in human myeloid cells. *FEBS Lett* **540**: 245-250.

Dever, G., C.L. Wainwright, S. Kennedy and C.M. Spickett (2006) Fatty acid and phospholipid chlorohydrins cause cell stress and endothelial adhesion. *Acta Biochim Pol* **53**: 761-768.

Dukan, S., S. Belkin and D. Touati (1999) Reactive oxygen species are partially involved in the bacteriocidal action of hypochlorous acid. *Arch Biochem Biophys* **367**: 311-316.

Dukan, S. and D. Touati (1996) Hypochlorous acid stress in Escherichia coli: resistance, DNA damage, and comparison with hydrogen peroxide stress. *Journal of bacteriology* **178**: 6145-6150.

Eiserich, J.P., C.E. Cross, A.D. Jones, B. Halliwell and A. van der Vliet (1996) Formation of nitrating and chlorinating species by reaction of nitrite with hypochlorous acid. A novel mechanism for nitric oxide-mediated protein modification. *The Journal of biological chemistry* **271**: 19199-19208.

El Hassani, R.A., N. Benfares, B. Caillou, M. Talbot, J.C. Sabourin, V. Belotte *et al.* (2005) Dual oxidase2 is expressed all along the digestive tract. *Am J Physiol Gastrointest Liver Physiol* **288**: G933-942.

Erental, A., I. Sharon and H. Engelberg-Kulka (2012) Two Programmed Cell Death Systems in Escherichia coli: An Apoptotic-Like Death Is Inhibited by the mazEF-Mediated Death Pathway. *PLoS Biol* **10**: e1001281.

Eriksson, S., S. Lucchini, A. Thompson, M. Rhen and J.C. Hinton (2003) Unravelling the biology of macrophage infection by gene expression profiling of intracellular Salmonella enterica. *Mol Microbiol* **47**: 103-118.

Fenton, H.J.H. (1894) Oxidation of tartaric acid in presence of iron. *J. Chem. Soc., Trans.* **65**: 899-911.

Ferguson, G.P., S. Totemeyer, M.J. MacLean and I.R. Booth (1998) Methylglyoxal production in bacteria: suicide or survival? *Arch Microbiol* **170**: 209-218.

Folkes, L.K., L.P. Candeias and P. Wardman (1995) Kinetics and mechanisms of hypochlorous acid reactions. *Arch Biochem Biophys* **323**: 120-126.

Ford, D.A. (2010) Lipid oxidation by hypochlorous acid: chlorinated lipids in atherosclerosis and myocardial ischemia. *Clin Lipidol* **5**: 835-852.
Fraval, H.N. and D.C. McBrien (1980) The effect of methyl glyoxal on cell division and the synthesis of protein and DNA in synchronous and asynchronous cultures of Escherichia coli B/r. *J Gen Microbiol* **117**: 127-134.
Fu, X., J.L. Kao, C. Bergt, S.Y. Kassim, N.P. Huq, A. d'Avignon *et al.* (2004) Oxidative cross-linking of tryptophan to glycine restrains matrix metalloproteinase activity: specific structural motifs control protein oxidation. *J Biol Chem* **279**: 6209-6212.
Fu, X., Y. Wang, J. Kao, A. Irwin, A. d'Avignon, R.P. Mecham *et al.* (2006) Specific sequence motifs direct the oxygenation and chlorination of tryptophan by myeloperoxidase. *Biochemistry* **45**: 3961-3971.
Furano, A.V. (1975) Content of elongation factor Tu in Escherichia coli. *Proc Natl Acad Sci U S A* **72**: 4780-4784.
Gebendorfer, K.M., A. Drazic, Y. Le, J. Gundlach, A. Bepperling, A. Kastenmuller *et al.* (2012) Identification of a Hypochlorite-specific Transcription Factor from Escherichia coli. *The Journal of biological chemistry* **287**: 6892-6903.
Gentleman, R.C., V.J. Carey, D.M. Bates, B. Bolstad, M. Dettling, S. Dudoit *et al.* (2004) Bioconductor: open software development for computational biology and bioinformatics. *Genome Biol* **5**: R80.
Giles, N., Watts, AB., Giles, GI., Fry, FH., Littlechild, JA., and Jacob, C. (2003) Metal and redox modulation of cysteine protein function. *Chem. Biol.* **10**: 677-693.
Gonzalez-Perez, M.M., P. van Dillewijn, R.M. Wittich and J.L. Ramos (2007) Escherichia coli has multiple enzymes that attack TNT and release nitrogen for growth. *Environ Microbiol* **9**: 1535-1540.
Guzman, L.M., D. Belin, M.J. Carson and J. Beckwith (1995) Tight regulation, modulation, and high-level expression by vectors containing the arabinose PBAD promoter. *J Bacteriol* **177**: 4121-4130.
Ha, E.M., C.T. Oh, Y.S. Bae and W.J. Lee (2005) A direct role for dual oxidase in Drosophila gut immunity. *Science* **310**: 847-850.
Hampton, M.B., A.J. Kettle and C.C. Winterbourn (1998) Inside the neutrophil phagosome: oxidants, myeloperoxidase, and bacterial killing. *Blood* **92**: 3007-3017.
Hamza, I., S. Chauhan, R. Hassett and M.R. O'Brian (1998) The bacterial irr protein is required for coordination of heme biosynthesis with iron availability. *J Biol Chem* **273**: 21669-21674.
Hanson, G.T., R. Aggeler, D. Oglesbee, M. Cannon, R.A. Capaldi, R.Y. Tsien and S.J. Remington (2004) Investigating mitochondrial redox potential with redox-sensitive green fluorescent protein indicators. *J Biol Chem* **279**: 13044-13053.
Harwood, D.T., A.J. Kettle and C.C. Winterbourn (2006) Production of glutathione sulfonamide and dehydroglutathione from GSH by myeloperoxidase-

derived oxidants and detection using a novel LC-MS/MS method. *Biochem J* **399**: 161-168.
Hawkins, C.L. and M.J. Davies (2002) Hypochlorite-induced damage to DNA, RNA, and polynucleotides: formation of chloramines and nitrogen-centered radicals. *Chem Res Toxicol* **15**: 83-92.
Hawkins, C.L. and M.J. Davies (2005) Inactivation of protease inhibitors and lysozyme by hypochlorous acid: role of side-chain oxidation and protein unfolding in loss of biological function. *Chem Res Toxicol* **18**: 1600-1610.
Hawkins, C.L., D.I. Pattison and M.J. Davies (2003) Hypochlorite-induced oxidation of amino acids, peptides and proteins. *Amino Acids* **25**: 259-274.
Hayatsu, H., S. Pan and T. Ukita (1971) Reaction of sodium hypochlorite with nucleic acids and their constituents. *Chem Pharm Bull (Tokyo)* **19**: 2189-2192.
Heinecke, J.W. (1999) Mechanisms of oxidative damage by myeloperoxidase in atherosclerosis and other inflammatory disorders. *J Lab Clin Med* **133**: 321-325.
Heinecke, J.W., W. Li, D.M. Mueller, A. Bohrer and J. Turk (1994) Cholesterol chlorohydrin synthesis by the myeloperoxidase-hydrogen peroxide-chloride system: potential markers for lipoproteins oxidatively damaged by phagocytes. *Biochemistry* **33**: 10127-10136.
Herring, C.D. and F.R. Blattner (2004) Global transcriptional effects of a suppressor tRNA and the inactivation of the regulator frmR. *J Bacteriol* **186**: 6714-6720.
Hopper, D.J. and R.A. Cooper (1972) The purification and properties of Escherichia coli methylglyoxal synthase. *Biochem J* **128**: 321-329.
Humphries, K.M. and L.I. Szweda (1998) Selective inactivation of alpha-ketoglutarate dehydrogenase and pyruvate dehydrogenase: reaction of lipoic acid with 4-hydroxy-2-nonenal. *Biochemistry* **37**: 15835-15841.
Hyslop, P.A., D.B. Hinshaw, W.A. Halsey, Jr., I.U. Schraufstatter, R.D. Sauerheber, R.G. Spragg *et al.* (1988) Mechanisms of oxidant-mediated cell injury. The glycolytic and mitochondrial pathways of ADP phosphorylation are major intracellular targets inactivated by hydrogen peroxide. *J Biol Chem* **263**: 1665-1675.
Ilbert, M., J. Horst, S. Ahrens, J. Winter, P.C. Graf, H. Lilie and U. Jakob (2007) The redox-switch domain of Hsp33 functions as dual stress sensor. *Nat Struct Mol Biol* **14**: 556-563.
Imlay, J.A. (2008) Cellular defenses against superoxide and hydrogen peroxide. *Annual review of biochemistry* **77**: 755-776.
Iuliano, L. (2011) Pathways of cholesterol oxidation via non-enzymatic mechanisms. *Chem Phys Lipids* **164**: 457-468.
Iwao, Y., Y. Ishima, J. Yamada, T. Noguchi, U. Kragh-Hansen, K. Mera *et al.* (2012) Quantitative evaluation of the role of cysteine and methionine residues in the antioxidant activity of human serum albumin using recombinant mutants. *IUBMB Life*.

Jacob, C. (2011) Redox signalling via the cellular thiolstat. *Biochemical Society transactions* **39**: 1247-1253.
Jakob, U., W. Muse, M. Eser and J.C. Bardwell (1999) Chaperone activity with a redox switch. *Cell* **96**: 341-352.
Jarboe, L.R. (2011) YqhD: a broad-substrate range aldehyde reductase with various applications in production of biorenewable fuels and chemicals. *Appl Microbiol Biotechnol* **89**: 249-257.
Jeong, K.C., K.F. Hung, D.J. Baumler, J.J. Byrd and C.W. Kaspar (2008) Acid stress damage of DNA is prevented by Dps binding in Escherichia coli O157:H7. *BMC Microbiol* **8**: 181.
Jeudy, S., V. Monchois, C. Maza, J.M. Claverie and C. Abergel (2006) Crystal structure of Escherichia coli DkgA, a broad-specificity aldo-keto reductase. *Proteins* **62**: 302-307.
Kawai, Y., H. Kiyokawa, Y. Kimura, Y. Kato, K. Tsuchiya and J. Terao (2006) Hypochlorous acid-derived modification of phospholipids: characterization of aminophospholipids as regulatory molecules for lipid peroxidation. *Biochemistry* **45**: 14201-14211.
Kawai, Y., H. Morinaga, H. Kondo, N. Miyoshi, Y. Nakamura, K. Uchida and T. Osawa (2004) Endogenous formation of novel halogenated 2'-deoxycytidine. Hypohalous acid-mediated DNA modification at the site of inflammation. *The Journal of biological chemistry* **279**: 51241-51249.
Kellum, M.W., B. Oray and S.J. Norton (1978) A convenient quantitative synthesis of methylglyoxal for glyoxalase I assays. *Anal Biochem* **85**: 586-590.
Kenmoku, S., Y. Urano, H. Kojima and T. Nagano (2007) Development of a highly specific rhodamine-based fluorescence probe for hypochlorous acid and its application to real-time imaging of phagocytosis. *J Am Chem Soc* **129**: 7313-7318.
Kettle, A.J., Winterbourn, C. C. (1997) Myeloperoxidase: a key regulator of neutrophil oxidant production. *Redox. Rep* **3**: 3-15.
Khor, H.K., M.T. Fisher and C. Schoneich (2004) Potential role of methionine sulfoxide in the inactivation of the chaperone GroEL by hypochlorous acid (HOCl) and peroxynitrite (ONOO-). *The Journal of biological chemistry* **279**: 19486-19493.
Klebanoff, S.J. (1980) Oxygen metabolism and the toxic properties of phagocytes. *Ann Intern Med* **93**: 480-489.
Klebanoff, S.J. (1999) Myeloperoxidase. *Proc Assoc Am Physicians* **111**: 383-389.
Klebanoff, S.J. (2005) Myeloperoxidase: friend and foe. *Journal of leukocyte biology* **77**: 598-625.
Kornberg, A., S.R. Kornberg and E.S. Simms (1956) Metaphosphate synthesis by an enzyme from Escherichia coli. *Biochim Biophys Acta* **20**: 215-227.

Kudlicki, W., A. Coffman, G. Kramer and B. Hardesty (1997) Renaturation of rhodanese by translational elongation factor (EF) Tu. Protein refolding by EF-Tu flexing. *J Biol Chem* **272**: 32206-32210.
Kulcharyk, P.A. and J.W. Heinecke (2001) Hypochlorous acid produced by the myeloperoxidase system of human phagocytes induces covalent cross-links between DNA and protein. *Biochemistry* **40**: 3648-3656.
Kumar, A., A.K. Pandey, S.S. Singh, R. Shanker and A. Dhawan (2011) Engineered ZnO and TiO(2) nanoparticles induce oxidative stress and DNA damage leading to reduced viability of Escherichia coli. *Free Radic Biol Med* **51**: 1872-1881.
Kumsta, C. and U. Jakob (2009) Redox-regulated chaperones. *Biochemistry* **48**: 4666-4676.
Lau, D. and S. Baldus (2006) Myeloperoxidase and its contributory role in inflammatory vascular disease. *Pharmacol Ther* **111**: 16-26.
Lee, B.C. and V.N. Gladyshev (2011) The biological significance of methionine sulfoxide stereochemistry. *Free radical biology & medicine* **50**: 221-227.
Leichert, L.I., F. Gehrke, H.V. Gudiseva, T. Blackwell, M. Ilbert, A.K. Walker *et al.* (2008) Quantifying changes in the thiol redox proteome upon oxidative stress in vivo. *Proceedings of the National Academy of Sciences of the United States of America* **105**: 8197-8202.
Leichert, L.I. and U. Jakob (2004) Protein thiol modifications visualized in vivo. *PLoS Biol* **2**: e333.
Levine, R.L., L. Mosoni, B.S. Berlett and E.R. Stadtman (1996) Methionine residues as endogenous antioxidants in proteins. *Proc Natl Acad Sci U S A* **93**: 15036-15040.
Ligeza, A., A.N. Tikhonov, J.S. Hyde and W.K. Subczynski (1998) Oxygen permeability of thylakoid membranes: electron paramagnetic resonance spin labeling study. *Biochim Biophys Acta* **1365**: 453-463.
Lin, W., L. Long, B. Chen and W. Tan (2009) A ratiometric fluorescent probe for hypochlorite based on a deoximation reaction. *Chemistry* **15**: 2305-2309.
Litman, G.W., J.P. Rast and S.D. Fugmann (2010) The origins of vertebrate adaptive immunity. *Nat Rev Immunol* **10**: 543-553.
Liu, B., X. Hou, Q. Zhou, J. Tian, P. Zhu, J. Xu *et al.* (2011) Detection of advanced oxidation protein products in patients with chronic kidney disease by a novel monoclonal antibody. *Free radical research* **45**: 662-671.
Luo, S. and R.L. Levine (2009) Methionine in proteins defends against oxidative stress. *FASEB J* **23**: 464-472.
MacLean, M.J., L.S. Ness, G.P. Ferguson and I.R. Booth (1998) The role of glyoxalase I in the detoxification of methylglyoxal and in the activation of the KefB K+ efflux system in Escherichia coli. *Mol Microbiol* **27**: 563-571.
Macomber, L., C. Rensing and J.A. Imlay (2007) Intracellular copper does not catalyze the formation of oxidative DNA damage in Escherichia coli. *J Bacteriol* **189**: 1616-1626.

Maitra, D., J. Byun, P.R. Andreana, I. Abdulhamid, M.P. Diamond, G.M. Saed *et al.* (2011) Reaction of hemoglobin with HOCl: mechanism of heme destruction and free iron release. *Free radical biology & medicine* **51**: 374-386.

Makui, H., E. Roig, S.T. Cole, J.D. Helmann, P. Gros and M.F. Cellier (2000) Identification of the Escherichia coli K-12 Nramp orthologue (MntH) as a selective divalent metal ion transporter. *Mol Microbiol* **35**: 1065-1078.

Malle, E., L. Hazell, R. Stocker, W. Sattler, H. Esterbauer and G. Waeg (1995) Immunologic detection and measurement of hypochlorite-modified LDL with specific monoclonal antibodies. *Arteriosclerosis, thrombosis, and vascular biology* **15**: 982-989.

Malle, E., G. Waeg, R. Schreiber, E.F. Grone, W. Sattler and H.J. Grone (2000) Immunohistochemical evidence for the myeloperoxidase/H2O2/halide system in human atherosclerotic lesions: colocalization of myeloperoxidase and hypochlorite-modified proteins. *European journal of biochemistry / FEBS* **267**: 4495-4503.

Marcinkiewicz, J., A. Grabowska, J. Bereta and T. Stelmaszynska (1995) Taurine chloramine, a product of activated neutrophils, inhibits in vitro the generation of nitric oxide and other macrophage inflammatory mediators. *J Leukoc Biol* **58**: 667-674.

Marcinkiewicz, J., E. Olszowska, S. Olszowski and J.M. Zgliczynski (1992) Enhancement of trinitrophenyl-specific humoral response to TNP proteins as the result of carrier chlorination. *Immunology* **76**: 385-388.

Marquez, L.A. and H.B. Dunford (1994) Chlorination of taurine by myeloperoxidase. Kinetic evidence for an enzyme-bound intermediate. *J Biol Chem* **269**: 7950-7956.

Matsuura, E., G.R. Hughes and M.A. Khamashta (2008) Oxidation of LDL and its clinical implication. *Autoimmun Rev* **7**: 558-566.

McCall, M.R., A.C. Carr, T.M. Forte and B. Frei (2001) Ldl modified by hypochlorous acid is a potent inhibitor of lecithin-cholesterol acyltransferase activity. *Arteriosclerosis, thrombosis, and vascular biology* **21**: 1040-1045.

McKenna, S.M. and K.J. Davies (1988) The inhibition of bacterial growth by hypochlorous acid. Possible role in the bactericidal activity of phagocytes. *Biochem J* **254**: 685-692.

Miller, R.A. and B.E. Britigan (1997) Role of oxidants in microbial pathophysiology. *Clin Microbiol Rev* **10**: 1-18.

Mironova, R., T. Niwa, Y. Handzhiyski, A. Sredovska and I. Ivanov (2005) Evidence for non-enzymatic glycosylation of Escherichia coli chromosomal DNA. *Mol Microbiol* **55**: 1801-1811.

Mironova, R., T. Niwa, H. Hayashi, R. Dimitrova and I. Ivanov (2001) Evidence for non-enzymatic glycosylation in Escherichia coli. *Mol Microbiol* **39**: 1061-1068.

Mohiuddin, I., H. Chai, P.H. Lin, A.B. Lumsden, Q. Yao and C. Chen (2006) Nitrotyrosine and chlorotyrosine: clinical significance and biological functions in the vascular system. *J Surg Res* **133**: 143-149.

Mokgatla, R.M., V.S. Brozel and P.A. Gouws (1998) Isolation of Salmonella resistant to hypochlorous acid from a poultry abattoir. *Lett Appl Microbiol* **27**: 379-382.

Mokgatla, R.M., P.A. Gouws and V.S. Brozel (2002) Mechanisms contributing to hypochlorous acid resistance of a Salmonella isolate from a poultry-processing plant. *J Appl Microbiol* **92**: 566-573.

Moskovitz, J., E. Flescher, B.S. Berlett, J. Azare, J.M. Poston and E.R. Stadtman (1998) Overexpression of peptide-methionine sulfoxide reductase in Saccharomyces cerevisiae and human T cells provides them with high resistance to oxidative stress. *Proc Natl Acad Sci U S A* **95**: 14071-14075.

Mueller, N.J., C. Steuckler, B. Hauer, N. Baudendistel, H. Housden, N.C. Bruce and K. Faber (2010) The Substrate Spectra of Pentaerythritol Tetranitrate Reductase, Morphinone Reductase, N-Ethylmaleimide Reductase and Estrogen-Binding Protein in the Asymmetric Bioreduction of Activated Alkenes. *Advanced Synthesis and Catalysis* **352**: 387-394.

Munch, G., B. Westcott, T. Menini and A. Gugliucci (2010) Advanced glycation endproducts and their pathogenic roles in neurological disorders. *Amino Acids*.

Muz, B., E. Kontny, J. Marcinkiewicz and W. Maslinski (2008) Heme oxygenase-1 participates in the anti-inflammatory activity of taurine chloramine. *Amino Acids* **35**: 397-402.

Navratil, T. and L.L. Spremulli (2003) Effects of mutagenesis of Gln97 in the switch II region of Escherichia coli elongation factor Tu on its interaction with guanine nucleotides, elongation factor Ts, and aminoacyl-tRNA. *Biochemistry* **42**: 13587-13595.

Nystrom, T. (2005) Role of oxidative carbonylation in protein quality control and senescence. *EMBO J* **24**: 1311-1317.

Okun, D.A., (2005) Drinking water and public health protection. In: Water Encyclopedia. J. Lehr, J. Keeley & J. Lehr (eds). Hoboken, NJ: John Wiley & Sons, pp. 281-292.

Ozyamak, E., S.S. Black, C.A. Walker, M.J. Maclean, W. Bartlett, S. Miller and I.R. Booth (2010) The critical role of S-lactoylglutathione formation during methylglyoxal detoxification in Escherichia coli. *Mol Microbiol* **78**: 1577-1590.

Palmer, L.J., P.R. Cooper, M.R. Ling, H.J. Wright, A. Huissoon and I.L. Chapple (2012) Hypochlorous acid regulates neutrophil extracellular trap release in humans. *Clin Exp Immunol* **167**: 261-268.

Panizzi, P., M. Nahrendorf, M. Wildgruber, P. Waterman, J.L. Figueiredo, E. Aikawa *et al.* (2009) Oxazine conjugated nanoparticle detects in vivo hypochlorous acid and peroxynitrite generation. *J Am Chem Soc* **131**: 15739-15744.

Papayannopoulos, V. and A. Zychlinsky (2009) NETs: a new strategy for using old weapons. *Trends Immunol* **30**: 513-521.
Parry, J. and D.P. Clark (2002) Identification of a CysB-regulated gene involved in glutathione transport in Escherichia coli. *FEMS Microbiol Lett* **209**: 81-85.
Pattison, D.I. and M.J. Davies (2001) Absolute rate constants for the reaction of hypochlorous acid with protein side chains and peptide bonds. *Chem Res Toxicol* **14**: 1453-1464.
Pattison, D.I., M.J. Davies and C.L. Hawkins (2012) Reactions and reactivity of myeloperoxidase-derived oxidants: differential biological effects of hypochlorous and hypothiocyanous acids. *Free Radic Res*.
Pattison, D.I., C.L. Hawkins and M.J. Davies (2003) Hypochlorous acid-mediated oxidation of lipid components and antioxidants present in low-density lipoproteins: absolute rate constants, product analysis, and computational modeling. *Chem Res Toxicol* **16**: 439-449.
Pattison, D.I., C.L. Hawkins and M.J. Davies (2007) Hypochlorous acid-mediated protein oxidation: how important are chloramine transfer reactions and protein tertiary structure? *Biochemistry* **46**: 9853-9864.
Patzer, S.I. and K. Hantke (2001) Dual repression by Fe(2+)-Fur and Mn(2+)-MntR of the mntH gene, encoding an NRAMP-like Mn(2+) transporter in Escherichia coli. *J Bacteriol* **183**: 4806-4813.
Pedersen, S., P.L. Bloch, S. Reeh and F.C. Neidhardt (1978) Patterns of protein synthesis in E. coli: a catalog of the amount of 140 individual proteins at different growth rates. *Cell* **14**: 179-190.
Perez, J.M., F.A. Arenas, G.A. Pradenas, J.M. Sandoval and C.C. Vasquez (2008) Escherichia coli YqhD exhibits aldehyde reductase activity and protects from the harmful effect of lipid peroxidation-derived aldehydes. *J Biol Chem* **283**: 7346-7353.
Peskin, A.V., R. Turner, G.J. Maghzal, C.C. Winterbourn and A.J. Kettle (2009) Oxidation of methionine to dehydromethionine by reactive halogen species generated by neutrophils. *Biochemistry* **48**: 10175-10182.
Peskin, A.V. and C.C. Winterbourn (2001) Kinetics of the reactions of hypochlorous acid and amino acid chloramines with thiols, methionine, and ascorbate. *Free Radic Biol Med* **30**: 572-579.
Peskin, A.V. and C.C. Winterbourn (2006) Taurine chloramine is more selective than hypochlorous acid at targeting critical cysteines and inactivating creatine kinase and glyceraldehyde-3-phosphate dehydrogenase. *Free radical biology & medicine* **40**: 45-53.
Pfaffl, M.W. (2001) A new mathematical model for relative quantification in real-time RT-PCR. *Nucleic Acids Res* **29**: e45.
Pirillo, A., P. Uboldi and A.L. Catapano (2010) Dual effect of hypochlorite in the modification of high density lipoproteins. *Biochem Biophys Res Commun* **403**: 447-451.

Pitt, A.R. and C.M. Spickett (2008) Mass spectrometric analysis of HOCl- and free-radical-induced damage to lipids and proteins. *Biochemical Society transactions* **36**: 1077-1082.

Pomposiello, P.J., M.H. Bennik and B. Demple (2001) Genome-wide transcriptional profiling of the Escherichia coli responses to superoxide stress and sodium salicylate. *Journal of bacteriology* **183**: 3890-3902.

Prokopowicz, Z., J. Marcinkiewicz, D.R. Katz and B.M. Chain (2012) Neutrophil myeloperoxidase: soldier and statesman. *Arch Immunol Ther Exp (Warsz)* **60**: 43-54.

Prokopowicz, Z.M., F. Arce, R. Biedron, C.L. Chiang, M. Ciszek, D.R. Katz *et al.* (2010) Hypochlorous acid: a natural adjuvant that facilitates antigen processing, cross-priming, and the induction of adaptive immunity. *J Immunol* **184**: 824-835.

Prutz, W.A. (1996) Hypochlorous acid interactions with thiols, nucleotides, DNA, and other biological substrates. *Archives of biochemistry and biophysics* **332**: 110-120.

Prutz, W.A. (1998a) Interactions of hypochlorous acid with pyrimidine nucleotides, and secondary reactions of chlorinated pyrimidines with GSH, NADH, and other substrates. *Archives of biochemistry and biophysics* **349**: 183-191.

Prutz, W.A. (1998b) Reactions of hypochlorous acid with biological substrates are activated catalytically by tertiary amines. *Archives of biochemistry and biophysics* **357**: 265-273.

Pullar, J.M., M.C. Vissers and C.C. Winterbourn (2001) Glutathione oxidation by hypochlorous acid in endothelial cells produces glutathione sulfonamide as a major product but not glutathione disulfide. *J Biol Chem* **276**: 22120-22125.

Pullar, J.M., C.C. Winterbourn and M.C. Vissers (1999) Loss of GSH and thiol enzymes in endothelial cells exposed to sublethal concentrations of hypochlorous acid. *Am J Physiol* **277**: H1505-1512.

Pulvermacher, S.C., L.T. Stauffer and G.V. Stauffer (2009) Role of the sRNA GcvB in regulation of cycA in Escherichia coli. *Microbiology* **155**: 106-114.

Puri, S., T.H. Hohle and M.R. O'Brian (2010) Control of bacterial iron homeostasis by manganese. *Proceedings of the National Academy of Sciences of the United States of America* **107**: 10691-10695.

Rabbani, N. and P.J. Thornalley (2010) Methylglyoxal, glyoxalase 1 and the dicarbonyl proteome. *Amino Acids*.

Rachmilovich-Calis, S., A. Masarwa, N. Meyerstein and D. Meyerstein (2011) The effect of pyrophosphate, tripolyphosphate and ATP on the rate of the Fenton reaction. *J Inorg Biochem* **105**: 669-674.

Raftery, M.J., Z. Yang, S.M. Valenzuela and C.L. Geczy (2001) Novel intra- and inter-molecular sulfinamide bonds in S100A8 produced by hypochlorite oxidation. *J Biol Chem* **276**: 33393-33401.

Rao, N.N., M.R. Gomez-Garcia and A. Kornberg (2009) Inorganic polyphosphate: essential for growth and survival. *Annu Rev Biochem* **78**: 605-647.

Rees, M.D., D.I. Pattison and M.J. Davies (2005) Oxidation of heparan sulphate by hypochlorite: role of N-chloro derivatives and dichloramine-dependent fragmentation. *Biochem J* **391**: 125-134.

Resch, U., M. Semlitsch, A. Hammer, H. Susani-Etzerodt, H. Walczak, W. Sattler and E. Malle (2011) Hypochlorite-modified low-density lipoprotein induces the apoptotic machinery in Jurkat T-cell lines. *Biochem Biophys Res Commun* **410**: 895-900.

Rosen, H., S.J. Klebanoff, Y. Wang, N. Brot, J.W. Heinecke and X. Fu (2009) Methionine oxidation contributes to bacterial killing by the myeloperoxidase system of neutrophils. *Proceedings of the National Academy of Sciences of the United States of America* **106**: 18686-18691.

Rossmann, C., A. Rauh, A. Hammer, W. Windischhofer, S. Zirkl, W. Sattler and E. Malle (2011) Hypochlorite-modified high-density lipoprotein promotes induction of HO-1 in endothelial cells via activation of p42/44 MAPK and zinc finger transcription factor Egr-1. *Archives of biochemistry and biophysics* **509**: 16-25.

Rutala, W.A. and D.J. Weber (1997) Uses of inorganic hypochlorite (bleach) in health-care facilities. *Clin Microbiol Rev* **10**: 597-610.

Saeed, A.I., V. Sharov, J. White, J. Li, W. Liang, N. Bhagabati *et al.* (2003) TM4: a free, open-source system for microarray data management and analysis. *Biotechniques* **34**: 374-378.

Sandoval, J.M., F.A. Arenas and C.C. Vasquez (2011) Glucose-6-phosphate dehydrogenase protects Escherichia coli from tellurite-mediated oxidative stress. *PLoS One* **6**: e25573.

Schurdell, M.S., G.M. Woodbury and W.R. McCleary (2007) Genetic evidence suggests that the intergenic region between pstA and pstB plays a role in the regulation of rpoS translation during phosphate limitation. *J Bacteriol* **189**: 1150-1153.

Senthilmohan, R. and A.J. Kettle (2006) Bromination and chlorination reactions of myeloperoxidase at physiological concentrations of bromide and chloride. *Archives of biochemistry and biophysics* **445**: 235-244.

Shepherd, J., S.A. Hilderbrand, P. Waterman, J.W. Heinecke, R. Weissleder and P. Libby (2007) A fluorescent probe for the detection of myeloperoxidase activity in atherosclerosis-associated macrophages. *Chem Biol* **14**: 1221-1231.

Skaff, O., D.I. Pattison and M.J. Davies (2009) Hypothiocyanous acid reactivity with low-molecular-mass and protein thiols: absolute rate constants and assessment of biological relevance. *Biochem J* **422**: 111-117.

Spickett, C.M., N. Rennie, H. Winter, L. Zambonin, L. Landi, A. Jerlich *et al.* (2001) Detection of phospholipid oxidation in oxidatively stressed cells by reversed-phase HPLC coupled with positive-ionization electrospray [correction of electroscopy] MS. *Biochem J* **355**: 449-457.

Storz, G. and J.A. Imlay (1999) Oxidative stress. *Curr Opin Microbiol* **2**: 188-194.
Subedi, K.P., D. Choi, I. Kim, B. Min and C. Park (2011) Hsp31 of Escherichia coli K-12 is glyoxalase III. *Mol Microbiol* **81**: 926-936.
Sun, Z.N., F.Q. Liu, Y. Chen, P.K. Tam and D. Yang (2008) A highly specific BODIPY-based fluorescent probe for the detection of hypochlorous acid. *Org Lett* **10**: 2171-2174.
Suquet, C., J.J. Warren, N. Seth and J.K. Hurst (2010) Comparative study of HOCl-inflicted damage to bacterial DNA ex vivo and within cells. *Arch Biochem Biophys* **493**: 135-142.
Tatsumi, T. and H. Fliss (1994) Hypochlorous acid and chloramines increase endothelial permeability: possible involvement of cellular zinc. *Am J Physiol* **267**: H1597-1607.
Thamsen, M. and U. Jakob (2011) The redoxome: Proteomic analysis of cellular redox networks. *Curr Opin Chem Biol* **15**: 113-119.
Thomas, E.L., M.B. Grisham and M.M. Jefferson (1986) Preparation and characterization of chloramines. *Methods Enzymol* **132**: 569-585.
Thompson, R.C., D.B. Dix and A.M. Karim (1986) The reaction of ribosomes with elongation factor Tu.GTP complexes. Aminoacyl-tRNA-independent reactions in the elongation cycle determine the accuracy of protein synthesis. *J Biol Chem* **261**: 4868-4874.
Thornalley, P.J. (2008) Protein and nucleotide damage by glyoxal and methylglyoxal in physiological systems--role in ageing and disease. *Drug Metabol Drug Interact* **23**: 125-150.
Ullman, T.A. and S.H. Itzkowitz (2011) Intestinal inflammation and cancer. *Gastroenterology* **140**: 1807-1816.
Umezawa, Y., T. Shimada, A. Kori, K. Yamada and A. Ishihama (2008) The uncharacterized transcription factor YdhM is the regulator of the nemA gene, encoding N-ethylmaleimide reductase. *J Bacteriol* **190**: 5890-5897.
van der Vliet, A. (2008) NADPH oxidases in lung biology and pathology: host defense enzymes, and more. *Free Radic Biol Med* **44**: 938-955.
Vissers, M.C., A.C. Carr and C.C. Winterbour (2001) Fatty acid chlorohydrins and bromohydrins are cytotoxic to human endothelial cells. *Redox Rep* **6**: 49-55.
Weijland, A. and A. Parmeggiani (1994) Why do two EF-Tu molecules act in the elongation cycle of protein biosynthesis? *Trends Biochem Sci* **19**: 188-193.
Weiss, S.J. and A.F. LoBuglio (1982) Phagocyte-generated oxygen metabolites and cellular injury. *Lab Invest* **47**: 5-18.
Weitzman, S.A. and L.I. Gordon (1990) Inflammation and cancer: role of phagocyte-generated oxidants in carcinogenesis. *Blood* **76**: 655-663.
Whiteman, M., S.H. Chu, J.L. Siau, P. Rose, K. Sabapathy, J.T. Schantz *et al.* (2007) The pro-inflammatory oxidant hypochlorous acid induces Bax-dependent mitochondrial permeabilisation and cell death through AIF-/EndoG-dependent pathways. *Cell Signal* **19**: 705-714.

Wholey, W.Y. and U. Jakob (2012) Hsp33 confers bleach resistance by protecting elongation factor Tu against oxidative degradation in Vibrio cholerae. *Mol Microbiol* **83**: 981-991.
Wild, J. and B. Obrepalska (1982) Regulation of expression of the dadA gene encoding D-amino acid dehydrogenase in Escherichia coli: analysis of dadA-lac fusions and direction of dadA transcription. *Mol Gen Genet* **186**: 405-410.
Winter, J., M. Ilbert, P.C. Graf, D. Ozcelik and U. Jakob (2008) Bleach activates a redox-regulated chaperone by oxidative protein unfolding. *Cell* **135**: 691-701.
Winter, J., K. Linke, A. Jatzek and U. Jakob (2005) Severe oxidative stress causes inactivation of DnaK and activation of the redox-regulated chaperone Hsp33. *Mol Cell* **17**: 381-392.
Winterbourn, C.C. (1985) Comparative reactivities of various biological compounds with myeloperoxidase-hydrogen peroxide-chloride, and similarity of the oxidant to hypochlorite. *Biochim Biophys Acta* **840**: 204-210.
Winterbourn, C.C. (2002) Biological reactivity and biomarkers of the neutrophil oxidant, hypochlorous acid. *Toxicology* **181-182**: 223-227.
Winterbourn, C.C. and S.O. Brennan (1997) Characterization of the oxidation products of the reaction between reduced glutathione and hypochlorous acid. *Biochem J* **326 (Pt 1)**: 87-92.
Winterbourn, C.C., M.B. Hampton, J.H. Livesey and A.J. Kettle (2006) Modeling the reactions of superoxide and myeloperoxidase in the neutrophil phagosome: implications for microbial killing. *J Biol Chem* **281**: 39860-39869.
Winterbourn, C.C. and A.J. Kettle (2000) Biomarkers of myeloperoxidase-derived hypochlorous acid. *Free radical biology & medicine* **29**: 403-409.
Winterbourn, C.C., J.J. van den Berg, E. Roitman and F.A. Kuypers (1992) Chlorohydrin formation from unsaturated fatty acids reacted with hypochlorous acid. *Archives of biochemistry and biophysics* **296**: 547-555.
Witko-Sarsat, V., M. Friedlander, C. Capeillere-Blandin, T. Nguyen-Khoa, A.T. Nguyen, J. Zingraff *et al.* (1996) Advanced oxidation protein products as a novel marker of oxidative stress in uremia. *Kidney Int* **49**: 1304-1313.
Wu, D. and P. Yotnda (2011) Production and detection of reactive oxygen species (ROS) in cancers. *J Vis Exp*.
Yang, N.C., W.M. Ho, Y.H. Chen and M.L. Hu (2002) A convenient one-step extraction of cellular ATP using boiling water for the luciferin-luciferase assay of ATP. *Anal Biochem* **306**: 323-327.
Yang, Y.C., H.H. Lu, W.T. Wang and I. Liau (2011) Selective and absolute quantification of endogenous hypochlorous acid with quantum-dot conjugated microbeads. *Anal Chem* **83**: 8267-8272.

Yu, M.S., H.W. Park, H.J. Kwon and Y.J. Jang (2011) The effect of a low concentration of hypochlorous acid on rhinovirus infection of nasal epithelial cells. *Am J Rhinol Allergy* **25**: 40-44.

Yuan, L., W. Lin, Y. Xie, B. Chen and J. Song (2012) Fluorescent Detection of Hypochlorous Acid from Turn-On to FRET-Based Ratiometry by a HOCl-Mediated Cyclization Reaction. *Chemistry* **18**: 2700-2706.

Zander, T., N.D. Phadke and J.C. Bardwell (1998) Disulfide bond catalysts in Escherichia coli. *Methods Enzymol* **290**: 59-74.

Zengel, J.M. and L. Lindahl (1990) Mapping of two promoters for elongation factor Tu within the structural gene for elongation factor G. *Biochim Biophys Acta* **1050**: 317-322.

Zhang, Z., Y. Zheng, W. Hang, X. Yan and Y. Zhao (2011) Sensitive and selective off-on rhodamine hydrazide fluorescent chemosensor for hypochlorous acid detection and bioimaging. *Talanta* **85**: 779-786.

Zhao, G., P. Ceci, A. Ilari, L. Giangiacomo, T.M. Laue, E. Chiancone and N.D. Chasteen (2002) Iron and hydrogen peroxide detoxification properties of DNA-binding protein from starved cells. A ferritin-like DNA-binding protein of Escherichia coli. *J Biol Chem* **277**: 27689-27696.

Zhou, Y., J.Y. Li, K.H. Chu, K. Liu and C. Yao (2012) Fluorescence turn-on detection of hypochlorous acid via HOCl-promoted dihydrofluorescein-ether oxidation and its application in vivo. *Chem Commun (Camb)*.